U.PORTO

INSTITUTO DE CIÊNCIAS BIOMÉDICAS ABEL SALAZAR
UNIVERSIDADE DO PORTO

universidade de aveiro
theoria poiesis praxis

MODELAÇÃO DA INTRUSÃO DA PLUMA DO RIO MINHO NAS RIAS BAIXAS

MODELLING THE MINHO RIVER PLUME INTRUSION INTO THE RIAS BAIXAS

MAGDA CATARINA FERREIRA DE SOUSA

Tese de doutoramento em Ciências do Mar e do Ambiente
(ciclo de estudos conjunto entre a Universidade de Aveiro e a Universidade do Porto)

2013

U.PORTO

INSTITUTO DE CIÊNCIAS BIOMÉDICAS ABEL SALAZAR
UNIVERSIDADE DO PORTO

universidade de aveiro
theoria poiesis praxis

MODELAÇÃO DA INTRUSÃO DA PLUMA DO RIO MINHO NAS RIAS BAIXAS

MODELLING THE MINHO RIVER PLUME INTRUSION INTO THE RIAS BAIXAS

MAGDA CATARINA FERREIRA DE SOUSA

O autor foi financiado pela Fundação para a Ciência e Tecnologia - FCT, através da bolsa de doutoramento SFRH/BD/60209/2009, no âmbito do Quadro de Referência Estratégico Nacional (QREN) e do Programa Operacional de Potencial Humano (POPH), comparticipado pelo Fundo Social Europeu e por fundos nacionais do Ministério da Educação e Ciência (MEC).

Este trabalho foi desenvolvido no âmbito do projeto DyEPlume: Estuarine Dynamics and Plume Propagation in the Portuguese Coast - Impacts of Climate Change (PTDC/MAR/107939/2008) com o apoio financeiro da Fundação para a Ciência e Tecnologia - FCT.

MAGDA CATARINA FERREIRA DE SOUSA

MODELAÇÃO DA INTRUSÃO DA PLUMA DO RIO MINHO NAS RIAS BAIXAS

MODELLING THE MINHO RIVER PLUME INTRUSION INTO THE RIAS BAIXAS

Tese de Candidatura ao grau de Doutor em Ciências do Mar e do Ambiente (Especialidade em: Oceanografia e Ecossistemas Marinhos) submetida à Universidade de Aveiro.

Orientador: Doutor João Miguel Sequeira Silva Dias
Categoria: Professor Auxiliar
Afiliação: Centro de Estudos do Ambiente e do Mar (CESAM) e Departamento de Física da Universidade de Aveiro

Co-orientador: Doutor Nuno Alexandre Firmino Vaz
Categoria: Investigador Auxiliar
Afiliação: Centro de Estudos do Ambiente e do Mar (CESAM) da Universidade de Aveiro

Co-orientadora: Doutora Maria Ines Alvarez Fernandez
Categoria: Professora Associada
Afiliação: Departamento de Física Aplicada da Faculdade de Ciências de Ourense da Universidade de Vigo

O JÚRI

Presidente

Doutor Aníbal Guimarães Costa
Professor Catedrático do Departamento de Engenharia Civil da Universidade de Aveiro

Doutor Rámon Gomez-Gesteira
Professor Catedrático do Departamento de Física Aplicada da Faculdade de Ciências de Ourense da Universidade de Vigo

Doutor Ramiro Joaquim de Jesus Neves
Professor Associado do Departamento de Engenharia Mecânica do Instituto Superior Técnico da Universidade Técnica de Lisboa

Doutor José Carlos Pinto Bastos Teixeira da Silva
Professor Associado do Departamento de Geociências, Ambiente e Ordenamento do Território da Faculdade de Ciências da Universidade do Porto

Doutor João Miguel Sequeira Silva Dias
Professor Auxiliar do Departamento de Física da Universidade de Aveiro

Acknowledgments

During my journey as a PhD student, I had the help, encouragement and friendship of a few people, and it is hard to know how to begin and end my acknowledgements to them.

Firstly, a special thanks to my three supervisors Professor João Miguel Dias, Ines Alvarez and Nuno Vaz, for their guidance, enthusiasm, patient and trust they have given.

I want to acknowledge Moncho Gomez-Gesteira for his guidance and advice. This work would not be the same without his suggestions.

I would like to thank Madalena Malhadas and Paulo Leitão for their help when I started with MOHID, which is the main tool of this work.

I want to acknowledge Martinho Almeida for providing some data and technical support that improved the model implementation.

I also wish to thank Ana Picado, António Trindade, Carina Lopes and Renato Mendes for helping me in many things.

I am especially thankful to Ana Pires for her help and especially for her friendship, which was crucial during this journey.

Thanks to my colleagues at NMEC (Estuarine and Coastal Modelling Division) for their availability.

I would to like to thank my colleagues at EPHYSLAB (Environmental Physics Laboratory) for their friendly welcome during my stays in Ourense.

I wish to thank my parents for their kindness, support and affection.

Finally, I also would like to thank Daniel, for his love and support, which encouraged my decisions. His faith in my abilities directed this work in the right way.

Resumo

O Rio Minho, situado a 30 km a sul das Rias Baixas, é o rio mais importante que desagua na costa ocidental Galega (NO da Península Ibérica). A descarga da água doce proveniente deste rio é importante para a determinação dos padrões hidrológicos adjacentes à sua foz, particularmente perto das regiões costeiras galegas. Esta água doce pode inundar as Rias Baixas por períodos prolongados, invertendo a distribuição normal de densidade. Deste modo, é fundamental caracterizar a dinâmica da pluma do Rio Minho, assim como os padrões termohalinos das áreas afetadas pela sua dispersão.

Assim, os principais objetivos deste trabalho consistiram no estudo da propagação da pluma estuarina do Minho em direção às Rias Baixas, e na deteção das condições nas quais esta afeta a circulação e as características hidrográficas destes sistemas costeiros, através do desenvolvimento e aplicação do modelo numérico MOHID.

Com este propósito avaliaram-se inicialmente as características hidrográficas das embocaduras das Rias Baixas. Verificou-se então que, no caso das embocaduras norte, devido à sua reduzida profundidade, os fluxos de calor entre a atmosfera e o oceano são o forçamento principal que determina a temperatura da água, enquanto que nas embocaduras sul os eventos de afloramento costeiro e a descarga de água doce são os fatores determinantes mais frequentes. Observou-se ainda um aumento de salinidade de sul para norte, o que indica que os menores valores detetados poderão ser explicados pela descarga de água doce proveniente do Rio Minho.

Seguidamente efetuou-se uma avaliação de dados de vento na costa Galega, com o objetivo de verificar a sua aplicabilidade no estudo da dispersão da pluma estuarina do Minho. Inicialmente compararam-se ventos medidos ao longo da costa em estações meteorológicas terrestres, com ventos medidos ao largo pelo satélite QuikSCAT. Esta análise permitiu estabelecer que os dados do satélite são uma boa aproximação no estudo de fenómenos costeiros induzidos pelo vento. No entanto, visto que para forçar o modelo numérico MOHID são necessários dados de vento com grande resolução espácio-temporal perto da costa, acrescentou-se ao estudo anterior dados resultantes de simulações de um modelo de previsão (WRF). Da comparação com os dados provenientes de boias oceanográficas, conclui-se que a melhor base de dados para representação do vento perto

da costa provém do modelo WRF.

Para efetuar o estudo da influência da pluma estuarina do Minho nas Rias Baixas, foi desenvolvido e implementado um sistema de modelação integrado de três níveis encaixados, baseado na utilização do modelo numérico MOHID. O primeiro domínio é um modelo de maré barotrópico, englobando toda a costa da Península Ibérica. O segundo e o terceiro domínios são modelos baroclínicos tridimensionais, sendo o segundo uma representação grosseira das Rias Baixas e da costa adjacente, enquanto que o terceiro domínio inclui a mesma área com maior resolução. Neste âmbito, foi também implementado em modo 2D um modelo para o estuário do Minho, de forma a quantificar o fluxo (e as suas propriedades) que o estuário injeta no oceano.

Devido à disponibilidade de dados foi escolhido o período de maio de 1998 para a validação da implementação numérica desenvolvida, efetuando a simulação da propagação da pluma estuarina do Minho para este período. Note-se que durante esta época foi detetada uma descarga elevada do Rio Minho, bem como ventos favoráveis à dispersão da pluma em direção às Rias Baixas. Os resultados obtidos mostraram que a metodologia de modelos encaixados foi implementada com sucesso, uma vez que os modelos reproduzem com precisão aceitável os padrões hidrodinâmicos e termohalinos do estuário do Minho e das Rias Baixas. Também foi avaliada a importância da descarga do Rio Minho e do vento no evento de maio de 1998. Os resultados revelaram que uma descarga moderada e contínua combinada com ventos de sul é suficiente para inverter o padrão de circulação das Rias Baixas, reduzindo a importância da existência de eventos específicos de elevado caudal.

No âmbito do objetivo princial deste estudo, foram avaliadas as condições nas quais a pluma estuarina do Minho afeta a circulação e hidrografia das Rias Baixas. Os resultados numéricos indicaram que a dispersão da pluma estuarina do Minho responde rapidamente às variações do vento e às variações de batimetria e morfologia da linha de costa. Sem vento, a pluma expande-se para o largo, criando um bojo em frente da embocadura do rio. Sob condições de vento de norte, a pluma estende-se numa maior dimensão para o largo. Por outro lado, sob condições de vento de sul, a pluma fica confinada junto à costa, chegando às Rias Baixas ao fim de um dia e meio. No entanto, para descargas do Rio Minho superiores a 800 m^3 s^{-1}, a pluma estuarina do Minho inverte os padrões de circulação das Rias Baixas. Verificou-se também que a variabilidade do vento e da descarga do Rio Minho são os fatores que mais influenciam o tamanho e forma da pluma.

Sob as mesmas condições analisou-se a troca de água nas Rias Baixas seguindo a trajetória de partículas lançadas perto da embocadura do estuário do Minho. Para descargas do Rio Minho superiores a 2100 m^3 s^{-1} combinadas com ventos de sul de 6 m s^{-1} e numa escala superior a cinco dias, observou-se uma intensa troca de água entre as Rias. Cerca de 20% das partículas detetadas na Ria de Pontevedra provêm diretamente do Rio Minho.

Em suma, a aplicação do modelo desenvolvido neste trabalho contribuiu para o conhecimento da influência do Rio Minho na circulação e hidrografia das Rias Baixas, evidenciando que esta metodologia também pode ser replicada para outros sistemas costeiros.

Abstract

The Minho River, situated 30 km south of the Rias Baixas is the most important freshwater source flowing into the Western Galician Coast (NW of the Iberian Peninsula). This discharge is important to determine the hydrological patterns adjacent to its mouth, particularly close to the Galician coastal region. The buoyancy generated by the Minho plume can flood the Rias Baixas for long periods, reversing the normal estuarine density gradients. Thus, it becomes important to analyse its dynamics as well as the thermohaline patterns of the areas affected by the freshwater spreading.

Thus, the main aim of this work was to study the propagation of the Minho estuarine plume to the Rias Baixas, establishing the conditions in which this plume affects the circulation and hydrographic features of these coastal systems, through the development and application of the numerical model MOHID.

For this purpose, the hydrographic features of the Rias Baixas mouths were studied. It was observed that at the northern mouths, due to their shallowness, the heat fluxes between the atmosphere and ocean are the major forcing, influencing the water temperature, while at the southern mouths the influence of the upwelling events and the Minho River discharge were more frequent. The salinity increases from south to north, revealing that the observed low values may be caused by the Minho River freshwater discharge.

An assessment of wind data along the Galician coast was carried out, in order to evaluate the applicability of the study to the dispersal of the Minho estuarine plume. Firstly, a comparative analysis between winds obtained from land meteorological stations and offshore QuikSCAT satellite were performed. This comparison revealed that satellite data constitute a good approach to study wind induced coastal phenomena. However, since the numerical model MOHID requires wind data with high spatial and temporal resolution close to the coast, results of the forecasted model WRF were added to the previous study. The analyses revealed that the WRF model data is a consistent tool to obtain representative wind data near the coast, showing good results when comparing with *in situ* wind observations from oceanographic buoys.

To study the influence of the Minho buoyant discharge influence on the Rias Baixas, a set of three one-way nested models was developed and implemented, using the numerical

model MOHID. The first model domain is a barotropic model and includes the whole Iberian Peninsula coast. The second and third domains are baroclinic models, where the second domain is a coarse representation of the Rias Baixas and adjacent coastal area, while the third includes the same area with a higher resolution. A bi-dimensional model was also implemented in the Minho estuary, in order to quantify the flow (and its properties) that the estuary injects into the ocean.

The chosen period for the Minho estuarine plume propagation validation was the spring of 1998, since a high Minho River discharge was reported, as well as favourable wind patterns to advect the estuarine plume towards the Rias Baixas, and there was field data available to compare with the model predictions. The obtained results show that the adopted nesting methodology was successful implemented. Model predictions reproduce accurately the hydrodynamics and thermohaline patterns on the Minho estuary and Rias Baixas. The importance of the Minho river discharge and the wind forcing in the event of May 1998 was also studied. The model results showed that a continuous moderate Minho River discharge combined with southerly winds is enough to reverse the Rias Baixas circulation pattern, reducing the importance of the occurrence of specific events of high runoff values.

The conditions in which the estuarine plume Minho affects circulation and hydrography of the Rias Baixas were evaluated. The numerical results revealed that the Minho estuarine plume responds rapidly to wind variations and is also influenced by the bathymetry and morphology of the coastline. Without wind forcing, the plume expands offshore, creating a bulge in front of the river mouth. When the wind blows southwards, the main feature is the offshore extension of the plume. Otherwise, northward wind spreads the river plume towards the Rias Baixas. The plume is confined close to the coast, reaching the Rias Baixas after 1.5 days. However, for Minho River discharges higher than 800 m^3 s^{-1}, the Minho estuarine plume reverses the circulation patterns in the Rias Baixas. It was also observed that the wind stress and Minho River discharge are the most important factors influencing the size and shape of the Minho estuarine plume.

Under the same conditions, the water exchange between Rias Baixas was analysed following the trajectories particles released close to the Minho River mouth. Over 5 days, under Minho River discharges higher than 2100 m^3 s^{-1} combined with southerly winds of 6 m s^{-1}, an intense water exchange between Rias was observed. However, only 20% of the particles found in Ria de Pontevedra come directly from the Minho River.

In summary, the model application developed in this study contributed to the characterization and understanding of the influence of the Minho River on the Rias Baixas circulation and hydrography, highlighting that this methodology can be replicated to other coastal systems.

Publications and Communications in the context of this dissertation

Several publications in peer reviewed journals and presentations at international and national conferences were accomplished as result of the research developed in this thesis, and used as base for several chapters of this dissertation.

Papers in international scientific periodicals with referees:

- Sousa M.C., Alvarez I., Vaz N. and Dias J.M. (2011). Physical forcing of the hydrography of the Ria de Vigo mouth. *Journal of Coastal Research*, SI64, 1589-1593. (Chapter 2)

- Sousa M.C., Alvarez I., Vaz N. and Dias J.M. (2011). Evaluating QuikSCAT wind data to study wind induced coastal phenomena in the Galician Coast. *Journal of Coastal Research*, SI64, 445-449. (Chapter 3)

- Sousa M.C., Alvarez I., Vaz N., Gomez-Gesteira M. and Dias J.M. (2013). Assessment of wind patterns accuracy from the QuikSCAT satellite and the WRF model along the Galician coast (NW Iberian Peninsula). *Monthly Weather Review*, 141, 2, 742-753. (Chapter 3)

- Sousa M.C., Vaz N., Alvarez I. and Dias J.M. (2013). Effect of Minho estuarine plume on Rias Baixas: numerical modeling approach. *Journal of Coastal Research*, SI65, 2059-2064. (Chapter 5)

- Sousa M.C., Vaz N., Alvarez I., Gomez-Gesteira M. and Dias J.M. (in review). Modelling the Minho River plume intrusion into the Rias Baixas (NW Iberian Peninsula). *Continental Shelf Research*. (Chapter 5)

- Sousa M.C., Vaz N., Alvarez I., Gomez-Gesteira M. and Dias J.M. (in review). Influence of the Minho River plume on the Rias Baixas (NW Iberian Peninsula). *Journal of Marine Systems*. (Chapter 6)

Other publications:

- Sousa M.C., Alvarez I., Vaz N., Gomez-Gesteira M., Dias J.M. (2012). Análisis de la precisión de los datos de viento obtenidos del satélite QuikSCAT y el modelo WRF en la costa gallega. *Revista Avances en Ciencias de la Tierra (ACT)*, 3, 39-53.

Conference abstracts, proceedings and communications:

- Sousa M.C., Alvarez I., Vaz N., Dias J.M. (2010). Wind Analysis in the Western Galician Coast. *IV Congresso Brasileiro de Oceanografia*. 17-21 May, Rio Grande, Brazil.

- Sousa M.C., Alvarez I., Vaz N., Dias J.M. (2011). Physical forcing of the hydrography of the Ria de Vigo mouth. *11th International Coastal Symposium 2011 (ICS 2011)*. 9-14 May, Szczecin, Poland.

- Sousa M.C., Alvarez I., Vaz N., Dias J.M. (2011). Evaluating QuikSCAT wind data to study wind induced coastal phenomena in the Galician Coast. *11th International Coastal Symposium 2011 (ICS 2011)*. 9-14 May, Szczecin, Poland.

- Sousa M.C., Vaz N., Alvarez I., Dias J.M. (2012). Wind forcing response of the dispersal of Minho estuarine plume. *European Geosciences Union, General assembly 2012*. 22-27 April 2012, Vienna, Austria.

- Sousa M.C., Vaz N., Alvarez I., Dias J.M. (2012). Dispersão da Pluma Estuarina do Minho: Resposta ao Forçamento do Vento. *Encontro de Oceanografia Física*. 15-16 June, Quiaios, Portugal.

- Vaz N., Sousa M.C., Mendes R., Picado A., Plecha S., Dias J.M. (2012). Estudo do Impacto das Plumas Estuarinas na Costa Oeste de Portugal Continental: Uso de Malhas Tridimensionais Encaixadas. *V Congresso Brasileiro de Oceanografia*. 13-16 November, Rio de Janeiro, Brazil.

- Sousa M.C., Vaz N., Alvarez I., Picado A., Dias J.M. (2012). Modelação da Pluma Estuarina do Rio Minho: Influência do Caudal e do Vento. *V Congresso Brasileiro de Oceanografia*. 13-16 November, Rio de Janeiro, Brazil.

- Sousa M.C., Vaz N., Alvarez I., Dias J.M. (2013). Effect of Minho estuarine plume on Rias Baixas: Numerical modeling approach. *12th International Coastal Symposium (ICS 2013)*. 8-12 April, Plymouth University, Plymouth, UK.

- Plecha, S., Sousa M.C., Mendes R., Vaz N., Alvarez I., Dias J.M. (2013). Dynamics of Estuarine Plumes Along the NW Portuguese Coast. *Research Day*. 19 June, Aveiro University, Aveiro, Portugal.

Contents

List of Figures

List of Tables

Chapter 1

Introduction

1.1 Motivation

Freshwater inputs from rivers have great influence on coastal waters, changing the distribution of various parameters, such as particles, dissolved matter, pollutants, nutrients, biogeochemical and phytoplankton communities [Dortch and Whitledge, 1992; Kortzinger, 2003; Warrick and Milliman, 2003; Bruland et al., 2008; Reifel et al., 2009].

Generally, river plumes are turbid and rich in nutrients, remaining near surface due to their buoyancy and breaking up into lenses of less saline water, stimulating phytoplankton growth [Lunven et al., 2005]. Some studies suggest that the areas corresponding to river plumes are preferred feeding places for zooplankton [Pearcy, 1992]. The plume dynamics is controlled by the interaction of outflow inertia [Horner-Devine et al., 2009], buoyancy forcing [Jurisa and Chant, 2012], Earth's rotation effect [Monteiro et al., 2011], wind forcing [Choi and Wilkin, 2007] and alongshore coastal current [Fong and Geyer, 2002]. All these factors contribute to change the dynamics of river and estuarine plumes. Different plume classifications have been carried out. Several authors established relationships relating the extension, velocity of the discharged freshwater and the depth of the river at the mouth [Garvine, 1995; Yankovsky and Chapman, 1997; Lentz and Largier, 2006].

Due to their large spatial and temporal dynamics and considering the importance of the driving factors, the development and exploitation of ocean circulation models has become an important tool to study the evolution of estuarine plumes. From their application, individual effects of the driving factors (e.g. river discharge, tide or wind direction) on a buoyant plume may be evaluated under different conditions. Several numerical studies related to coastal plumes characterization have been performed worldwide [Fong and Geyer, 2002; García-Berdeal et al., 2002; Choi and Wilkin, 2007; Guo and Valle-Levinson, 2007; Otero and Ruiz-Villarreal, 2008; Horner-Devine et al., 2009; Jurisa and Chant, 2012], indicating the

utility of a numerical model to analyse their dynamics as well as the thermohaline patterns of the areas affected by its propagation. These studies have shown that downwelling favourable wind compresses the plume towards the coast and the vertical mixing reduces the stratification in the plume, where velocities are stronger. On the other hand, during upwelling favourable winds, the main feature is the offshore extension of the plume, increasing the vertical stratification in the area under its influence [Otero and Ruiz-Villarreal, 2008]. Moreover, the tidal effect contributes to increase the mixing processes, reducing the stratification.

In general, the magnitude of the impact of river plumes on coastal regions is proportional to the amount of river discharge [Tian et al., 1993; Dagg et al., 2004]. Extreme events of river discharges associated to torrential rain episodes and favourable wind patterns can flood the major coastal estuaries located north of the river for long periods, reversing the normal estuarine density and salinity gradients.

The Rias Baixas (Figure 1.1) are located in the northern limit of the NW Africa upwelling system [Wooster et al., 1976] and are ecosystems of enormous potential, both economical (e.g. exploration of marine resources: fisheries, aquaculture and fishing industry) and social (e.g. tourism: beaches and natural beauty), leading to a wide population establishment in this area. Thus, the quality of its inhabitant's life depends on the conservation of the natural ecosystems and mitigation of the negative impacts of anthropogenic activities. They are also situated along one of the most important maritime routes and numerous merchant ships navigate through its waters and even close to the coast. The frequent storms which affect the coast during winter time can provoke accidents with important consequences as oil spills. These spills may seriously affect the local economy, which depends on the richness of marine ecosystems (bivalves, octopus, sardine, sole and barnacle). The seasonal coastal upwelling induced by favourable winds in spring-summer months is the main recognized source of primary production, supporting the high fishery and aquaculture yields. Nowadays, the number of suspended rafts in the Rias Baixas is 3237, with an estimated annual mussel production per raft of 75×10^3 kg raft^{-1} y^{-1} (around 15% of the world production), rendering a total estimated production of 243×10^6 kg y^{-1} of edible mussels, representing enough biomass to have clear impact on the Rias as an entire ecosystem [Alonso-Perez et al., 2010].

The primary production generated by the upwelling events can also be affected by the estuarine discharge that flow in the interior of the Rias and continental shelf. The freshwater discharge from the rivers is particularly important in near coastal regions. The Rias Baixas have numerous rivers flowing inside, modifying their thermohaline properties. The Minho River, situated south of the Rias Baixas (Figure 1.1), is the most important river that flows into the Western Galician coast. The Minho estuarine plume intrusion can generate an important salinity decrease at the Rias Baixas mouths, reversing the normal circulation pattern and affecting the primary production distribution [deCastro et al., 2006a]. This

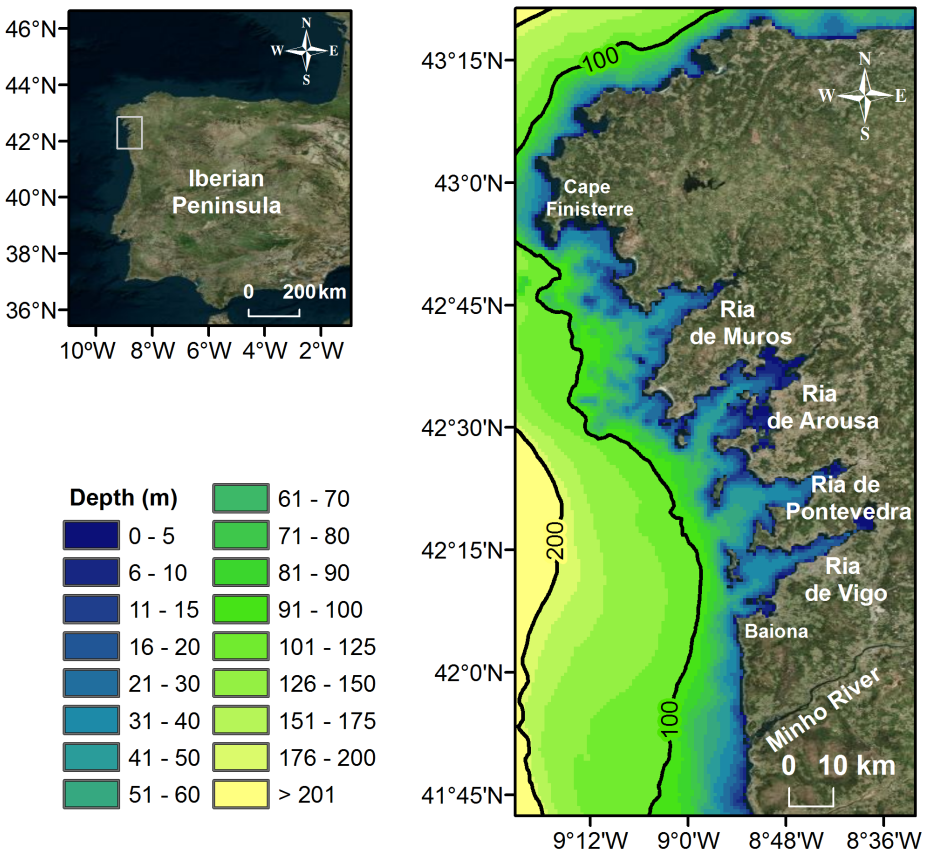

Figure 1.1: Location and bathymetry of study area.

reverse circulation pattern is characterized by the intrusion of warm and less saline coastal waters at the surface, which accumulates in the Rias interior and finally flows towards the ocean through the bottom. The Minho freshwater intrusion can rise both positive and negative effects. It can generate an inverse estuarine circulation, which tends to stop water exchange between the Rias and the shelf, increasing residence time and hence affecting water quality. Conversely, extreme freshwater pulses can induce phytoplankton blooms at the shelf, which penetrates into the Rias embedded in a water fresher than the estuarine one, fertilizing the area. Consequently, knowledge of freshwater effects in these areas greatly facilitates the management of many exploited and protected species. Due to the lack of continuous and simultaneous *in situ* measurements along coastal estuaries as the Rias Baixas, it is important to develop numerical models to understand the complex structure of the oceanographic features and circulation patterns that characterize these particular environments.

The numerical models are used worldwide, in order to quantify and understand different process occurring in coastal waters. They have the ability to answer questions and investigate hypothetical scenarios (e.g. changes in wind and river discharge), which observations alone cannot provide. In addition, they afford the capability to study processes

independently. The Minho estuarine plume influence inside the western Galician estuaries has not been studied in detail, namely by means of numerical model applications, specifically designed for this purpose. Therefore, this study aims the implementation of a high resolution circulation and transport model, in order to study the influence of the Minho buoyant discharge influence upon Rias Baixas.

1.2 Aims

The main goal of this work is to study the evolution of the Minho estuarine plume and its effect on the circulation and hydrography of the Rias Baixas, as well as the dependence of the estuarine plume impact on these coastal systems in terms of its major forcing mechanisms. In particular, this work aims to:

- compare surface winds from weather forecast model, satellite and *in situ* measurements along the Galician coast, in order to evaluate its applicability to study wind induced coastal phenomena;

- characterize the hydrography and dynamics of the NW Iberian Peninsula, with special emphasis to the Rias Baixas adjacent area;

- develop a high resolution numerical model application to reproduce the propagation of the Minho estuarine plume towards the Rias Baixas;

- study specific events of the Minho estuarine plume intrusion inside the Rias Baixas;

- analyse the dynamics of the Minho estuarine plume in terms of the major forcing (tides, river discharge and wind conditions);

- investigate the necessary conditions for the establishment of the reverse circulation in the Rias Baixas;

- assess the water renovation and mixture between Rias Baixas through the analysis of the trajectories of passive particles released at the Minho River mouth;

The approach used to achieve the specific aims listed above involves the implementation of a three-dimensional baroclinic model and *in situ* and remote sensing data analysis, allowing to research the evolution of the Minho estuarine plume along the NW Iberian Peninsula, and especially its influence in the Rias Baixas dynamics.

1.3 Literature review

1.3.1 Estuarine plumes

Rivers often discharge in the coastal zone in the form of plumes and are essential for the exportation of fine sediments, nutrients and organic material from land to the coastal ocean. They can directly influence coastal sediment budgets, ocean biogeochemistry and circulation in coastal waters [Garvine, 1984; Kourafalou, 1999]. The estuarine plume structure may take a variety of shapes, depending on the complex interactions with the ambient flow, tides, bottom topography, freshwater volume discharged, the shape of the river mouth and wind stress [Garvine, 1974; Yankovsky and Chapman, 1997; Fong and Geyer, 2002; García-Berdeal et al., 2002].

Since the 1950s, various studies including observational, laboratory and numerical model studies have been adopted to understand the dynamics and structures of estuarine plumes. The first steady state theory of a river plume entering the sea off a straight coast were presented by Takano [1954a,b, 1955]. From 1960s to 1980s, observational studies of several plume dynamics had been made around the world: for example the Columbia River estuary (USA) [Stefansson and Richards, 1963; Park, 1966], Connecticut Estuary (USA)[Garvine, 1974], Fraser River (Canada) [Royer and Emery, 1982], Rhine River estuary (Netherlands) [van Alphen et al., 1988] and the Rhone River estuary (France) [Szekielda and Kupferman, 1973].

Chao [1988a,b] and Chao and Boicourt [1986] were the first authors to apply an ocean model with idealized topography, to examine the effect of wind and river discharge on buoyant plumes. Latter, Garvine [1995] introduced a classification scheme for unforced plumes to assess the contribution of advection terms and the Coriolis force to the buoyant plume. A different classification scheme was suggested by Yankovsky and Chapman [1997], using the plume's vertical structure and discriminating between bottom and surface advected plumes. In spite of the absence of external forcing mechanisms in their theory, they correctly predicted the plume type for several numerical and real cases. In the mid-1990s and in the early 2000s, the dependence of three-dimensional plume characteristics on model parameters were investigated by Garvine [1999, 2001], Kourafalou et al. [1996] and Kourafalou [1999]. To study the impact of upwelling winds to the surface advected plume, a conceptual model was developed by Fong and Geyer [2001]. Their model simulations demonstrated that the plume thins and is advected offshore by the cross-shore Ekman transport. García-Berdeal et al. [2002] and Choi and Wilkin [2007] also used numerical simulations to study the influence of wind stress and ambient flow in a high discharge river plume. These studies showed that the wind speed and direction play an important role in determining plume structure and the fate of freshwater, as demonstrated by Hetland

[2005]. That is, downwelling favourable wind compresses the plume towards the coast, increasing the mixing process and inducing the coastal current formation, while upwelling favourable wind induces an offshore advection on the surface Ekman layer. The results also showed that the river runoff is one of the most important environmental factors leading to the seaward expansion of the plume.

A modulation effect was attributed to the tidal action, which contributes to mixing processes, reducing stratification generated by the wind and spreading the freshwater over the shelf [Chao, 1990; Garvine, 1999; Guo and Valle-Levinson, 2007; Marques et al., 2009]. This was further confirmed with laboratory experiments by Horner-Devine et al. [2006, 2009]. Therefore, it is of great significance to have a comprehensive understanding of the plume shaping in relationship with the river discharge, wind and ambient current.

1.3.2 Western Galician coast

1.3.2.1 Hydrodynamical and hydrographical patterns

During the last few years the Western Galician coast has been extensively studied taking into account its hydrodynamical and hydrographical patterns. This area has an important hydrologic and biogeochemical activity, mainly attributable to coastal upwelling processes which occur from April to October [McClain et al., 1986; Tilstone et al., 1994]. This upwelling is commonly attributed to the action of northerly winds along the shelf which produce an offshore Ekman transport, displacing surface water seaward.

The Rias Baixas have been extensively studied by means of *in situ* measurements and by numerical models. Prego and Fraga [1992] analysed scattered measurements at the Ria de Vigo from February to October 1986, by means of stationary box model. It was observed that the Ria de Vigo behaves as a partially mixed estuary with residual positive circulation. An interannual study to describe thermohaline and biogechemical properties of the Ria de Vigo from May 1994 to September 1995 was carried out by Doval et al. [1998], showing the Ria also behaves like an extension of the shelf during the upwelling season and like a partially mixed estuary during the downwelling season. More recently, Alvarez et al. [2013] analysed the response of thermohaline properties to the occurrence of upwelling events at the Ria de Vigo from October 2003 to September 2004. Eastern North Atlantic Central Water (ENACW) was observed during spring-summer (summer) at the southern (northern) mouth of Ria de Vigo.

deCastro et al. [2000] performed hydrodynamical and thermohaline measurements at the Ria de Pontevedra from February to July 1998, through nine stations spreaded along the Ria, and an anchored station located in the inner-middle part of the Ria. These measurements were used to identify the current patterns. It was observed that the wind

direction is strongly dependent on topography and that wind velocity higher than 4 m s^{-1} dominate the current at surface layers, even against tidal effect. Prego et al. [2001] assessed the physical-hydrodynamical characteristics of the Ria de Pontevedra, studying its hydrography and spring upwelling events during a year. Four distinct water bodies penetrating inside the Ria during the course of a year were observed: (1) autumnal shelf water, (2) seawater showing characteristics of the poleward current in winter, (3) subsurface shelf water in May to September when the upwelling relaxes and (4) the ENACW in summer. In the same period, an unusual two-layered tidal circulation pattern in this Ria was also studied in terms of thermohaline stratification and wind forcing by Gomez-Gesteira et al. [2001]. This unusual positive tidal circulation showed dependency on the particular summer stratification conditions and on the presence of easterly winds inside the estuary. The stratification was generated by solar heating and favourable upwelling conditions on the adjacent shelf, which reinforced the estuarine positive circulation and originates near bed inflow of ENACW. The unusual winter upwelling event observed in the Ria de Pontevedra, during a cruise carried out on the 27 January 1998, corresponds to the water mass transported by the poleward current, which is saltier and warmer, though less dense water than the ENACW observed in spring and summer [Alvarez et al., 2003]. deCastro et al. [2004] studied the along estuary negative circulation in the Ria de Pontevedra, revealing a two-layered circulation pattern generated by the existence of two different water masses at intermediate depths. This pattern was due to a sudden transition between upwelling and downwelling combined with a fast decrease of river discharge. This negative estuarine circulation was also described in Ria de Arousa [Alvarez-Salgado et al., 1996a,b], which is 30 km North of Ria de Pontevedra. Moreover, deCastro et al. [2006b] analysed the seasonal evolution of the spatial thermohaline asymmetry. This asymmetry varies throughout the year depending on two external parameters: the river discharge and the seawater inflow (characterized by upwelling index).

The Rias de Vigo, Pontevedra and Arousa were studied in simultaneous by Alvarez et al. [2005a], through the analysis of inter and intra-annual evolution of water temperature and salinity (between October 1997 and October 2002) in the boundary between the Rias and the adjacent ocean. All Rias were observed to share some common features: thermal inversion from November to February, intense upwelling events from April to September. The Rias de Vigo and Pontevedra behave in a similar way, even quantitatively, and they differ slightly from the Ria de Arousa. This difference is especially important at the northern mouth of Arousa, where water is fresher in winter and upwelling events are less frequent during the summer. The water exchange between the Ria de Pontevedra and the shelf, under tidal effects, wind and freshwater input was studied during the past few years, while in the other Rias fewer studies were performed on this subject.

The first studies carried out off the Rias Baixas were performed by Wooster et al. [1976]. They analysed the seasonal upwelling cycle along the eastern boundary of the

North Atlantic from 1850 to 1970. It was found that this system is the northernmost limit of the Eastern North Atlantic upwelling system, which extends from 10° N to about 44° N. Fraga [1981] was also among the first to describe the upwelling off Galician coast, using scattered measurements obtained from 1974 to 1977. Tenore et al. [1982] studied the benthic distribution on the continental shelf in order to describe the coastal upwelling offshore. McClain et al. [1986] analysed the wind driven upwelling using a grid of stations covering the continental shelf from Cape Finisterre to Vigo during April 1982. They observed a salinity increase and a water temperature decrease during the upwelling season. Alvarez-Salgado et al. [1993] studied the hydrographic variability off the Rias Baixas during the upwelling season (May-October 1989) by means of samples taken at a station located on the shelf, about 9 km from the mouth of the Ria de Pontevedra. They observed that the upwelling events occur with biweekly periodicity, bringing Eastern North Atlantic Water (ENAW) to the subsurface layer at the station. The observations show that the thermohaline properties of the upwelled water tend to increase over time. Perez et al. [1995] studied the correlation between inter-annual variations in wind stress and changes in ENACW by means of the combination of data obtained from the eastern North Atlantic region from 1974 to 1992 and data obtained near the Iberian coast (around 42° N, 10° W) in 1991 and 1993. Fiuza et al. [1998] analysed water masses and their circulation in the eastern North Atlantic region based on CTD measurements in May 1993. They concluded that this episodically circulation is enhanced, especially from April to October, by coastal upwelling events induced by northerly shelf winds, during which cold and nutrient-laden ENACW ascends to the shelf and eventually enters the Rias. Torres et al. [2003] used sea surface temperature (SST) to describe the Galician upwelling region from July 1999 to May 2001, although they covered a larger area and their study was mainly focused on wind patterns. They verified that the wind measured at Finisterre itself, is not always representative of the overall wind field.

Alvarez et al. [2005b] also studied the variation in upwelling intensity along the northwest Iberian Peninsula. They observed that the intensity of coastal upwelling is strongly dependent on the wind pattern. The maximum amplitudes of wind stress were observed at the western coast (0.30 N m^{-2}) with southward direction and these are shown to be related to low water temperature (12 ℃) and high salinity (35.8) in the estuary mouth. In order to describe the Ekman transport patterns in the area close to the Galician coast, Cabanas and Alvarez [2005] analysed a 40-year time series of daily and monthly Ekman transport. The Ekman transport shows different seasonal patterns: the summer pattern is characterized by seaward transport (upwelling favourable), while the winter pattern is characterized by landward transport (downwelling favourable).

Alvarez et al. [2008a] described the wind forcing over the area extending from 36° N to 44° N by means of two different but complementary databases: QuikSCAT satellite database was used for the period between 2000-2006 with high spatial resolution (0.25°×

0.25°) and Pacific Fisheries Environmental Laboratory (PFEL) database provided longer records (from 1967-2006) with a coarser spatial resolution (1°$\times$ 1°). They found that the upwelling events occur along the full western coast of the Iberian Peninsula, although these are definitively more complex on particular coastal features, due to the interaction between the macroscopic wind regime and coastal orography. More recently, Santos et al. [2012] studied the differences in the variability of water temperature along the western Iberian Peninsula. The difference between coastal and ocean values was related to the generation of coastal upwelling, which partially inhibits the warming from surface of coastal waters.

1.3.2.2 Minho River

The Minho River, situated south of Rias Baixas, is the most important river flowing into the Western Galician coast. The discharge of freshwater is particularly important in near coastal regions. Freshwater can flood the major coastal estuaries located north of the river for prolonged periods, reversing the normal estuarine density and salinity gradients [Fiedler and Laurs, 1990]. Because the freshwater intrusion can occur in these estuaries, its presence or absence can provide an important environmental distinction between estuaries as well as between near coastal regions. This river is also one of the most important contributing to the formation of an extensive buoyant plume known as the Western Iberian Buoyant Plume (WIBP)[Peliz et al., 2002; Otero et al., 2008, 2013].

The influence of the Minho estuarine plume along the western Galician coast has never been studied in detail. There are previous works which have been carried out analysing changes in thermohaline variables: Mourino and Fraga [1982] analysed variations in water temperature, salinity, nitrate, nitrite and silicate at the southern mouth of the Ria de Vigo from October 1976 to December 1977. They found an important salinity decrease in the estuary mouth from December to March that they attributed to the Minho River freshwater. More recently, the effect of the Minho River intrusion in the hydrographic behaviour of the Rias Baixas was assessed by Alvarez et al. [2006] using thermohaline observations. This study was carried out in the spring of 1998 under high Minho River discharge and favourable wind patterns, which spread the estuarine plume northward from the river mouth. The generated buoyancy reverses the normal salinity gradient in the Rias of Vigo and Pontevedra, but not in Ria de Arousa. deCastro et al. [2006a] also observed an intrusion of low salinity water coming from the Minho River for the same period, which can be related to the high discharge from the dams that control the Minho River discharge. This release resulted in a strong cross-axis salinity gradient, in which salinity decreases seawards, giving rise to a two-layered circulation pattern and a high concentration of the phytoplankton *Skeletonema costatum*.

1.3.2.3 Numerical modelling

Several developments and applications of numerical models have been made in the last decades to investigate the interaction between the Rias Baixas and their adjacent coastal waters.

Pascual [1987a,b] studied the circulation produced by tides and wind in the Ria de Arousa with a 2D finite difference model. Bermudez et al. [1997, 1996] studied the circulation inside the Ria de Vigo driven by tides using also a 2D model but based on finite elements. Some studies have been done to quantify the long term processes and the seasonal variations inside the Rias, by means of a box model [Prego and Fraga, 1992; Nogueira et al., 1997b] or using data from a fixed station [Nogueira et al., 1997a]. The results were used to describe the dynamics of the system, the seasonal patterns and the long term trends. On the other hand, some authors [Montero et al., 1992, 1997] used lagrangian models coupled with 2D eulerian models to carry out dispersion studies in Galician Rias. Taboada et al. [1998] developed a 3D baroclinic model to study the seasonal variations of the Ria de Vigo residual circulation. This circulation model was compared to and found to be in reasonable agreement with the box model [Prego and Fraga, 1992]. The results showed that the Ria de Vigo has a two-layered circulation, where most of water enters the estuary through the southern mouth and leaves it through the northern one. Gomez-Gesteira et al. [1999] used the model of Taboada et al. [1998] in a 2D mode to track the dispersion of passive pollutants in the Ria de Vigo, concluding that the Ria de Vigo has a small residence time. Some modelling efforts have evaluated residual fluxes in Ria de Vigo and indicate a two-layered pattern [Montero et al., 1999; Torres-López et al., 2001; Souto et al., 2003].

Only few studies have dealt with the hydrodynamics modelling of the Ria de Pontevedra. Ruiz-Villarreal et al. [2002] applied a numerical model to understand the hydrodynamics and its influence on nutrients cycles and on the productivity in the Ria. This Ria was found to be a partially mixed estuary with a double-layered residual pattern, with water flowing seaward at the surface layers and upstream at the bottom layers. The combination of these characteristics has an important effect in biogeochemical cycles and productivity in the estuary. Gomez-Gesteira et al. [2003] used numerical modelling to relate the residence time estimated by a stationary box model to the upwelling index and river discharge considering biweekly surveys in the Ria de Pontevedra. The calculated residence time varies from around 3 days at upstream region to around 8 days near the mouth and it depends simultaneously on the river discharge and seawater inflow. More recently, Gilcoto et al. [2007] developed a 3D kinematic box model based on tracer and volume balances. However, through the analysis of the model results the existence of a bidirectional flow originated by a barotropic interaction with the shelf upwelling was found.

Recently, Otero et al. [2008, 2013] also used a numerical model for study the variability of the Western Iberian Buoyant Plume in response to wind events in the adjacent shelf of

Rias Baixas, identifying three characteristic situations: a) confinement of the plume to the coast during downwelling-southerly-winds, b) expansion of the plume during the declining phase of the downwelling event by relaxation of the wind and c) expansion of the plume by upwelling-northerly-winds.

All these studies provide insight on the dynamics of the adjacent coast of the Rias Baixas. In this work, in order to give a step forward, a high resolution numerical model was implemented for this region. This was performed to study the propagation of the Minho estuarine plume to the Rias Baixas, establishing the conditions in which this plume affects the circulation and hydrographic features of the Rias Baixas.

1.4 Structure of this work

This dissertation is divided in 7 chapters. Chapter 1 presents the Introduction, where the motivations, general objectives, a general literature review and the structure of the work are described. This is followed by Chapter 2, where a review of the hydrography and dynamics characterization of the NW of the Iberian Peninsula, with special attention to the Rias Baixas adjacent area is performed. In Chapter 2, the hydrography of the Ria de Vigo, Ria de Pontevedra and Ria de Arousa mouth is studied in terms of its major mechanisms and identifying their influence on the establishment of the observed patterns. In Chapter 3 an assessment of wind patterns accuracy from the QuikSCAT satellite, WRF model and *in situ* wind along the Galician coast is carried out, allowing to evaluate its applicability to study wind induced coastal phenomena. Chapter 4 presents the general overview of MOHID numerical model as well as the setup of the coastal and estuarine models. The model ability to reproduce the Minho estuarine plume, as well as the study of the propagation and influence of Minho estuarine plume on Rias Baixas circulation and hydrography can be found in Chapters 5 and 6. Finally, in Chapter 7, the conclusions of the dissertation are drawn and suggestions for further work are presented.

Chapter 2

Characterization of the Minho River, Rias Baixas and adjacent coastal zone

2.1 Introduction

Circulation and exchange processes in estuaries are forced by waves, tides, freshwater inflow, wind stress and exchanges with the atmosphere. These processes determine the patterns found for the salinity and water temperature inside estuaries, which are perhaps the most important physical factors confronting an organism here.

The northwest of the Iberian Peninsula is characterized by the presence of four estuaries located south of Cape Finisterre locally named as Rias Baixas (Figure 2.1), which are similar from a morphological point of view and sharing several common features [Alvarez et al., 2005a]. They are located in the northernmost limit of the Eastern North Upwelling System, which extends from 10°N to about 44°N [Wooster et al., 1976], and therefore in an area where the along-shore winds interact with the coastal topography to generate upwelling-downwelling dynamics on the continental shelf. The seasonal coastal upwelling induced by favorable winds in spring-summer months is the main recognized source of primary production related to the presence of ENACW near coast and inside these estuaries [Rios et al., 1992b; Perez et al., 1995; Fiuza et al., 1998]. Although this coastal upwelling is basically a spring-summer process linked to northeast winds, several autumn-winter upwelling events have been characterized along the Galician coast [Alvarez et al., 2003; deCastro et al., 2006c; Prego et al., 2007; deCastro et al., 2008; Varela et al., 2008, 2010; Alvarez et al., 2009], indicating that the upwelling process along the Galician coast cannot be considered a limited phenomenon to the spring-summer seasons and that

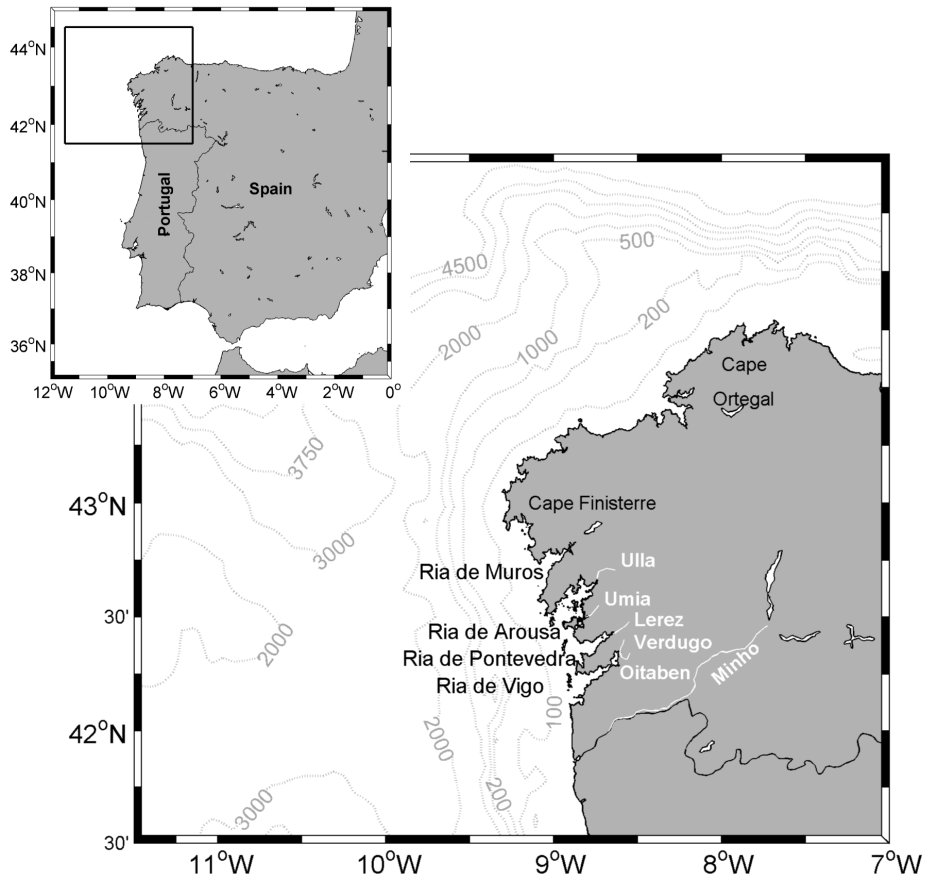

Figure 2.1: Map of the Western Galician Coast.

should be observed under favourable conditions independently of the season. Due to the proximity with the Minho River, the Rias Baixas considered in this thesis are from south to north: the Ria de Vigo, the Ria de Pontevedra and the Ria de Arousa.

In this chapter, a review of the hydrography and dynamics characterization of the NW of the Iberian Peninsula, with special attention to the Rias Baixas adjacent area is carried out, based on published papers and data collected from surveys. It is intended, therefore to understand and evaluate the importance of the physical processes in the study area. Thus, this chapter is structured as follows. First, general atmospheric, topographic and hydrographic features of the Minho River and Rias Baixas are briefly presented. This is followed by an overview of the additional aspects to the water masses and circulation patterns in the Rias Baixas adjacent area. Next, the hydrography of the Ria de Vigo, Ria de Pontevedra and Ria de Arousa mouth is studied, in terms of its major mechanisms, identifying their influence on the establishment of the observed patterns. Finally, the main conclusions from the work are discussed.

2.2 General description

The Rias Baixas between 42°N and 43°N are characterized by a fairly topography and a jagged SSE-NNW coastline. They are V shaped widening progressively from the innermost part of the estuary toward the mouth, with volume comprised between 3.0 and 4.3 km^3. They are connected to the open sea by means of two entrances due to the existence of islands in the outermost part. Freshwater contributions come from four small rivers: the Verdugo-Oitabén River at the Ria de Vigo head, the Lérez River at the Ria de Pontevedra and the Umia e Ulla Rivers at the Ria de Arousa (Figure 2.1). The Table 2.1 shows the main fundamental dimensions of Rias Baixas.

The Ria de Vigo supports the highest population among the Rias. The Ria de Arousa is the one with higher surface, while the Ria de Pontevedra is the second largest estuary of the Rias Baixas in terms of water volume content. The volume of freshwater flowing into the Rias is higher in Ria de Arousa, because two main rivers discharge into this estuary. It is the shallowest of the Rias.

The Rias Baixas are characterized by an oceanic climate, which tends to aridity in summer. The climate of the area can be related to the seasonal evolution of two major atmospheric systems the Azores High and the Iceland Low [Wooster et al., 1976; Fiuza et al., 1982; Vitorino et al., 2002]. Typically, during the summer months, when the Azores high-pressure cell is located over the central North Atlantic, the associated trade wind blows southward along the coast of Iberia inducing upwelling and associated southward currents. The summer wave regime is characterized by low energy wave conditions, with significant wave heights of 2 m and period of about 8-9 s [Vitorino et al., 2002; Dodet et al., 2010]. During the winter, the Azores High is usually located farther south of the North West Africa and the Iceland low pressure is deeper and located in southeastern Greenland. Thus, the pressure gradient between the two systems results in an onshore and slightly northward wind along the west coast of the Iberian Peninsula. During the winter months, the significant wave heights are of the order of about 3-4 m, with a period of 11 and 13 s [Dodet et al., 2010].

Table 2.1: Rias Baixas dimensions.

	Ria de Vigo	Ria de Pontevedra	Ria de Arousa
Location	42°06' - 42°21'N 8°36' - 8°54'W	42°15' - 42°25'N 8°39' - 8°56'W	42°27' - 42°41'N 8°44' - 9°01'W
Surface (km^2)	156	141	239
Volume (km^3)	3.12	3.47	4.34
Mean width (km)	4.80	3.80	9.00
Mean depth (m)	21	31	19
Main axis length (km)	32.50	22.00	33.00
Mouth width (km)	southern: 5.10 northern: 2.80	southern: 7.30 northern: 3.60	southern: 4.60 northern: 3.70
Mouth depth (m)	southern: 45 northern: 25	southern: 60 northern: 15	southern: 55 northern: 5

2.2.1 Rias Baixas

2.2.1.1 Ria de Vigo

Around 30 km northwards of the Minho River mouth is located the Ria de Vigo (Figure 2.2), which is the most meridional of the Rias Baixas. It is located near the border between Portugal and Spain, between 42° 06'N and 42° 21'N, and 8° 36'W and 8° 54'W.

The Ria de Vigo is 32.5 km long, presenting an NE-SW direction, with 1 km width in its inner part (NE) and 10 km at the mouth of the Ria (SW). The mean width and depth are 4.8 km and 21 m, respectively. The connection of the Ria with the shelf is separated by the Cíes Islands, forming two distinct estuary mouths. The northern mouth is 2.8 km wide and has a maximum depth of 25 m and the southern mouth is 5.1 km wide and 45 m depth.

It can be divided into three zones according to the degree of continental or oceanic influence. The innermost zone includes San Simón bay and shows the characteristics of a typical estuary, due to the effects of tides ($\sim$ 3 m of averaged tidal range) and to the influence of the Verdugo-Oitabén River [Perez et al., 1992]. This River is the main tributary of freshwater into Ria de Vigo with a catchment area of 333 km^2. The Verdugo-Oitabén River has a annual mean discharge of 13 m^3 s^{-1}, with a greatest seasonal variability, with values ranging from 120 m^3 s^{-1} in winter to values of 1 m^3 s^{-1} in summer [Rios et al., 1992a]. The middle zone, which spreads from the Rande Strait to Mar Cape, is under the influence of both continental and oceanic contributions. Finally, the outer zone, which is under dominant oceanic influence, includes the area lying between Mar Cape and the Cíes islands, providing a natural protection from Atlantic swell. The almost north-south orientation of these islands leaves two relatively narrow corridors at the north and south entrances of the Ria.

The tidal forcing is mainly semidiurnal with a Form Number significantly lower than 0.25 [Varela et al., 2005]. The tidal range varies between 2 and 4 m, so this Ria is a

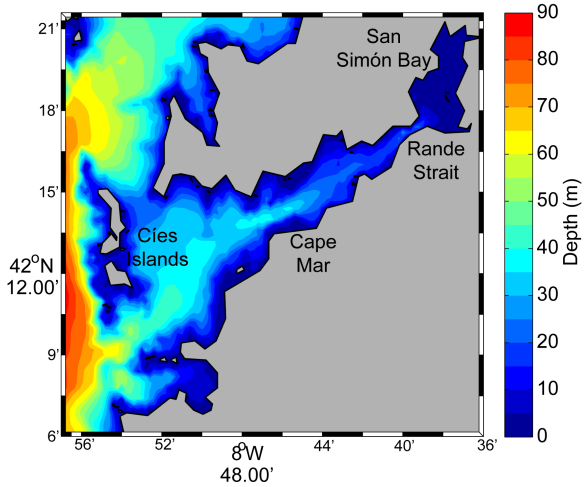

Figure 2.2: Map of the Ria de Vigo.

mesotidal estuary [Fraga and Margalef, 1979]. The Ria de Vigo behaves as partially mixed estuary, with positive residual circulation and a two layer circulation pattern, with surface water outflow and inflow on the bottom [Fraga and Margalef, 1979; Prego and Fraga, 1992].

2.2.1.2 Ria de Pontevedra

The Ria de Pontevedra is located between 42°15'N and 42°25'N, and 8°39'W and 8°56'W. It is connected to the ocean by means of two mouths (Figure 2.3). The northern mouth is narrow (3.6 km) and shallow (15 m), while the southern mouth is wide (7.3 km) and has a depth of 60 m. The southern mouth provides the main channel for water exchange and the Ons and Onza islands behave as protective barriers against the swell from the open sea.

It is the second largest estuary of the Rias Baixas in terms of water volume content (3.47 km^3) and has a mean depth of 31 m and a surface of 141 km^2 This Ria is oriented in the SW-NE direction, with the Lérez River being in the innermost part of the Ria and the Onza and Ons islands in the outermost part of the estuary. This river is the main freshwater runoff that flows into the estuary. This river has a catchment area of 450 km^2 and an annual mean discharge of 27.5 m^3 s^{-1}. The monthly mean discharge oscillates between 2 and 80 m^3 s^{-1} and follows a similar pattern to the rainfall, as its runoff is not controlled by dams. In this way, the level of the discharge is high from December to March, with a maximum discharge in February and a low discharge from July to September and a minimum in September. The Ria may be considered as an extension of the river Lérez valley where there is tidal influence [Ruiz-Villarreal et al., 2002].

The Ria de Pontevedra is an estuarine-like system that has a semi-diurnal and mesotidal regime, which is characterized by a two-layered residual circulation pattern [Prego et al., 2001]. Typical spring vertical profiles of density show a pycnocline at depths that are close to -10 m with density anomaly values around 27 kg m^3 near the riverbed and lower density values near the surface due to the Lerez River influence. The surface density values

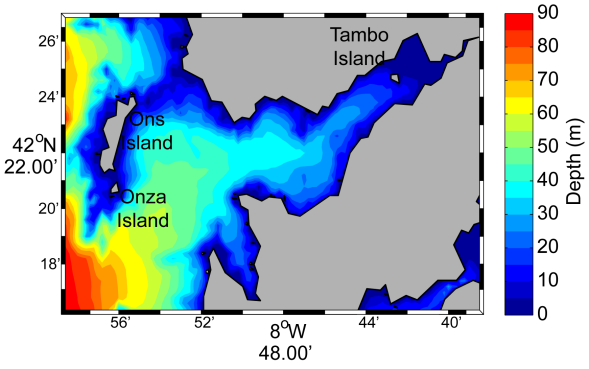

Figure 2.3: Map of the Ria de Pontevedra.

range from around 21 kg m^3 at the inner part of the estuary to around 24 kg m^3 at the outer one. The partial stratification of the estuary is maintained by salinity in winter and water temperature in summer [Gomez-Gesteira et al., 2001].

2.2.1.3 Ria de Arousa

The Ria de Arousa is the largest of the estuaries of Galicia (Figure 2.4) and is located between the estuary of Muros and Noia to the north and the Pontevedra estuary to the south (42° 27' - 42° 41'N, 8° 44' - 9° 01'W).

The Ria de Arousa is 33 km in length, 9 km wide on average (8 km in the mouth, 15 km in its wider central area and 2.5 km in the inner area), with a surface area of 239 km^2, a volume of 4.34 km^3 and an average depth of 19 m. The Sálvora Island divides the entrance of the estuary into a narrow and shallow northern mouth (5 m deep) and the wider and deeper southern mouth (55 m deep), through which almost all the water exchange is occurring. The middle area has intermediate hydrographic characteristics (INTECMAR, Xunta de Galicia) depending on the river discharge, but mainly on the wind regime over the shelf, which is the main factor governing the hydrodynamic of the Ria [Roson et al., 1995]. The Ulla River is responsible by freshwater discharge into the estuary, with a catchment area of 2924 km^2 and an annual mean discharge of 76.3 m^3 s^{-1}, which range from about 5 m^3 s^{-1} in summer up to 140 m^3 s^{-1} in winter [Otto, 1975]. Small rivers, of which the Umia River is the largest, also discharge into the estuary (Figure 2.1). This river has a catchment area of 250 km^2 and a annual mean discharge of 16.3 m^3 s^{-1} [Roson et al., 1995]. These rivers and the topography determine the division of the estuary into three well defined areas, inner, central and outer [Otto, 1975]. The inner area is less than 20 m deep and is strongly influenced by the River Ulla. The outer area (30-60 m deep) has a strong oceanic influence.

The Ria de Arousa, as the other Rias Baixas, is a partially mixed estuary with a two-

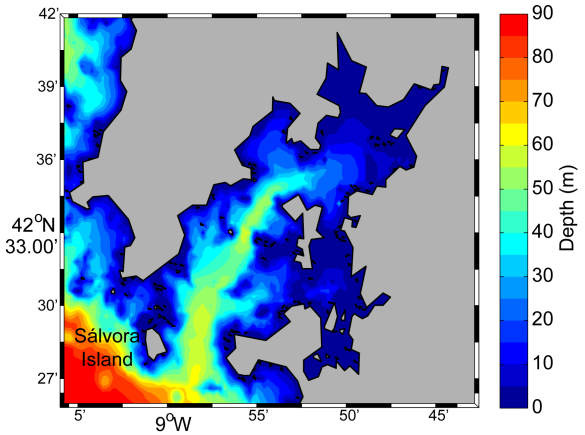

Figure 2.4: Map of the Ria de Arousa.

layer positive residual estuarine circulation [Fraga and Margalef, 1979]. The tidal range is 1.1 m and 3.5 m during neap and spring tides, respectively [Hanson et al., 1986].

2.2.2 Minho River

Minho River is an international river in the north of Portugal that crosses Portuguese and Spanish territory (Figure 2.1). It rises in Serra de Meira (Spain) and flows into the Atlantic Ocean (in front of Caminha and A Guardia) in Portugal, after a total length of about 300 km. The upper part of the river is in Spain and the lower 70 km lie within Portuguese territory. The river has a catchment area of 17080 km^2, 95% of which is located in Spain, and only 5%, in Portugal, and an annual average discharge of 300 m^3 s^{-1}. The monthly average discharge oscillates between 100 m^3 s^{-1} in August and 800 m^3 s^{-1} in February [Rio-Barja and Rodriguez-Lestegas, 1996].

The Minho estuary (41° 49.0'N - 41° 55.1'N, 8° 26.4'- 8° 56.7'W) is approximately 38 km long with a total area of 23 km^2 (Figure 2.5). The estuary has a maximum width of about 2 km near the mouth, decreasing to about 10 m at the head. In the middle estuary there is a region of sediment accumulation, which forms several sand banks and islands. The mean depth of the estuary is 2.6 m and the maximum depth is about 4 m near the mouth [Freitas et al., 2009]. It presents a semidiurnal, high-mesotidal regime and the range of the astronomical tide varies between 2 m, during neap tides, and almost 4 m, in spring tides [IH, 2006]. The estuary can be considered as a partially mixed system, although it may present salt wedge characteristics during high river flow events [Sousa et al., 2005]. The limit of salt intrusion is about 35 km from the mouth [Bettencourt et al., 2003].

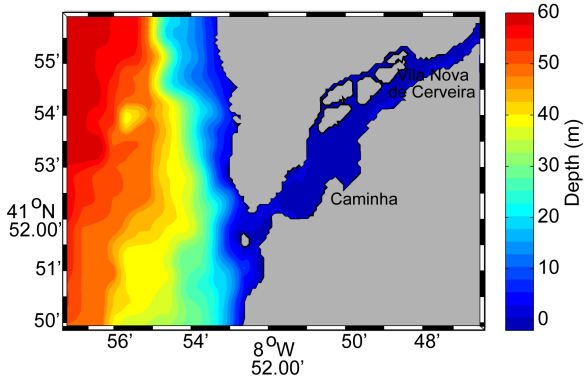

Figure 2.5: Map of the Minho estuary.

2.2.3 Circulation patterns

The general circulation of the NE Atlantic region is directly dependent on two major current systems that transport surface water masses from west to east across the Atlantic: the North Atlantic Current extending to the north of the Iberian Peninsula (48°N to 53°N) and the Azores Current south of Iberia centred at about 34-35°N [Saunders, 1982; Pollard and Pu, 1985; Peliz et al., 2005].

The surface circulation off the NW of the Iberian Peninsula is dominated by the Portugal Current System, which is composed of the slow, equatorward, Iberian basin-scale flow of the Portugal Current (PC) proper in the open ocean, and the fast, seasonally Portugal Coastal Current (PCC) closer to the shelf break (Figure 2.6).

The PC is estimated, on average, to extend about 300 km beyond the shelf, transporting about 2.0 $\pm$ 1.2 Sv [Mazé et al., 1997] at an average of 1.6 cm s^{-1} [Pollard and Pu, 1985] with maximum speeds reaching up to 5.7 cm s^{-1} [Martins et al., 2002]. The surface current can range between 0.3-12 Sv region-wide (10 Sv at 37.2°N, 12 Sv at 43°N and in the narrow strip between 10.5°W and 1000 m water depths, 9 Sv at 37.2°N and 4 Sv at 43°N) [Huthnance et al., 2002; Martins et al., 2002].

During summer, the PCC is 30-40 km wide and 50-100 m deep and flows southward (with maximum values of about 40 cm s^{-1} [Peliz et al., 2002]) in the vicinity of the shelf break, being driven by upwelling favourable northerly winds. It then transports upwelled, cold and nutrient-rich ENACW of subpolar origin ($>$ 45°N, $ENACW_{sp}$) in the north, and warmer and nutrient-poor ENACW of subtropical origin ($<$ 40°N, $ENACW_{st}$) formed along the Azores Front in the south, while during September to April the PCC piratically vanishes [Alvarez-Salgado et al., 2003].

During the winter, beneath the near-surface equatorward flow of the Portugal and

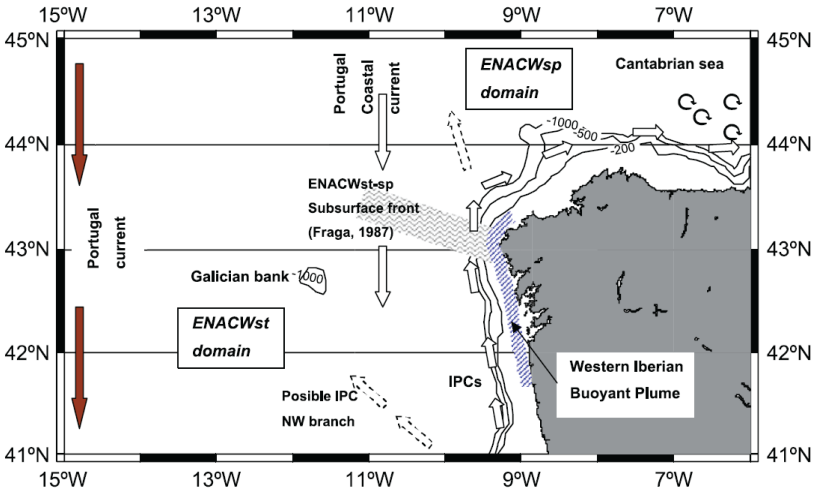

Figure 2.6: Schematic map of the main circulation features at the NW of the Iberian Peninsula. From Varela et al. [2005].

Canary Currents, there is another current called Iberian Poleward Current (IPC) [Frouin et al., 1990; Peliz et al., 2005]. The IPC is a saltier and warmer poleward current. It is a narrow (25-40 km) slope trapped tongue like structure that flows northerly along a distance exceeding 1500 km off the coasts of the Iberian Peninsula and its magnitude is of the order of 20 cm s^{-1}. It is a salty surface current (about 200 m deep) geographically trapped by the bathymetric discontinuity at the shelf break upper slope zone. Moderately strong upwelling and downwelling favourable winds, can modify the poleward flow but do not significantly change the density-driven current structure at the slope. The alongshore transport within the slope region is reduced by 0.2-0.3 Sv (from 1.2 Sv), under the influence of either downwelling or upwelling winds [Peliz et al., 2003]. In the coastal region, the surface circulation is also influenced by freshwater plumes resulting of the discharge from rivers (Verdugo-Oitabén, Lérez, Ulla, Umia, Tambre and to the south by the Minho and Douro), generating a persistent buoyant plume, the WIBP [Peliz et al., 2002]. Thus, the WIBP is a low-salinity lens ($<$35.7) formed by river discharge and continental runoff expanding all over the shelf, that could reach the 100 m isobath and is about 20 m deep, its thickness being reduced as it approaches to the coast due to the raise of the isopycnals [Varela et al., 2005]. According to Peliz et al. [2002], under typical winter conditions, the onshore Ekman transport driven by southerly winds induces the confinement of the plume to the coast, thus forcing the WIBP to develop into a narrow coastal current with strong velocities [Otero et al., 2008]. When the southerly winds weaken or turn northerly, it is advected both southward with the upwelling jet and offshore in the Ekman layer, even when wind variation has a short duration (1-3 h) [Otero et al., 2008].

The dynamics on the coastal shelf interact with Rias Baixas circulation in distinct ways. On one hand, as the Rias Baixas show a positive circulation with surface water leaving the Rias and bottom water entering it [Otto, 1975; Prego and Fraga, 1992]. Coastal upwelling enhanced this positive circulation, introducing colder and saltier water inside the estuaries [Wooster et al., 1976; Fiuza et al., 1998]. One the other hand, coastal downwelling causes a reversal of this circulation pattern, characterized by the intrusion of warm coastal waters at the surface, which accumulates in the Rias interior and finally flows towards the ocean through the bottom [Figueiras et al., 1994, 2002].

2.3 Material and methods

The data used in this study are: hydrographic parameters surveyed in the two mouths of the Rias de Vigo, Pontevedra and Arousa, wind data, air temperature and Minho River discharge.

Salinity and water temperature were measured weekly from October 1997 to October 2002 at the surface and deep for the southern (35 m deep) and northern (20 m deep)

mouth of each estuary (Figure 2.7). Table 2.2 shows the location of sampling stations. These measurements were made using a conductivity-temperature-depth (CTD) instrument (Seabird19 and 25). Salinity calibration was previously performed by means of an "Autosal" salinometer. Salinity and water temperature time series were smoothed in order to analyse their seasonal evolution in both mouths of the Rias de Vigo, Pontevedra and Arousa. The methodology followed can be summarized in several stages: (1) raw data were analysed in such a way that data out of the range of $\pm 3\sigma$ (where σ is the standard deviation) were removed; (2) data were filtered using a low-pass filter, in such a way that frequencies higher than one month were smoothed out, and (3) data gaps (less than 5%), generated by bad weather conditions and problems in the measuring devices, were filled using a cubic interpolation scheme.

The wind data consists of surface wind fields obtained by the QuikSCAT satellite. This dataset consists of global grid values of meridional and zonal components of wind, measured twice a day in an approximately $0.25° \times 0.25°$ global coverage grid. Data are given in an ascending (6 AM) and descending (6 PM) pass. The reference height of wind data is 10 m. In addition, it is necessary to note that the wind data close to the coast ($\sim$25 km) are not available due to the existence of a small land mask. The time series used in this study result of the extraction of the data in a point located at 42° 15'N, 10°W .

The air temperature was provided by the "Agencia Estatal de Meteorología" of Spain from a meteorological station situated at Peinador (42° 13'N, 8° 38'W).

Daily Minho River discharge was supplied by the "Confederación Hidrográfica del Miño Sil". The river discharge considered is the result of averaging the river runoff from the

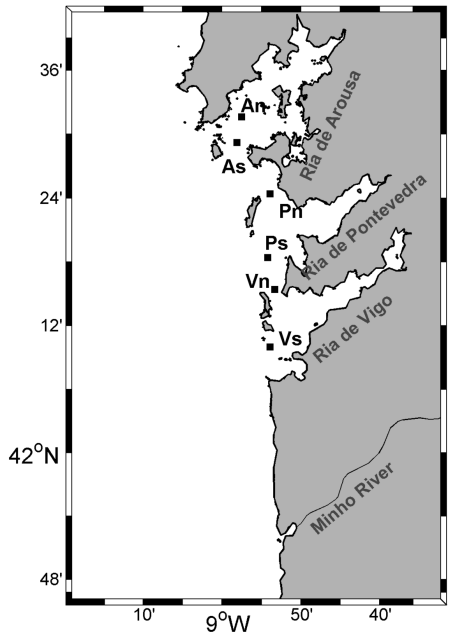

Figure 2.7: Map of Rias Baixas and sampling stations position (black dots).

Table 2.2: Location of the sampling stations.

	Southern station	Northern station
Ria de Vigo	42° 10.7'N, 8° 52.5'W	42° 14'N, 8° 52.7'W
Ria de Pontevedra	42° 19.5'N, 8° 53'W	42° 23.5'N, 8° 53.5'W
Ria de Arousa	42° 28.5'N, 8° 58'W	42° 30.8'N, 8° 58.8'W

previous 7 days to the day of hydrographic sampling [Alvarez et al., 2003].

All of these datasets cover the period October 1997 to October 2002, except the wind data provided by the QuikSCAT satellite, which are from July 1999 to October 2002.

Upwelling index was calculated at 43 ºN, 11 ºW by means of the geostrophic wind speed obtained from atmospheric fields [Lavin et al., 1991, 2000] and was averaged for 4 days before each cruise. Negative values of upwelling index indicate downwelling conditions, while positive values indicate upwelling conditions.

Additionally, in order to evaluate the influence of the upwelling index, wind, air temperature and Minho River discharge over the salinity and water temperature patterns in the Ria de Vigo, correlations between these variables were determined using the correlation coefficient ($r_{x,y}$), which can be calculated by:

$$r_{x,y} = \frac{cov(x,y)}{\sigma_x \sigma_y} \tag{2.1}$$

where *cov(x,y)* is the covariance between data and $r_{x,y}$ ranges from -1 to 1.

2.4 Results and discussion

2.4.1 Forcing mechanisms

In order to study the effect of the major forcing mechanisms in the hydrography of the Rias Baixas, it is necessary to analyze their seasonal behavior. Upwelling index, air temperature measured at Peinador meteorological station and Minho River discharge were monthly averaged from October 1997 to October 2002. These means are depicted in Figure 2.8.

A positive or negative upwelling index values indicates favorable (northerly winds) or unfavourable (southerly winds) upwelling conditions, respectively. As it can be observed in Figure 2.8a , the upwelling season occurs from April (114.2 $m^3s^{-1}km^{-1}$) to September (33.5 $m^3s^{-1}km^{-1}$). For the rest of the months, winds are predominantly from the south and south-west, favouring the predominance of downwelling conditions.

The air temperature (Figure 2.8b) shows the highest value in August (19.8 ºC), while the lowest values corresponds to January (9.2 ºC) and December (9.1 ºC), presenting a marked seasonality.

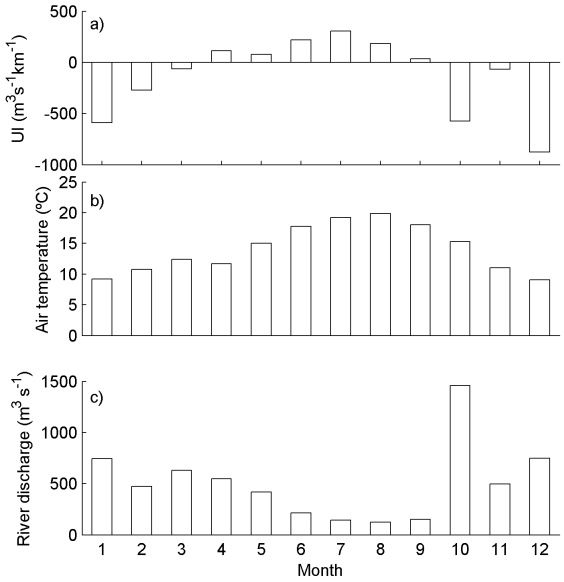

Figure 2.8: Monthly mean (October 1977-October 2002) upwelling index (a), air temperature (b) and Minho River discharge (c).

The monthly Minho River discharge shows a typical pattern with high values during winter and low values during summer. The maximum value corresponds to October (1457 m^3 s^{-1}), and the minimum values are reached in July and August (144 and 123 m^3 s^{-1}).

2.4.2 Seasonal evolution of hydrographic parameters

The near surface and near bottom salinity and water temperature time series from October 1997 to October 2002 for the northern and southern mouths of the Ria de Vigo, Pontevedra and Arousa are shown in Figures 2.9, 2.10 and 2.11.

Regarding salinity, the surface salinity decreases in the beginning of 1998 (about 5) and 2001 (about 7) in the Ria de Vigo (Figure 2.9a) and Ria de Pontevedra (Figure 2.10a), synchronized with a high Minho River discharge, which reaches 900 m^3 s^{-1} [Alvarez et al., 2006]. Nevertheless, this decrease in surface salinity is higher for the Ria de Arousa (about 20 for the beginning of 2001) (Figure 2.11a), where the freshwater inflow is higher [Rio-Barja and Rodriguez-Lestegas, 1996]. The low surface salinities can be also induced by the southerly winds (downwelling favourable), which are predominant in the winter months (Figure 2.8a), and drives the water to enter the Ria through the surface layer. On the bottom (Figures 2.9b, 2.10b and 2.11b), the northern mouth of the three Rias presents the same pattern, which may be related to its shallowness. However, the bottom salinity does not exhibit seasonality, because the shelf water intrusion is controlled by the bathymetry [Guerrero et al., 1997]. However, the salinity difference between surface and bottom is higher during winter than summer (see Figures 2.12, 2.13 and 2.14), following the Minho

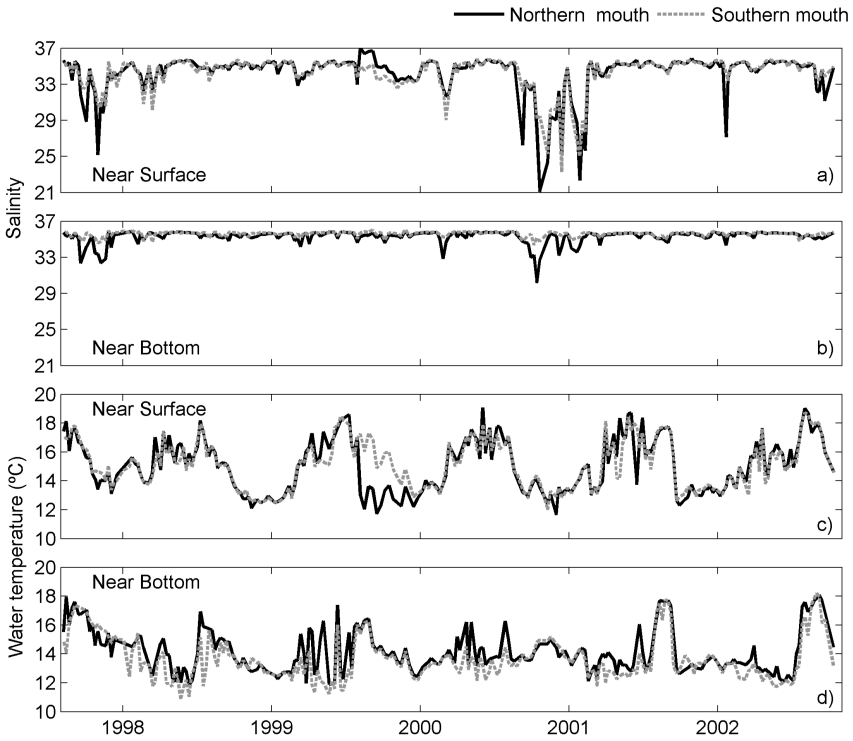

Figure 2.9: Near surface (a,c) and near bottom (b,d) salinity and water temperature time series from October 1997 to October 2002 for the northern and southern mouths of Ria de Vigo.

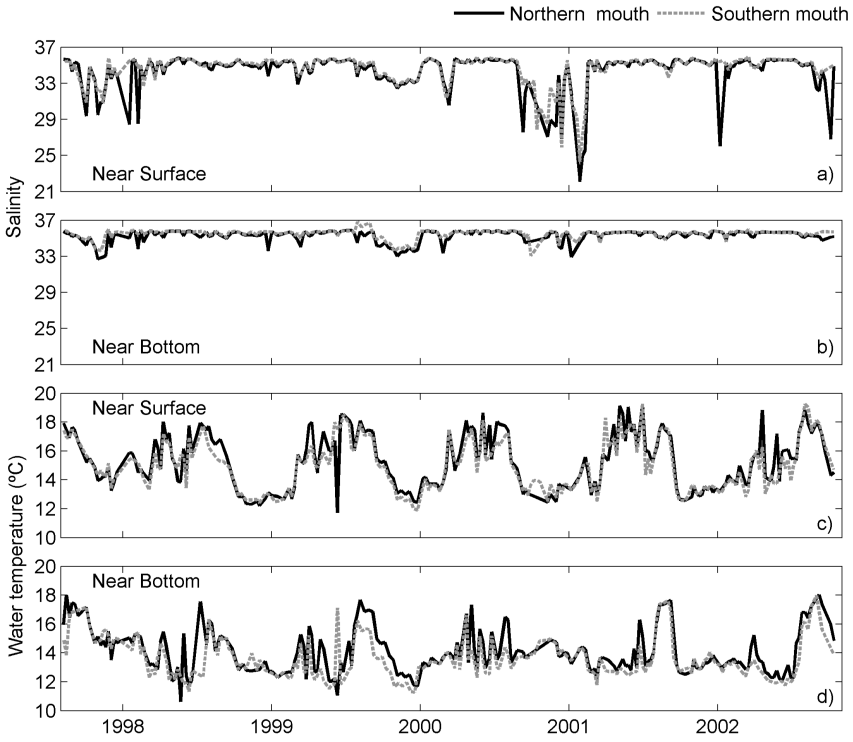

Figure 2.10: Near surface (a,c) and near bottom (b,d) salinity and water temperature time series from October 1997 to October 2002 for the northern and southern mouths of Ria de Pontevedra.

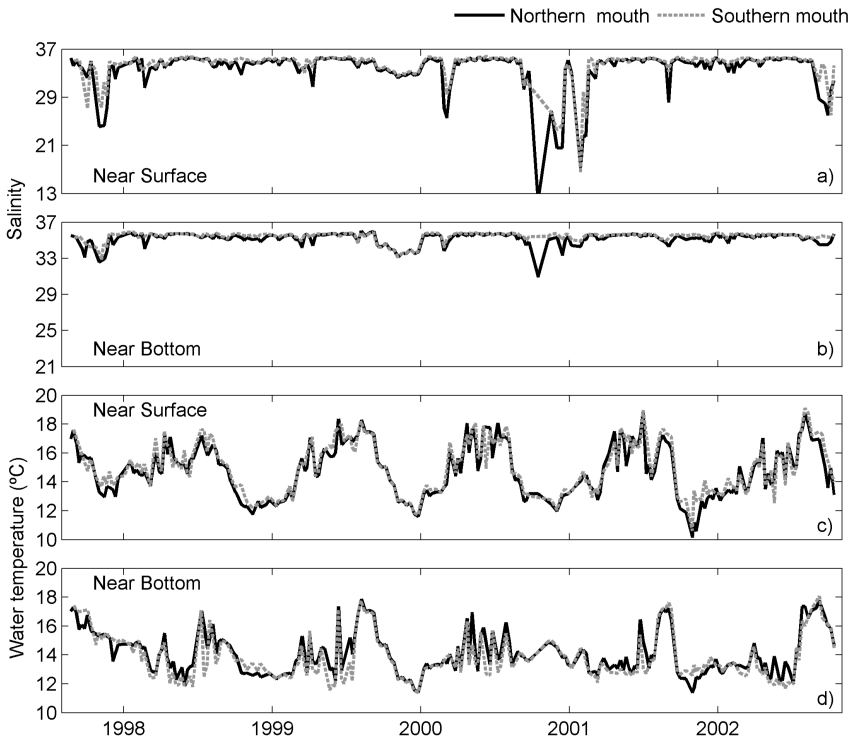

Figure 2.11: Near surface (a,c) and near bottom (b,d) salinity and water temperature time series from October 1997 to October 2002 for the northern and southern mouths of Ria de Arousa.

River and the freshwater inflow pattern (Figure 2.8c). A maximum salinity difference was observed between January and April in both mouths, with the stratification reaching 2.5. Stratification decreases in summer, due to the strong upwelling events and low rainfall occurring in this area [Alvarez et al., 2005a]. When comparing both mouths of the same Ria, near surface water in the southern mouth is saltier than in the northern mouth, which is consistent with northward surface freshwater deflection induced by the Coriolis force [Ruiz-Villarreal et al., 2002].

The water temperature is similar at the surface and near the bottom in both mouths (Figures 2.9c,d, 2.10c,d and 2.11c,d). Surface water temperature increases from April to October and decreases at the end of the year (Figures 2.12c, 2.13c and 2.14c). The bottom water temperature decreases from December to August and increases from August to November (Figures 2.12d, 2.13d and 2.14d). Surface water temperature is warmer at the southern mouths than at the northern ones, due to freshwater deflection to the northern mouth as mentioned above.

Water temperature values range from 12℃ (17℃) at the surface to 13℃ (15℃) near to bottom in the winter (summer) months. This pattern is related to the air temperature variability and freshwater input, since in winter the air is colder than the water, inducing the surface water cooling, and the freshwater input is much colder than the seawater. In summer it is found the opposite pattern. This superficial cooling affects sub-superficial

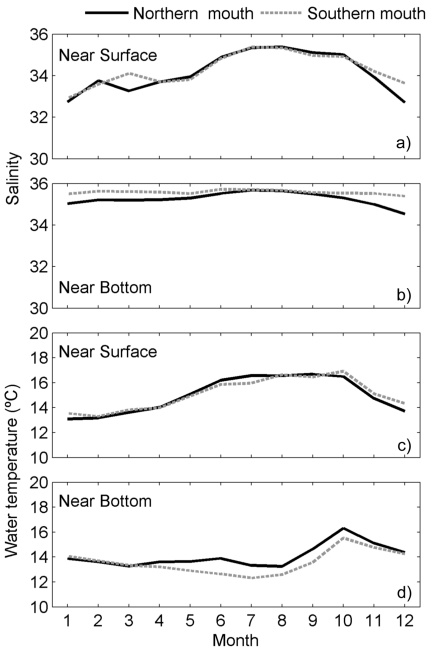

Figure 2.12: Monthly mean near surface (a,c) and near bottom (b,d) salinity and water temperature for the northern and southern mouths of the Ria de Vigo for the period from October 1997 to October 2002.

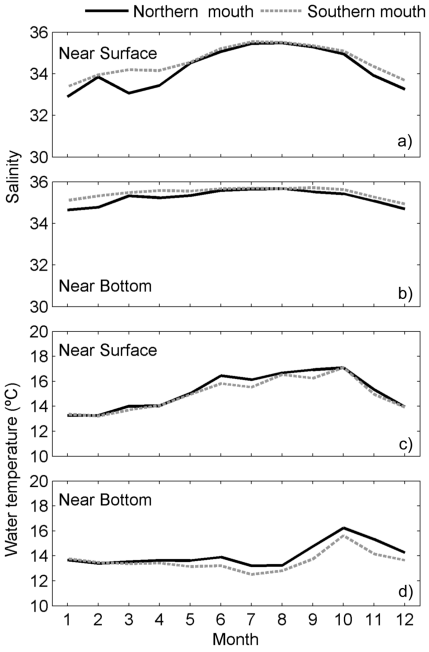

Figure 2.13: Monthly mean near surface (a,c) and near bottom (b,d) salinity and water temperature for the northern and southern mouths of the Ria de Pontevedra for the period from October 1997 to October 2002.

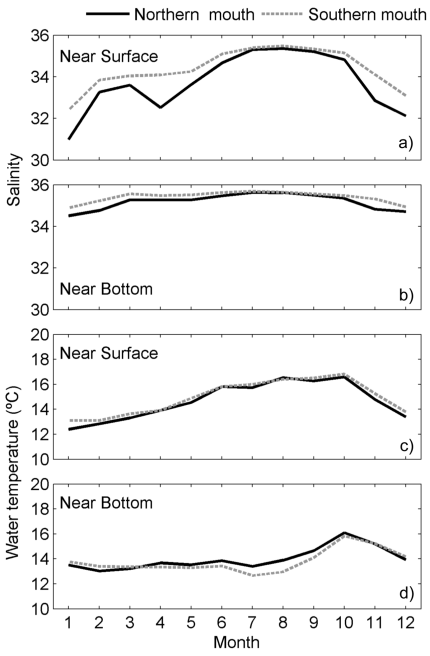

Figure 2.14: Monthly mean near surface (a,c) and near bottom (b,d) salinity and water temperature for the northern and southern mouths of the Ria de Arousa for the period from October 1997 to October 2002.

depths decreasing its effect as depth decreases.

Once again, when comparing both mouths, it can be observed that they have a similar behaviour. However, the highest surface-to-bottom water temperature difference is observed in the summer months, reaching 1 ºC for Rias de Vigo and Pontevedra and 2 ºC for Ria de Arousa, following the air temperature pattern (Figure 2.8b).

The bottom water temperature decreases from April to September (Figures 2.12d, 2.13d and 2.14d), due to the presence of a colder water mass (ENACW) and the prevalence of northerly winds (Figure 2.8a), which pump ENACW from the shelf [Rios et al., 1992b; Prego et al., 1999]. Moreover, a maximum value in October, associated with the presence of a warmer water mass on the adjacent shelf is also found, in accordance with previous results from Prego et al. [2001]. The same pattern is also observed at the southern mouth. When comparing both mouths of the same Ria, the water temperature is colder at the southern mouth than at the northern one. This situation can be explained by the depth difference between both mouths (southern mouths are considerably deeper) and by the different orientation of the mouths (the southern mouth is aligned with the axis of the Ria, while the northern one opens in the northwest direction) which affects the water circulation [Alvarez et al., 2005a].

2.4.3 Influence of external forcing on hydrographic variables

The correlations of water temperature and salinity with upwelling index, alongshore wind, Minho River discharge and air temperature were computed. Upwelling index values and alongshore wind were used in order to verify the possible upwelling response to the wind variability. The Minho River discharge and air temperature were used in order to evaluate their relationship on the establishment of the circulation patterns. The results are summarized in Tables 2.3, 2.4 and 2.5.

With respect to the correlation of upwelling index with bottom salinity and water temperature, the first is positive and the second is negative (Tables 2.3, 2.4 and 2.5). In both cases, correlations have significance levels greater than 95%. These results show possibility of occurrence of upwelling events, that is, when the winds blow predominantly from the North and Northwest (positive upwelling index), it is verified that the colder and

Table 2.3: Correlations coefficients between the forcing variables and hydrographic parameters for the Ria de Vigo (S: salinity; T: temperature) ([a] significance level >95%); [b] significance level of 95%); [c] significance level <95%).

	Northern mouth				Southern mouth			
	Surface		Bottom		Surface		Bottom	
	S	T	S	T	S	T	S	T
Upwelling Index	0.226[a]	0.009[a]	0.532[a]	-0.352[a]	0.229[a]	-0.049[c]	0.480[a]	-0.459[a]
Wind	-0.338[a]	-0.047[a]	-0.561[a]	0.379[a]	-0.324[a]	-0.007[c]	-0.513[a]	0.462[a]
Discharge	-0.795[a]	-0.317[a]	-0.591[a]	0.083[b]	-0.848[a]	-0.283[b]	-0.300[a]	0.247[a]
Air temperature	0.271[a]	0.659[a]	0.200[a]	-0.071[c]	0.269[a]	0.554[a]	0.108[c]	-0.284[a]

Table 2.4: Correlations coefficients between the forcing variables and hydrographic parameters for the Ria de Pontevedra (S: salinity; T: temperature) ([a] significance level >95%); [b] significance level of 95%); [c] significance level <95%).

	Northern mouth				Southern mouth			
	Surface		Bottom		Surface		Bottom	
	S	T	S	T	S	T	S	T
Upwelling Index	0.174[a]	0.020[a]	0.366[a]	-0.322[a]	0.277[a]	-0.066[c]	0.341[a]	-0.400[a]
Wind	-0.136[a]	-0.020[c]	-0.322[a]	0.366[a]	-0.217[c]	0.065[c]	-0.400[a]	0.341[a]
Discharge	-0.759[a]	-0.270[a]	-0.385[a]	0.093[b]	-0.762[a]	-0.241[a]	-0.319[a]	0.205[a]
Air temperature	0.334[a]	0.592[a]	0.391[a]	-0.061[c]	0.282[a]	0.547[a]	0.295[a]	-0.132[b]

Table 2.5: Correlations coefficients between the forcing variables and hydrographic parameters for the Ria de Arousa (S: salinity; T: temperature) ([a] significance level >95%); [b] significance level of 95%); [c] significance level <95%).

	Northern mouth				Southern mouth			
	Surface		Bottom		Surface		Bottom	
	S	T	S	T	S	T	S	T
Upwelling Index	0.283[a]	0.010[a]	0.369[a]	-0.302[a]	0.206[a]	-0.016[c]	0.262[a]	-0.390[a]
Wind	-0.165[a]	-0.030[c]	-0.307[a]	0.218[a]	-0.100[a]	0.017[c]	-0.201[a]	0.336[a]
Discharge	-0.713[a]	-0.209[a]	-0.489[a]	0.116[c]	-0.752[a]	-0.226[a]	-0.274[a]	0.163[a]
Air temperature	0.280[a]	0.596[a]	0.388[a]	0.083[c]	0.286[a]	0.554[a]	0.339[a]	-0.136[b]

saltier water enters the Rias. At surface the upwelling index correlation with salinity was low for the three Rias. Although the significance level is greater than 95%, the relationship between water temperature and upwelling index was not statistically significant, showing that upwelling events affect only the bottom layers.

The correlation between the alongshore wind and the bottom salinity in the northern and southern mouths shows negative values, both in Ria de Vigo (0.561 and -0.513), Pontevedra (-0.322 and -0.400) and Arousa (-0.307 and -0.201). This can be related to upwelling events, which pump salty water into the Rias mouths [Alvarez et al., 2005a]. A similar pattern can be observed when comparing bottom water temperature, although the correlation is positive in this case, since upwelling events pump cold water into the estuary (Tables 2.3, 2.4 and 2.5). As it can be observed, the correlation between water temperature and alongshore wind is lower in the northern mouth, which can be related to its low depth. At the surface, the correlation results are similar for salinity and close to zero for water temperature, with significance levels lower than 95%.

The correlations between air temperature and the surface water temperature are higher, ranging from 0.6 and 0.5 in northern and southern mouths, respectively (Tables 2.3, 2.4 and 2.5). Thus, in the northern mouth, the major forcing seems to be the air temperature (as a consequence of the shallowness of the region), revealing the high influence of the atmosphere.

The Minho River discharge is negatively correlated with the surface salinity, ranging from -0.759 and -0.713 (northern mouths) and from -0.848 and -0.752 (southern mouths). The negative correlation means that when the freshwater inflow increases, the salinity decreases in the mouths. Thereby, the increase in salinity from south to the north reveals that the observed values may be induced by the Minho River discharge [Mourino and Fraga, 1982].

As it can be observed in Tables 2.3, 2.4 and 2.5, the water temperature distribution is found to be weakly dependent on the river discharge and closely related to the air temperature. However, the salinity distribution is closely related to the wind variability and to the Minho River discharge. This result is in accordance with the results obtained for Espinheiro channel [Vaz and Dias, 2008], where the water temperature distribution is closely related to the freshwater temperature, tide and is also influenced by air temperature patterns due to the small depth of the channel. The salinity distribution is closely related with the tide and with the river discharge.

2.5 Conclusions

In this chapter was presented a characterization of the hydrography and dynamics of the NW of the Iberian Peninsula, with special attention to the Rias Baixas adjacent area. This

characterization allowed to identify and understand the role played by the major forcings on the dynamics in this area. A study of the hydrography of the Ria de Baixas mouth in terms of its major forcing mechanisms, identifying their influence on the establishment of the observed patterns was also performed. This study has shown the following:

- During winter the surface salinity decreases, synchronized with the high Minho River discharge. Nevertheless, the surface salinity in the Ria de Arousa was lower than in the rest of the Rias, due to the existence of a higher inside river inflow. In the summer, the surface-to-bottom salinity difference increases. This surface-to-bottom difference may be related to the upwelling events. No seasonality in salinity was observed at the bottom.

- The water temperature was similar on the surface and near the bottom, in both mouths. A surface-to-bottom difference of water temperature, with maximum amplitude of 1 ℃ in Rias de Vigo and Pontevedra and 2 ℃ in Ria de Arousa was observed, following the air temperature pattern. The water temperature reached a maximum value in October at all depths associated with the presence of a warmer mass on the adjacent shelf.

- At the southern mouths, the influence of the upwelling events and of the Minho River discharge is more frequent. At the northern mouths, due to the its shallowness, the air temperature is the major forcing.

- It was found that water temperature is weakly dependent on the river discharge and closely related to the air temperature pattern, and the salinity is closely related to wind variability and to the Minho River discharge.

Chapter 3

Wind data assessment to study coastal phenomena along the Galician coast

3.1 Introduction

Surface winds over open sea and near coastlines have a great impact on many economic activities, including ship routing, coastal management and fisheries. For example, in the absence of strong ambient flows, the spreading of plumes and local oceanographic features of ecological relevance, as upwelling regime, are highly dependent on wind stress. Thus, in coastal areas, the study of the wind induced phenomena becomes extremely important. In addition to their meteorological interest and importance, surface winds play a key role in numerical studies, being a major forcing mechanism of the circulation of coastal ocean models. This implies that errors in the determination of the surface wind will change the model forcing and consequently will modify the output of the ocean circulation models.

Therefore, for various offshore applications it is fundamental to have accurate wind speed and direction, and consequently appropriate tools for their observation or prediction are essential. A few years ago, the available data for observational studies over the oceanic regions have been based on anemometer wind measurements from land meteorological stations. More recently, *in situ* measurements using oceanographic buoys improve the knowledge about offshore winds. The data provided from these datasets are generally long enough in time and have great temporal resolution. However, these datasets are wind observations at a single point, coastal or offshore. Additionally, satellite scatterometry and high-resolution weather forecast models are also frequently used to provide useful winds. Satellite data and model predictions of the surface wind field refer to extended

gridded spatial and temporal scales, containing more information than isolated buoys or land meteorological stations. It should also be noted that satellite measurements are not available near coast, limiting its applications in those areas. In other hand, model predictions can also be less reliable close to the coast due to the discretization regarding the inland topography.

The Galician shoreline can be divided in three regions (Figure 3.1): the western coast, stretching from the northern part of Portugal to Cape Finisterre; the middle coast, from Cape Finisterre to Cape Ortegal; and the northern coast, eastward of Cape Ortegal. Several studies have been carried out in terms of wind patterns along the Galician coast [Torres et al., 2003; Alvarez et al., 2005b; Gomez-Gesteira et al., 2006; Alvarez et al., 2008b; Ospina-Alvarez et al., 2010; Alvarez et al., 2011]. According to these studies, wind field along this coast is far from homogeneous due to the particular coastal topography and orientation, which modulates wind direction and intensity. Wind observations at a single point, coastal or offshore, will not necessarily be representative of the wind conditions along the entire coast [Torres et al., 2003]. In this way, the analysis of wind regime along this coast constitutes an important task, although the lack of real wind measurements (e.g. buoys and land meteorological stations) obtained simultaneously and over long time periods makes the analysis of the wind patterns difficult near the shoreline. To overcome this difficulty, data provided by satellites as QuikSCAT and weather forecast models, can be used to study the wind regime over the area.

As it can be derived from previously published work [Pickett et al., 2003; Chelton and Freilich, 2005; Accadia et al., 2007; Alvarez et al., 2008b; Penabad et al., 2008; Otero and Ruiz-Villarreal, 2008; Pensieri et al., 2010], QuikSCAT is a useful tool to study the wind-induced phenomena in the open ocean and near the coast. However, it is necessary to keep in mind the existence of a small land mask (about 25 km) near shore where data are not available. In fact, it has been observed that QuikSCAT wind data tend to be more accurate offshore than near shore [Pickett et al., 2003; Tang et al., 2004]. This lack of satellite wind measurements near coast can be overcome using numerical models. Thus, weather forecast models also constitute an important tool to characterize the wind regime solving certain wind features that the satellite is roughly able to estimate, especially near shore. Since the main aim of this dissertation is to implement a high resolution coastal numerical model to study the Minho River plume intrusion into the Rias Baixas, it is crucial to know thoroughly the wind fields close to the coast. Once the wind data is assessed, it is possible to impose these data as boundary forcing in the coastal numerical model for simulating realistic scenarios. Therefore, the goals of this chapter are the following: to evaluate the reliability of offshore winds by the land meteorological stations and to determine the accuracy of wind patterns along the Galician coast through a comparative analysis between surface winds obtained from satellite, weather forecast model and *in situ* observations from buoys. This comparison will evaluate wind data quality close to the coast, assessing its applicability to

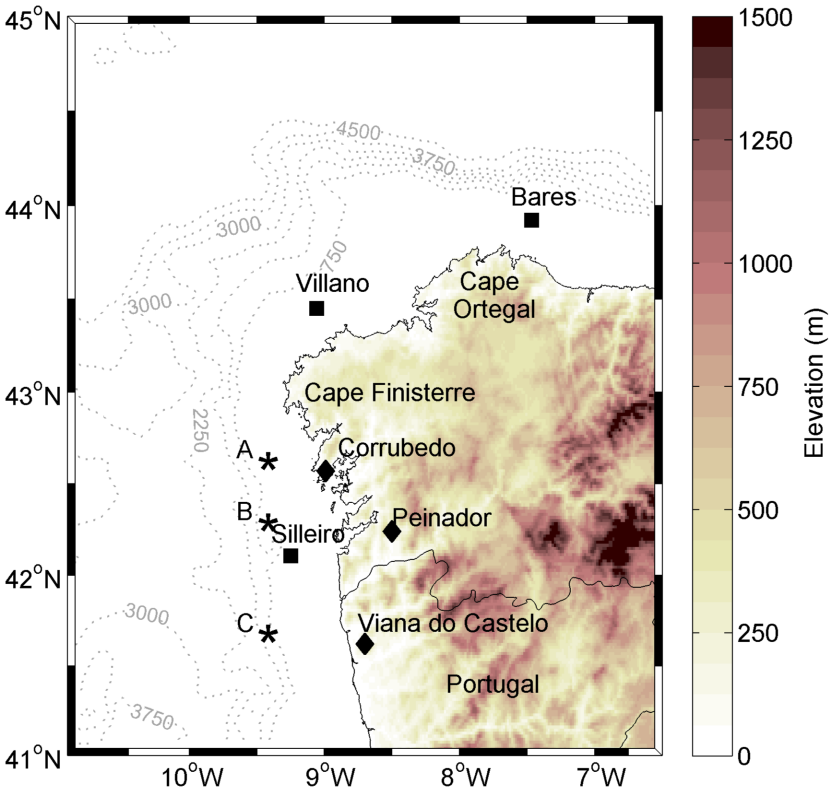

Figure 3.1: Bathymetry (m) and subaerial relief (m) of the Galician coast. Black squares, diamonds and stars correspond to the location of oceanographic buoys, meteorological stations and QuikSCAT data extraction points, respectively.

study the dispersal of Minho estuarine plume.

In a first approach, a comparative analysis between winds obtained from land meteorological stations and offshore QuikSCAT satellite is performed. Secondly, surface winds obtained from QuikSCAT data, WRF model predictions and *in situ* wind measurements from buoys along the Galician coast is also compared.

3.2 Material and methods

3.2.1 Data

Wind data used in this study were obtained from four different datasets. The wind supplied by the ”Agencia Estatal de Meteorología” of Spain for the land meteorological stations situated at Corrubedo (42° 35’N, 9° 6’W) and Peinador (42° 13’N, 8° 38’W), and ”Administração do Porto de Viana do Castelo” at the Viana do Castelo land meteorological station (41°41’N, 8°50’W)(Figure 3.1, diamonds) were considered. For the two first stations, the wind is measured four times a day over the period January 2000 to December 2001 and

for the last station it is measured every ten minutes over the period November 2008 to October 2009.

Wind data measured at three oceanographic buoys moored near the Galician shelf break were also considered. These buoys, supported by the Spanish Agency Puertos del Estado, are situated at Silleiro (42° 7.2'N, 9° 24'W at 44 km from land), Villano (43° 29.4'N, 9° 12.6'W at 30 km from land) and Bares (44° 3.6'N, 7° 37.2'W at 38 km from land) (Figure 3.1, squares). They measure wind vectors only over 10 minutes every hour at the 3 m level. Then an average is calculated and hourly wind vectors are stored.

Surface wind fields obtained by the QuikSCAT satellite are available from July 1999 to November 2009 and were retrieved from the Jet Propulsion Laboratory web site (`ftp://podaac-ftp.jpl.nasa.gov/allData/quikscat/L3/jpl/v2/hdf/`). This dataset consists of global grid values of meridional and zonal components of wind, measured twice a day in an approximately 0.25°×0.25° global coverage grid. Data are given in an ascending (6 AM) and descending (6 PM) pass and provided with a rain flag. Wind intensity measurements range from 3 to 20 m s^{-1}, with an accuracy of 2 m s^{-1} and 20° in direction [JPL, 2001]. The reference height of wind data is 10 m. In addition, it is necessary to note that the wind data close to the coast (∼25 km) are not available due to the existence of a small land mask. From the analysis carried out over several ocean regions [Portabella and Stoffelen, 2001; Stiles and Yueh, 2002; Milliff et al., 2004; Chelton and Freilich, 2005], it was found that the accuracy of QuikSCAT wind data is very low when the observations are taken under rainy conditions. This is because scattering from rain drops is higher than the scattering produced by wind action over the sea surface [Portabella and Stoffelen, 2001]. Thus, QuikSCAT data marked with a rain flag were discarded to carry out the study. To perform a spatial analysis of the entire area under study, some gaps detected in daily data were objectively interpolated between the four surrounding grid points. This interpolation affects less than 10% of the total data. The time series used in this study results of the data extraction at 3 points: A (42° 35'N, 9° 30'W), B (42° 13'N, 9°30'W) and C (41° 41'N, 9° 30'W) located at a distance of about 50 km from the nearest shoreline (Figure 3.1, stars).

Predicted wind data around the Galician coast were also provided by the Regional Forecast Agency Meteogalicia (`www.meteogalicia.es`) through the Weather Research and Forecasting model (WRF) (`http://www.wrf-model.org`). The ARW (Advanced Research WRF) core of WRF is ran operationally twice a day, producing numerical weather predictions up to 72 hours over Galicia. Three two-way nested domains are configured: a first one with 36 km resolution covering the SW of Europe; a second one with 12 km resolution covering the Iberian Peninsula; the last one with 4 km resolution over Galicia. In this study, results from the last domain are used. Table 3.1 summarizes the combinations of microphysics and cumulus parametrizations used with other physics options provided by Meteogalicia. The wind generated by the model at 10 m over the sea surface (outputted hourly) is from the PBL scheme (see Table 3.1). Only the measurements corresponding to 6 AM and 6 PM

Table 3.1: Summary of the WRF parameterizations.

WRF physics options (three domains)	
Cumulus	Grell
Microphysics	Thompson
Longwave radiation	Rapid Radiative Transfer Model scheme
Shortwave radiation	Dudhia scheme
Ground temperature	Five-layer soil model

were used for comparison purposes. A more detailed description of the model can be found in Skamarock et al. [2008].

Satellite and model datasets cover the period from November 2008 to October 2009 (the last year of available QuikSCAT data), except the wind data provided by the buoys, which do not contain continuous data for this period (Table 3.2).

3.2.2 Methodology

To evaluate wind quality close to the coast, two different approaches were applied. The first one consists of a simple statistical analysis between offshore QuikSCAT points (Figure 3.1, stars) and land meteorological stations (Figure 3.1, diamonds), in order to analyse the relation between offshore and land wind patterns in the Western Galician coast. This analysis was carried out in terms of the minimum, mean and standard deviation of the wind speed and direction. Due to the different location, satellite wind and wind measured by land meteorological station do not necessarily represent the same measurement. Austin and Pierson [1999] showed that satellite scatterometer winds represent synoptic scale winds with mesoscale fluctuations removed. Besides the tidal and other supra-inertial effects, coastal winds often exhibit diurnal cycles caused mainly by the land–sea interaction, in the form of breezes. These may be significant in locations with strong land–sea temperature gradients. With the purpose of removing the mesoscale fluctuations present in the land meteorological stations datasets, these data were low-pass filtered with an arbitrary low-pass filtered response of 33 h.

Table 3.2: Available data at the three ocean buoys during the period under study, covering the period November 2008-October 2009.

Station	Start	End
Silleiro	5 Dec 2008	6 Mar 2009
	31 Mar 2009	16 Jul 2009
Villano	1 Nov 2008	29 Jan 2009
	30 Mar 2009	24 Jul 2009
	31 Jul 2009	9 Aug 2009
Bares	1 Nov 2008	23 Jan 2009
	31 Mar 2009	17 Jul 2009
	31 Jul 2009	31 Oct 2009

The second approach followed consists on a comparative analysis between surface winds obtained from QuikSCAT, the WRF model and *in situ* observations from buoys along the Galician coast, with the objective of determining which database offers the best representation of the surface ocean wind close to the coast when compared to measured wind. To compare these different datasets, wind speed values provided by the oceanographic buoys were adjusted to a 10 m height, assuming neutral stability and a logarithmic wind profile [Large and Pond, 1981; Johnson, 1999]. The method of a logarithmically varying wind vertical profile [Ruti et al., 2008] was used instead of other methods considering algorithms based on neutral stability correction [Liu et al., 1979; Liu and Tang, 1996] due to the lack of atmospheric pressure, relative humidity and air and sea surface temperature data. To adjust the time in wind vectors from all databases, the measurements of buoy winds corresponding to 6 AM and 6 PM were used. The spatial collocation between databases was carried out with the QuikSCAT/WRF grid point closest to the location of each buoy.

To evaluate the adjustment between the different wind databases, a statistical analysis was carried out examining the wind speed and wind direction by means of the correlation coefficient,

$$r_{D,B} = \frac{cov(D,B)}{\sigma_D \sigma_B} \tag{3.1}$$

the root mean square error (RMSE),

$$RMSE = \left(\frac{1}{n} \sum_{i=1}^{n} (D_i - B_i)^2 \right)^{\frac{1}{2}} \tag{3.2}$$

the mean error (ME),

$$ME = (\overline{D_i - B_i}) \tag{3.3}$$

and the bias,

$$Bias = \frac{1}{n} \sum_{i=1}^{n} (D_i - B_i) \tag{3.4}$$

where *D* corresponds to wind data from QuikSCAT/WRF and *B* corresponds to buoys and meteorological stations. Positive (negative) values in direction bias indicate that the QuikSCAT/WRF is anticlockwise (clockwise) rotated with respect to meteorological/buoy data.A weighted mean was also calculated for the RMSE and bias following,

$$\bar{x} = \frac{\sum_{i=1}^{n} x_i w_i}{\sum_{i=1}^{n} w_i} \tag{3.5}$$

where *w* corresponds to the data weight (number of data).

The differences between QuikSCAT-buoy and WRF-buoy wind direction were also calculated to better evaluate the wind vector differences. To reduce the discontinuity between 0° and 360°, the QuikSCAT and WRF wind direction was modified using the

methodology proposed by Pensieri et al. [2010], which consists of $\theta_D = \theta_D - 360\,^\circ$ when $\theta_D - \theta_B > 180\,^\circ$ and $\theta_D = \theta_D + 360\,^\circ$ when $\theta_D - \theta_B < -180\,^\circ$.

3.3 Results and discussion

In this section, an assessment of wind data close to the Galician coast was investigated. Firstly, a comparative analysis between winds obtained from land meteorological stations and offshore QuikSCAT satellite was performed. Next, the accuracy of wind patterns along the Galician coast was also determined through a comparative analysis between wind obtained from QuikSCAT satellite, WRF model and *in situ* from buoys.

3.3.1 Offshore and land wind patterns along the Western Galician coast

The relation between offshore and land wind patterns in the Western Galician coast was addressed through an adequate statistical analysis between offshore QuikSCAT points and *in situ* land meteorological wind data. The details of this comparison are included as follows.

3.3.1.1 Statistics for the year 2000

An overview of the seasonal statistics computed for the offshore stations from QuikSCAT (A and B) and land meteorological stations (Corrubedo and Peinador) for the year 2000 is given in Figure 3.2. The winter is defined as January, February and March and summer as July, August and September.

In winter, the maximum wind speed presents 17.03 and 16.11 m s^{-1} and a minimum of 0.54 and 0.31 m s^{-1} at points A and B, respectively. For the Corrubedo and Peinador land meteorological stations the maxima are 12.50 and 6.39 m s^{-1} and minima are 0.28 and 0.56 m s^{-1}. During the summer, the maxima are 16.00 and 14.00 m s^{-1} at points A and B and minima are 8.61 and 5.56 m s^{-1}, respectively (Figure 3.2). The winds measured at the land meteorological stations are very much influenced by the orography [Sanchez et al., 2007]. Offshore satellite and land meteorological stations have similar wind direction values during both seasons.

A statistical analysis was performed in order to analyse both datasets. Correlations between wind from QuikSCAT and land stations, as well as calculation of bias, ME and RMSE for the year 2000 were performed (Tables 3.3 and 3.4).

The wind speed correlation between point A and the Corrubedo land meteorological station shows high values, both in winter and summer (0.78 and 0.54). Data from Point B are stronger correlated with the Peinador alnd meteorological station for the winter (0.83),

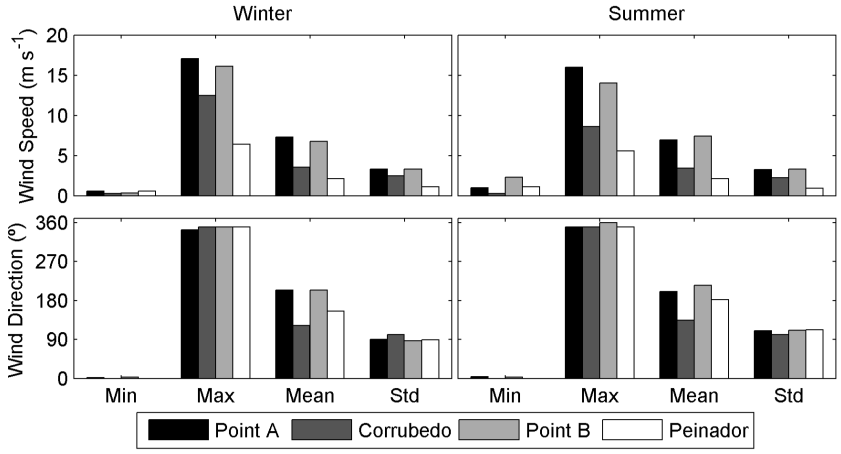

Figure 3.2: Wind speed and direction minimum, maximum, mean and standard deviation for offshore QuikSCAT points (A and B) and land meteorological stations (Corrubedo and Peinador) for winter and summer 2000.

as opposed to the summer (0.14) (Table 3.3). In respect to the wind direction, the correlation between data from Point A and the Corrubedo land meteorological station ranges from 0.30 (winter) to -0.63 (summer). On the other hand, data from Point B and from the Peinador land meteorological station presents a wind direction correlation ranging from -0.76 (winter) to 0.86 (summer). In both cases correlations have significance levels of 5%. The great variability of the wind direction and the correlation decreasing at Corrubedo land

Table 3.3: Wind speed comparison between offshore QuikSCAT points (A, B and C) and land meteorological stations (Cor-Corrubedo, Pei-Peinador, VC-Viana do Castelo) for winter (w) and summer (s) of 2000, 2001 and 2009.

Year		Wind Speed							
		r		Bias (m s^{-1})		ME (m s^{-1})		RMSE (m s^{-1})	
		w	s	w	s	w	s	w	s
2000	A/Cor	0.78	0.54	3.51	3.33	3.71	3.52	3.67	3.48
	B/Pei	0.83	0.14	3.91	4.28	4.81	5.25	4.44	4.81
2001	A/Cor	0.22	0.13	2.28	2.33	3.80	3.90	4.10	3.35
	B/Pei	0.66	0.87	5.27	4.69	6.33	5.13	5.87	4.93
2009	C/VC	0.24	-0.82	1.08	2.32	1.65	2.57	3.63	3.03

Table 3.4: Wind direction comparison between offshore QuikSCAT points (A, B and C) and land meteorological stations (Cor-Corrubedo, Pei-Peinador, VC-Viana do Castelo) for winter (w) and summer (s) of 2000, 2001 and 2009.

Year		Wind Direction							
		r		Bias (º)		ME (º)		RMSE (º)	
		w	s	w	s	w	s		
2000	A/Cor	0.30	-0.63	77.55	62.36	82.06	65.95	86.40	89.73
	B/Pei	-0.76	0.86	39.07	27.05	48.70	33.19	67.80	32.80
2001	A/Cor	-0.15	0.10	-3.44	24.78	-5.73	41.46	121.95	128.57
	B/Pei	-0.90	0.13	-51.64	44.70	-61.16	49.96	67.19	72.20
2009	C/VC	-0.02	-0.29	119.10	91.32	119.00	92.32	134.50	102.04

meteorological station in the summer may be related to diurnal fluctuations that reflect the sea-breeze regime. Moreover, results from the northern Portuguese shelf [Vitorino et al., 2002] indicated that the summer wind variability at time scales $>$ 2 days is about 25% less than in winter, and that the main factor affecting wind variability in summer is the sea-land breeze, at scales of 1 day.

As it can be observed in Tables 3.3 and 3.4, both wind speed and directional bias are always positive, indicating that offshore satellite data is anticlockwise rotated with respect to the land meteorological data. This result is in accordance with Penabad et al. [2008] findings for the Galician coast. With respect to the other variables, the values of wind direction ME are always higher for data from Point A and Corrubedo land meteorological station for both seasons. However, the opposite can be observed in ME wind speed, where it is higher in the Peinador land meteorological station. A seasonal behaviour arises in the ME and RMSE of wind speed, presenting higher error values in winter. These errors are mainly attributed to the effect of the distance from the points to the coast. These may be also caused by the local effects near shore, which are not resolved by the satellite. The southeasterly winds change frequently and abruptly, associated to passage of frontal systems [Penabad et al., 2008]. Some errors are due to the wind direction variability, contributing to the relatively high RMSE values (Table 3.4). Nevertheless, these results reveal that the wind regimes from the two datasets have similar wind direction patterns but some differences in wind speed along the Western Galician coast [Gomez-Gesteira et al., 2006].

3.3.1.2 Statistics for the year 2001

The statistical results of the wind speed and direction for the year 2001 for the offshore QuikSCAT (points A and B) and land meteorological stations (Corrubedo and Peinador) are presented in Figure 3.3.

The wind speed presents higher values than in 2000. In the offshore stations, the wind speed maximums are 20 and 13 m s^{-1} during winter and summer, respectively. At land meteorological stations of Corrubedo and Peinador, the maximums are 14.4 and 11.1 m s^{-1}, and 6.9 and 5.6 m s^{-1} during the winter and summer, respectively. The maxima occurring during the winter, in both locations, can be explained by the presence of cold fronts that affect the study area and are responsible for the wind variability. The wind speed differences between the offshore and land meteorological stations can be also explained by the presence of frontal systems, occurring during the winter [Vitorino et al., 2002]. When they reach land, these frontal systems lose speed due to the friction exerted by topography. Thus, it is expected that the wind speed at stations near the shore presents values lower than at offshore stations. According to the results presented in Figure 3.3, all the statistical variables studied herein for the wind direction shows a good agreement between both

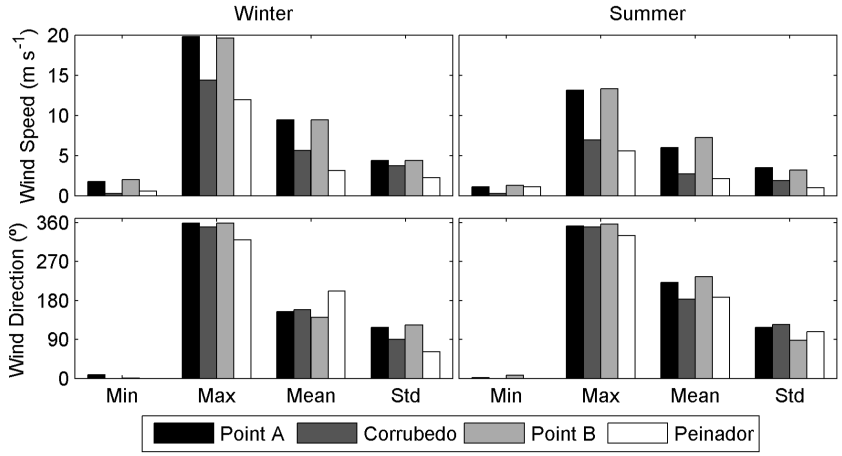

Figure 3.3: Wind speed and direction minimum, maximum, mean and standard deviation for offshore QuikSCAT points (A and B) and land meteorological stations (Corrubedo and Peinador) for winter and summer 2001.

datasets.

Taking into account wind speed, the higher correlation values are obtained between point B and the Peinador land meteorological station for the winter and summer (0.66 and 0.87). Point A and Corrubedo land meteorological station show lower correlations values (0.22 winter and 0.13 summer) (Table 3.3). During the winter, the correlation value may be related to the strong precipitation occurring in the study area [deCastro et al., 2006c; Lorenzo et al., 2010]. As previously referred, during this season the large-scale circulation is mainly driven by the position and the intensity of the Iceland Low. The Western Iberia is affected by westerly winds that carry moist air and produce rainfall events, affecting the wind variability. During this year occurred a negative phase in the North Atlantic Oscillation (NAO) index, which represents a reduced pressure gradient, resulting in fewer and weaker winter storms crossing the Galician coast [deCastro et al., 2008]. This analysis is confirmed by Torres et al. [2003], where the winter 2001 was characterized as an “atypical” winter season.

Relatively to the wind direction, the correlation between data from point B and from the Peinador land meteorological station ranges from -0.90 in winter to 0.13 in summer (Table 3.4). During the winter, the wind direction has a large variability, therefore it is expected that the wind direction varies largely between these two stations, since they are 75 km away. In general, according to Torres et al. [2003], the winter winds present larger variability than summer winds, showing a decrease in the wind direction correlation.

The wind speed bias is always positive, ranging from 2.28 m s^{-1} (A/Corrubedo) to 5.27 m s^{-1} (B/Peinador) in the winter and 2.33 m s^{-1}(A/Corrubedo) to 4.69 m s^{-1} (B/Peinador) in the summer (Table 3.3). During the winter (summer), for both datasets negative (positive) directional bias are observed, indicating that offshore satellite data are clockwise

(anticlockwise) rotated with respect to land meteorological data. It can be observed that ME is higher in the Peinador land meteorological station, that may be related to the influence of the orography (Table 3.3). For the wind speed, RMSE values range from 4.10 to 5.87 m s^{-1} for winter and 3.35 to 4.93 m s^{-1} for summer. The higher RMSE values may be related to the very low wind speed (mainly in Peinador).

These errors are also attributed to the effect of the distance from the points to the coast. Therefore, QuikSCAT satellite estimates wind speed as if it were in a neutral stable atmosphere, while land meteorological stations measure wind in real time. These are in accordance with the results obtained for Gulf of Finland [Soomere and Keevallik, 2003], where the wind speed over the open sea and coastal area differ from 40 to 100%.

3.3.1.3 Statistics for the year 2009

For the year 2009, the wind speed and direction statistical results for the offshore point C and Viana do Castelo land meteorological station is presented in Figure 3.4. In the winter (summer), the minimum was 1.34 (0.18) and 1.31 (0.63) m s^{-1} at offshore point C and Viana do Castelo land meteorological station, respectively. For offshore point C and Viana do Castelo land meteorological station, the maxima were 17.88 and 14.71 m s^{-1} (winter and summer) and 14.17 and 8.22 m s^{-1} (winter and summer), respectively (Figure 3.4).

In fact, the wind speed and direction correlation values for both seasons are lower than 0.29 (Tables 3.3 and 3.4), indicating that offshore and land meteorological stations winds are out of phase.

In spite of this low correlation, the values of the bias (1.08 and 2.32 m s^{-1}), ME (1.65 and 2.57 m s^{-1}) and RMSE (3.63 and 3.03 m s^{-1}) (Table 3.3) for the wind speed for the winter

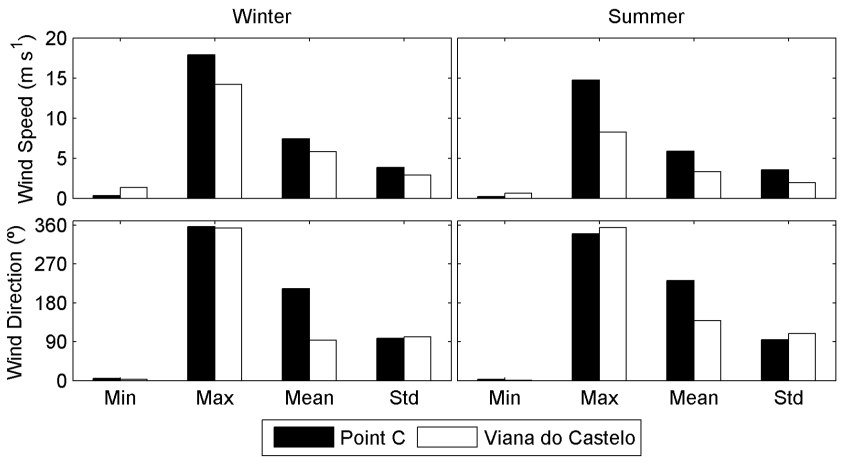

Figure 3.4: Wind speed and direction minimum, maximum, mean and standard deviation for the offshore QuikSCAT point C and Viana do Castelo land meteorological station for winter and summer 2009.

and summer respectively are low, showing the similarity of values into both datasets. The largest difference can be seen in the wind direction ME (119.1° and 92.3°), which can be attributed to the effect of the distance to the coast. Finally, the RMSE for the wind direction are 134.5° and 102.0° for winter and summer, respectively, showing once again the similarity of values.

Although the comparison of the two wind datasets shows that the offshore wind from QuikSCAT represents adequately the wind patterns measured at land meteorological station, in the next sections data from the weather forecast model will be added to the study due to the near-shore land contamination of satellite values and the lack of land meteorological stations in the coastal region.

3.3.2 Assessment of wind patterns accuracy along the Galician coast

Once wind conditions in the Galicia coast are highly variable due to the change of coastline orientation and the complex orographic features, it is crucial to accurately assess wind patterns by comparing observations at the same local and time. Therefore, only the comparison between surface winds obtained from QuikSCAT, WRF and *in situ* data from buoys was performed and the wind data from land meteorological stations were discarded from this analysis.

3.3.2.1 Oceanographic buoys wind data analysis

Buoy data were used to characterize the wind regime over the area under study, the percentage of events obtained for each range of wind speed according to the Beaufort wind force scale was summarized in Table 3.5. The wind speeds statistics reveal that the probability of light winds (lower than 3.3 m s^{-1}) ranges from 9 to 18%. Gentle, moderate and fresh breezes represent the prevailing wind regime of this region showing similar percentage values which correspond to a total amount of 63-69%. Finally, the probability of strong winds ($<$13.8 m s^{-1}) is very low, ranging from 3 to 8%.

Wind roses were also represented to analyse the distribution of wind vectors at the three stations measured by the oceanographic buoys (Figure 3.5). Bars indicate the direction from which the wind blows. At the Silleiro station, the wind blows predominantly from the North and Northwest directions (along shore). South winds are also observed although with a lower frequency. At the Villano station, the behaviour is slightly different showing northeast and southwest winds with similar frequencies. At the Bares station was found prevalence of intense easterly wind, whose amplitude tends to surpass 8 m s^{-1}. The second most prevailing winds are westerly showing lower intensity than observed for easterly winds. These results show that coastal winds tend to be aligned with coastal

Table 3.5: Percentage of events obtained for each range of wind speed according to the Beaufort scale at the three ocean buoys from November 2008 to October 2009.

Limits of wind speed (m s^{-1})	Wind descriptive terms	Silleiro (%)	Villano (%)	Bares (%)
<1.5	Calm	6	2	3
1.6-3.3	Light breeze	12	7	9
3.4-5.4	Gentle breeze	21	18	19
5.5-7.9	Moderate breeze	20	26	23
8.0-10.7	Fresh breeze	22	22	27
10.8-13.8	Strong breeze	16	17	15
>13.9	Near gale	3	8	4

orientation [Gomez-Gesteira et al., 2006; Alvarez et al., 2008b, 2011]. In addition, these wind patterns indicate upwelling favourable conditions during most of the period under study all along the Galician coast. This situation is especially remarkable at the western coast (Silleiro) which is characterized by the prevalence of intense north winds (upwelling favourable), indicating that these conditions can also occur during autumn-winter [Alvarez et al., 2003; deCastro et al., 2006c; Prego et al., 2007; deCastro et al., 2008; Varela et al., 2008, 2010; Alvarez et al., 2009]. The occurrence of upwelling events during these seasons can have implications on biogeochemical and phytoplankton patterns [Borja et al., 1996; Santos et al., 2004; Prego et al., 2007]. These circumstances indicate that the accurate wind regime characterization during periods as the one analysed in the present study is fundamental to clarify the occurrence of these phenomena and, consequently, to determine their possible impact on coastal ecosystems.

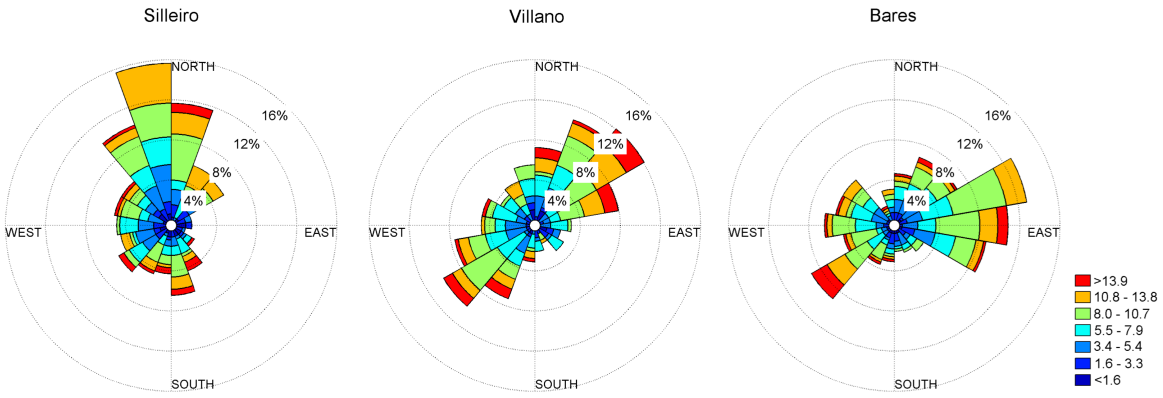

Figure 3.5: Wind rose diagrams (m s^{-1}) calculated at the three oceanographic buoys over the period November 2008 to October 2009.

3.3.2.2 Comparison of forecast and satellite winds with buoy data

Wind speed data from QuikSCAT, WRF and buoys were fitted to a Weibull distribution in order to characterize the variability among the different datasets and to calculate the probability of finding particular wind speeds at each coastal station (Figure 3.6). Weibull distribution gives an approximate but generally good fit to the observed wind speed distribution [Sanchez et al., 2007; Otero and Ruiz-Villarreal, 2008]. The selection of this distribution is often attributed to its flexibility, which assures a good fit to the observed data. Moderate winds are very common all along the coast, although some differences can be observed depending on the coastal area. At the western and middle coast a similar pattern can be observed between WRF and *in situ* wind observations showing almost the same behaviour. QuikSCAT tends to underestimate (overestimate) the occurrence of winds lower (higher) than 5-6 m s^{-1}. At the northern coast the distributions of QuikSCAT and WRF data are different from the buoy data, indicating a lower accuracy for both databases at this coastal area.

Table 3.6 shows the Weibull shape parameter (κ), which refers to the width of the distribution, and the scale parameter (λ) which is related to the mean wind speed. The most commonly occurring wind speed (W_m) was also considered. The shape parameter presents values about 2 at the three stations independently of the database. The maximum value

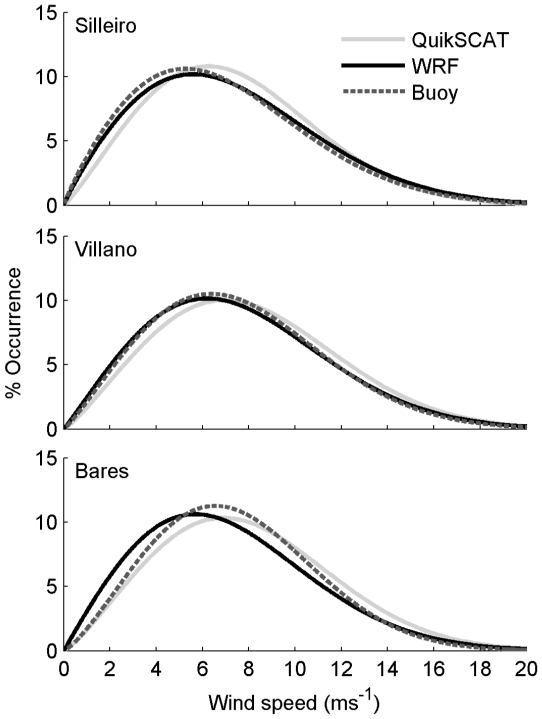

Figure 3.6: Wind speed occurrence at the three stations fitted to a Weibull distribution (grey-QuikSCAT; black-WRF; dashed black-buoy) over the period November 2008 to October 2009.

Table 3.6: Weibull shape parameter (κ), scale parameter (λ) and the most commonly occurring wind speed (W_m) corresponding to the Weibull distributions shown in Figure 3.6.

Station		κ	λ (m s^{-1})	W_m (m s^{-1})
Silleiro	Buoy	1.9	7.9	5.4
	WRF	1.9	8.2	5.6
	QuikSCAT	2.1	8.4	6.2
Villano	Buoy	2.1	8.6	6.4
	WRF	2.0	8.6	6.2
	QuikSCAT	2.2	9.1	6.9
Bares	Buoy	2.3	8.4	6.5
	WRF	2.0	8.1	5.7
	QuikSCAT	2.2	9.0	6.9

of the scale factor is obtained for QuikSCAT data at the three stations (between 8.4-9.1 m s^{-1}). In addition, the scale parameter corresponding to the model and buoys show a similar magnitude at the three stations indicating that the WRF model predictions presents better results than the satellite measurements. The most common wind speed ranges from about 5 to 7 m s^{-1} among the different databases and stations showing that moderate winds are very common. The highest value of W_m is also observed for QuikSCAT data at the three stations (between 6.2-6.9 m s^{-1}). At the western and middle coast model predictions and buoys data show a similar value. Nevertheless, at the northern coast, QuikSCAT data present a value of W_m closer to the buoy measurements showing a higher accuracy of the satellite to measure these winds.

A more detailed analysis can be carried out considering different limits of wind speed. According to the results shown in Table 3.5, three different intervals are considered. The first one includes calms and light breezes (0-3.3 m s^{-1}), the second corresponds to values between gentle and fresh breezes (3.4-10.7 m s^{-1}) and the last one considers values higher than strong breezes ($>$ 10.8 m s^{-1}). Table 3.7 shows the RMSE and bias calculated for these intervals using the QuikSCAT/WRF and buoy data. The different limits of wind speed are classified according to the values measured by the buoy. The bias is calculated as the difference between QuikSCAT/WRF values and buoy values. Thus, a positive bias in wind speed means that QuikSCAT/WRF tends to overestimate winds. The analysis by speed intervals shows similar RMSE results for QuikSCAT and WRF at the three stations. Bias distribution is less consistent. RMSE values tend to be higher at low winds ($<$ 3.3 m s^{-1}) for satellite and forecasted data at the three stations agreeing with the highest values of bias. Moderate winds show the lowest errors also at the three stations both for QuikSCAT and WRF. Note that these winds are the most commonly observed along the coast (Figure 3.6) and therefore, the highest number of samples is obtained within this interval. The statistical analysis was also carried out over the whole range speed (last row) and a weighted mean was calculated at the three stations, in terms of the number of samples existent in each bin. Thus, some data points contribute more than others to the final average. When comparing

wind speed results for the three locations, the RMSE values obtained for the satellite (about 1.5 m s^{-1}) are always lower than those for the model (about 2 m s^{-1}). Bias shows the opposite behaviour with the lowest absolute values found for the model. In addition, bias is always positive for QuikSCAT (about 0.5 m s^{-1}), indicating that the satellite overestimates wind intensity at the three stations. For the model there is a clear pattern showing a positive bias value at the western and middle coast and negative one at the northern coast. Thus, at the northern coast, forecasted data tend to be lower than *in situ* observations.

According to the previous results obtained from the Weibull analysis (Figure 3.6, Table 3.6), macroscopically at the western and middle coasts, forecasted data tend to present better results than the satellite data, showing wind patterns more similar to those determined from buoys measurements. Nevertheless, from the statistical analysis (Table 3.7) the RMSE values obtained for the satellite data are lower than the corresponding forecasted data, while the bias distribution shows the lowest absolute values for the model.

The wind direction variability was analysed considering the differences between QuikSCAT/WRF and buoy data. Figure 3.7 shows the dependence of wind direction difference between WRF-buoy (QuikSCAT-buoy) data on the buoy wind speed at the left column (right column) for the three stations.

A common pattern can be observed for WRF and QuikSCAT with most of the points distributed between -45° and 45°. The highest variations are observed for low wind speeds ($<$ 3 m s^{-1}). In fact, the standard deviations (bars) increase at low wind speeds for the three stations, as consequence of the complexity to define the direction for these events. For low wind speeds, it is more difficult to measure the wind direction. Winds over 15 m s^{-1} were not included in the calculations of the mean (black points) and standard deviation values (bars) due to the low number of samples, since their inclusion could result in a greater margin of error. In addition, high wind speeds are usually associated to bad weather conditions which can cause buoys oscillations in the higher waves as well as surface layer distortion [Large et al., 1995; Ebuchi et al., 2002] and therefore, buoys measurements become less reliable.

To better characterize the wind direction variability, a detailed analysis was carried out considering the four main direction sectors calculating the RMSE and bias for wind direction at the three stations for QuikSCAT and WRF data (Table 3.8). As in Table 3.7, direction sectors are classified according to the values measured by the buoy. The bias is calculated as the difference between QuikSCAT/WRF values and buoy data. Thus, a positive bias in wind direction means that QuikSCAT/WRF tends to rotate winds clockwise. Comparing the wind direction results analysed by sectors at the three stations, the RMSE is lower for the most frequent sectors (Figure 3.5), both for QuikSCAT and WRF. Thus, at the western coast the lowest RMSE values are obtained for S winds. At the middle coast, the lowest RMSE values correspond to the W direction and at the northern coast to the E and W direction. It is also important to note the higher RMSE obtained for the model at the western coast for W winds (65.5°) and at the northern coast for N winds (65.9°). According to Figure

Table 3.7: Statistics of the comparison between QuikSCAT, WRF and buoy wind speed at the three stations. Last row shows a weighted mean calculated over the whole range of wind speed.

Wind speed	Silleiro				Villano				Bares			
range (m s^{-1})	RMSE-Q	RMSE-W	Bias-Q	Bias-W	RMSE-Q	RMSE-W	Bias-Q	Bias-W	RMSE-Q	RMSE-W	Bias-Q	Bias-W
$<$3.3	1.6	2.2	1.2	1.3	2.3	2.5	1.6	1.3	1.5	1.8	0.9	0.6
3.4-10.7	1.3	1.9	0.2	0.1	1.3	1.8	0.3	-0.1	1.4	1.9	0.3	-0.5
$>$10.8	1.6	2.0	0.4	0.2	2.0	2.2	0.4	-0.2	1.6	1.9	0.9	0.1
Mean	1.4	2.0	0.4	0.3	1.5	2.0	0.4	0.1	1.5	1.9	0.5	-0.3

Table 3.8: Statistics of the comparison between QuikSCAT, WRF and buoy wind direction at the three stations. Last row shows a weighted mean calculated over the whole direction sectors.

Wind direction	Silleiro				Villano				Bares			
sectors	RMSE-Q	RMSE-W	Bias-Q	Bias-W	RMSE-Q	RMSE-W	Bias-Q	Bias-W	RMSE-Q	RMSE-W	Bias-Q	Bias-W
N	55.7	46.3	15.7	7.4	39.9	39.4	8.6	8.0	49.9	65.9	4.7	5.4
E	41.3	33.0	4.4	-4.9	45.3	37.2	-12.2	-5.3	26.3	30.7	-5.4	-2.0
S	25.6	32.3	1.4	-4.0	38.3	42.9	-10.7	-5.4	37.2	51.9	-11.5	-19.8
W	49.7	65.5	-16.6	17.5	29.1	27.9	-1.3	4.0	28.6	36.0	9.6	-7.0
Mean	36.5	38.8	5.4	0.4	38.1	37.1	-5.6	-0.8	32.5	41.7	-7.0	-6.5

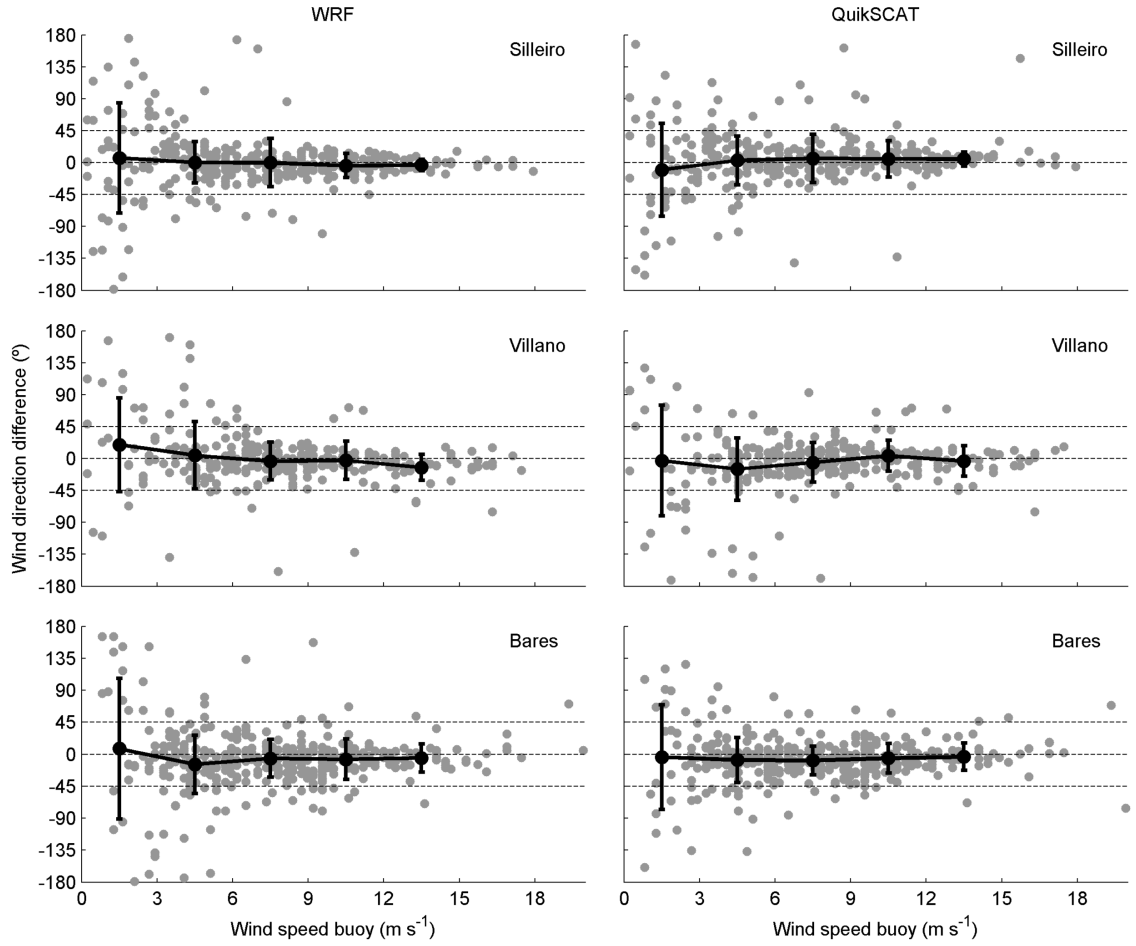

Figure 3.7: Dependences of wind direction differences (WRF-buoy and QuikSCAT-buoy) on the buoy wind speed at the three stations (grey points) calculated over the period November 2008 to October 2009. Black points represent the average of the differences based on 3 m s^{-1} bins and bars represent the standard deviation.

3.5, these winds are uncommon and the high RMSE can be due to the low number of samples. Nevertheless, the RMSE values obtained for QuikSCAT at the same sectors have considerable lower values which could indicate lower model accuracy when *in situ* measured winds come from land due to an insufficient model resolution regarding the complexity of coastal topography. For bias distribution there is not a clear pattern for QuikSCAT and WRF and values are dependent on the considered sector and station. Weighted means were also used to analyse the overall patterns (lower row). The RMSE values obtained for the satellite and the model are similar at the three stations (around 35 º). For both databases a positive bias is obtained at the western coast and a negative bias at the intermediate and northern coast. In terms of bias absolute value, the forecasted data present lower values at the three stations. Note that they can be dependent on the positive/negative distribution of bias values analysed by sectors. Thus, at the western coast QuikSCAT tends to present

positive bias values while at the middle and northern coasts bias values tend to be negative. The bias distribution corresponding to the model is less consistent.

3.3.3 QuikSCAT vs. WRF

With respect to the previous results, it was found that the WRF model and QuikSCAT data reproduce with reasonable accuracy the wind patterns measured by the buoys. In this section, the analysis of both datasets at each grid point around the Galician coast is also evaluated for the full period under study by means of an annual average. The annual mean wind pattern is calculated by averaging daily values provided by QuikSCAT and WRF at each grid point (Figure 3.8a, 3.8b). For the spatial comparison, model data were interpolated on a grid of $0.25° \times 0.25°$ using a bi-cubic interpolation. Both datasets reproduce approximately the same pattern in wind direction with some differences in wind speed. The wind speed increases from north to south for both databases showing higher values for satellite data over the entire domain. QuikSCAT minus WRF values were used to evaluate and quantify the differences in wind speed, through the computation of RMSE (Figure 3.8c) and bias (Figure 3.8d). The maximum RMSE values (about 2.2 m s^{-1}) are observed around Cape Finisterre mainly closer to coastline. Bias distribution shows positive values for the entire domain indicating that QuikSCAT tends to overestimate wind speed. The highest values of bias (about 0.7 m s^{-1}) are also observed north and south of Cape Finisterre near the shoreline. On the one hand, these results could be explained by the land mask for QuikSCAT data near shore. In fact, previous studies have shown that due to this mask, satellite measured winds tend to be more accurate offshore than near shore [Pickett et al., 2003; Tang et al., 2004]. On the other hand, it is necessary to consider the possibility of an insufficient model resolution regarding the complexity of the Galician coastal topography which could influence the model results near the shoreline. Wind direction differences were also analysed through the RMSE (Figure 3.8e) and bias (Figure 3.8f). The highest values of RMSE (about 38°) are observed at the western coast near the shoreline. These values could be explained by the fact that model results tend to be less accurate when measured winds come from land (see Table 3.8). At the most eastern part of the northern coast high values of RMSE are also observed, although they are more dependent on the low wind speed measured all over the northern coast (Figure 3.8a,3.8b). Bias distribution shows low values for the entire domain. Along the western coast the highest positive values (about 6°) near the shoreline are identified, indicating that QuikSCAT tends to rotate clockwise the wind direction. For the rest of the area bias values range between -1° and 2°.

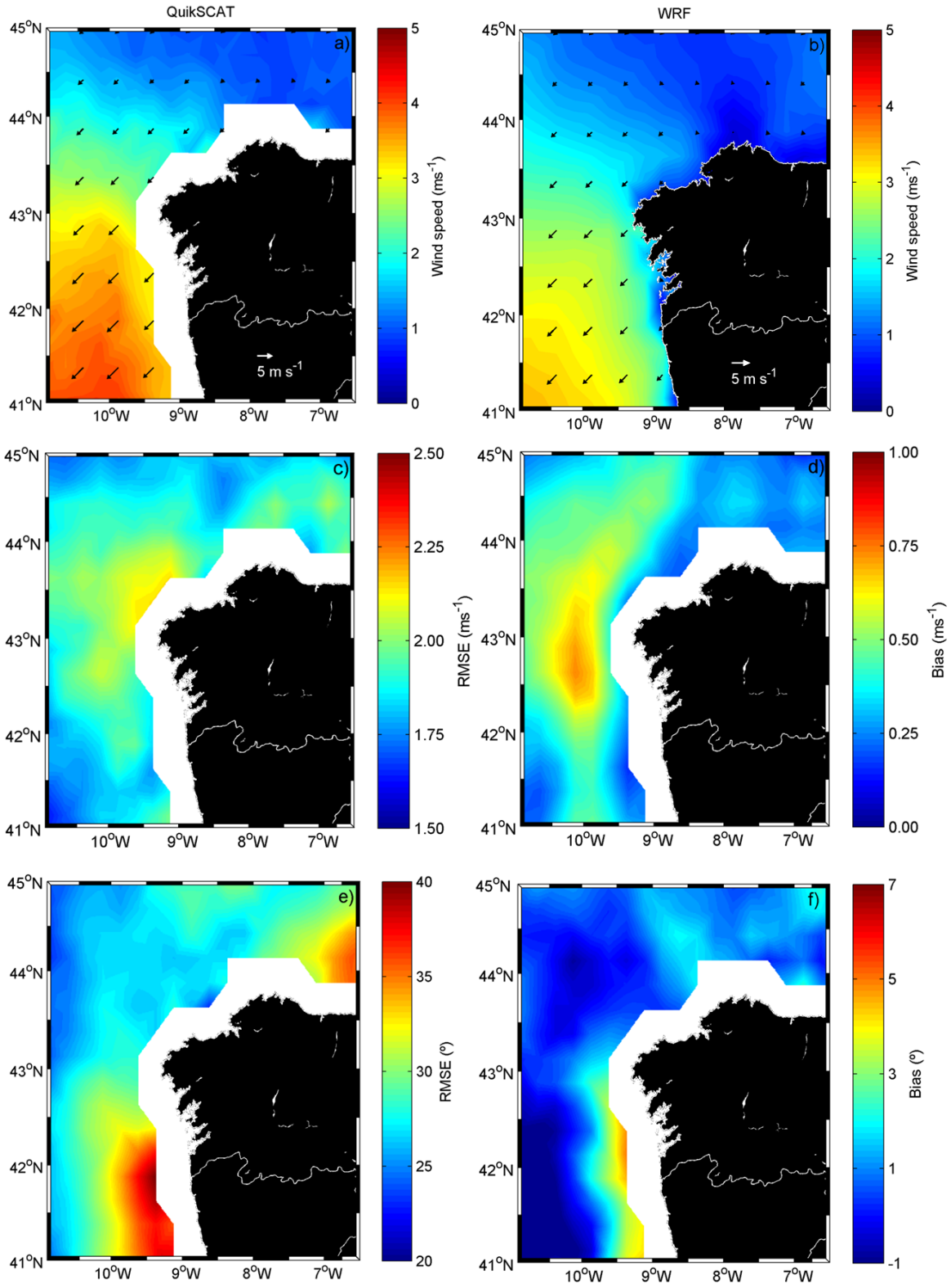

Figure 3.8: Mean annual wind circulation obtained from satellite (a) and model (b) along the Galician coast from November 2008 to October 2009. RMSE and bias for wind speed (c,d) and wind direction (e,f) from QuikSCAT-WRF data.

3.4 Conclusions

The main objectives of this chapter were to evaluate wind data quality close to the coast, assessing its applicability to study the dispersal of Minho estuarine plume. Thus, the relation between offshore and land wind patterns, and an assessment of wind patterns accuracy from the QuikSCAT satellite and the WRF model were performed. From these analysis, the following can be concluded:

- Despite the deviations found in the comparative analysis performed, the offshore data from the QuikSCAT satellite has revealed to constitute a good approach to the wind data measured in land meteorological stations.

- Near the coast, the wind pattern strongly depends on coastal geometry and orography. During the study periods, the wind regime was similar for the years 2000 and 2009. The winter 2001 was characterized by the passage of cold frontal systems that affected the study area. They induced important wind variability. Thereby, during the winter, the wind variability was larger than in the summer.

- The accuracy of the wind speed derived from the QuikSCAT and the WRF model was similar all along the coast, showing RMSE errors between 1.5 m s^{-1} and 2 m s^{-1}. The calculated bias for QuikSCAT data was positive at the three stations (0.5 m s^{-1}) while the bias for WRF predictions was positive at the western (0.3 m s^{-1}) and middle (0.1 m s^{-1}) coast and negative at the northern one (-0.3 m s^{-1}).

- Similar RMSE values were found for wind direction at the three stations (35°). Wind direction bias also showed a similar pattern between satellite and forecasted data, with positive values at the western coast and negative values at the middle and northern coasts, although always lower in absolute value for WRF data.

- From the analysis carried out considering different wind speed ranges, it was found that QuikSCAT tends to overestimate wind speeds within the whole ranges. RMSE and biases tend to be lower for moderate winds at the three stations both for satellite and forecasted data.

- Regarding the direction sectors analysis, the lowest errors and biases were observed at the same sectors for both databases at the three stations (S: Silleiro; W: Villano; E-W: Bares). The model tends to be less accurate when *in situ* measured winds come from land.

- From the spatial comparison between satellite and forecasted data it was found that the forecasted winds tend to be lower than satellite winds over the entire domain, with the highest RMSE and bias values found near shoreline.

In summary, the analyses revealed that the WRF model is a consistent tool to obtain representative wind data near the coast showing good results when comparing with *in situ* wind observations. Thus, in the oceanographic numerical modelling implementation that will be developed in this study, the WRF data will be used as the surface boundary condition.

Chapter 4

Numerical model

4.1 Introduction

To study the propagation and influence of the Minho estuarine plume on the Rias Baixas circulation and hydrography, the numerical model MOHID was used. MOHID (`www.mohid.com`) is a three-dimensional free surface numerical model under development at the Instituto Superior Técnico (Universidade Técnica de Lisboa) [Santos, 1995; Martins et al., 2001; Leitão, 2002; Leitão et al., 2005; Vaz et al., 2009b; Mateus et al., 2012]. This model has the ability to simulate flows in shallow systems, like the Minho estuary, as well as to study the Western Iberian coastal circulation, and it has been previously applied to simulate the Galician Rias [Taboada et al., 1998; Gomez-Gesteira et al., 1999; Ruiz-Villarreal et al., 2002]. Thus, to achieve the main objectives of this work two model applications composed by a coastal nested model and an estuarine model were designed. The first one is used to simulate the propagation of the Minho River plume towards the Rias Baixas and analyse the effects of the plume intrusion into these estuaries. The second one runs offline and it was developed to reproduce the Minho estuary-ocean interaction.

Therefore, a general overview of the MOHID is performed in this chapter, presenting the main formulations solved by the model. Also, a nesting numerical modeling methodology developed to reproduce the propagation of the Minho estuarine plume towards the Rias Baixas is described.

4.2 Model physics

4.2.1 Equations

The model solves the three-dimensional incompressible primitive equations. Hydrostatic equilibrium is assumed as well as Boussinesq and Reynolds approximation. All the equations below have been derived taken into account these approximations. Only a summary of the model information is presented here. A more detailed description of the numerical algorithms can be found in Santos [1995], Martins et al. [2001], Leitão [2002] and Vaz [2007]. The hydrodynamic model solve the primitive equations in Cartesian coordinates for incompressible flows. The momentum evolution equation is portrayed in Equation 4.1:

$$\frac{\partial u_i}{\partial t} + \frac{\partial (u_i u_j)}{\partial x_j} = -\frac{1}{\rho_0}\frac{\partial p_{atm}}{\partial x_i} - g\frac{\rho(\eta)}{\rho_0}\frac{\partial \eta}{\partial x_i} - \frac{g}{\rho_0}\int_{x_3}^{\eta}\frac{\partial \rho^{'}}{\partial x_i}dx_3 + \frac{\partial}{\partial x_j}\left(\nu\frac{\partial u_i}{\partial x_j}\right) - 2\epsilon_{ijk}\Omega_j u_k \quad (4.1)$$

where u_i is the velocity vector components in the Cartesian coordinates x_i directions, ν is the turbulent viscosity, η is the free surface elevation, g is the gravity acceleration and p_{atm} is the atmospheric pressure. ρ is the density, ρ' is its anomaly, ρ_0 is the reference density and $\rho(\eta)$ represents the density at the free surface, t is the time, h is the depth, Ω is the Earth velocity of rotation and ϵ is the alternate tensor.

The mass balance equation (continuity) is:

$$\frac{\partial u_i}{\partial x_i} = 0 \quad (4.2)$$

The vertical velocity is calculated from the continuity equation (Equation 4.2) by integrating between the bottom -h and the depth x_3 where u_3 is to be calculated:

$$u_3(x_3) = \frac{\partial}{\partial x_1}\int_{-h}^{\eta} u_1 dx_3 - \frac{\partial}{\partial x_2}\int_{-h}^{\eta} u_2 dx_3 \quad (4.3)$$

The free surface equation (Equation 4.4) is obtained by integrating the continuity equation over the whole water column (between the free surface elevation $\eta(x, y)$ and the bottom -h):

$$\frac{\partial \eta}{\partial t} = -\frac{\partial}{\partial x_1}\int_{-h}^{\eta} u_1 dx_3 - \frac{\partial}{\partial x_2}\int_{-h}^{\eta} u_2 dx_3 \quad (4.4)$$

The hydrostatic approximation gives:

$$p(z) = p_{atm} + \rho_0 g(\eta - z) + g\int_z^\eta \rho' dz \tag{4.5}$$

Equation 4.5 relates pressure at any depth with the atmospheric pressure at the free surface, the sea level and the anomaly pressure integrated between the level and the surface.

The model also solves a transport equation for salinity, water temperature or any other tracer:

$$\frac{\partial \alpha}{\partial t} + u_j \frac{\partial \alpha}{\partial x_j} = \frac{\partial}{\partial x_j}\left(K \frac{\partial \alpha}{\partial x_j}\right) + FP \tag{4.6}$$

where α is the transported property, *K* is the diffusion coefficient and FP is a possible source or sink term.

Finally, the density ρ is calculated as a function of water temperature and salinity by a simplified equation of state [Leendertse and Liu, 1978]:

$$\rho = \left(5890 + 38T - 0.375T^2\right)/(1179.5 + 11.25T - 0.0745T^2 - (3.8 - 0.01T)\,S + 0.698\left(5890 + 38T - 0.375T^2 + 3S\right)) \tag{4.7}$$

4.2.2 Lagrangian model

Lagrangian transport models are very useful to simulate localized processes with sharp gradients, such as discharge by submarine outfalls, sediment erosion due to dredging works, oil dispersion and water quality. This particle tracking model is a subset of the MOHID modelling system and has been used to study pollutant dispersion [Gomez-Gesteira et al., 1999; Braunschweig et al., 2003]. The Lagrangian module derives the hydrodynamic information (current fields) from the system and updates the calculations without having the need to solve all the variables at the same time. It uses the concept of passive tracers, characterized by their spatial coordinates, area and a list of properties. The particle tracking model assumes that the velocity of each particle (u_p) can be split into a large scale organized flow, characterized by a mean velocity (u_M), provided by the model, and a smaller scale random fluctuation (u_F) so that u_p=u_M+u_F. The particle tracking model used the equation:

$$\frac{dx_i}{dt} = u_i(x_i, t) \tag{4.8}$$

where u_i is the mean velocity and x_i the particle position, this equation is solved using and explicit method:

$$x_i^{t+\Delta t} = x_i^t + \Delta t u_i^t \tag{4.9}$$

The random movement is calculated following the procedure of Allen [1982], and the random displacement is calculated using the mixing length and the standard deviation of turbulent velocity provided from the hydrodynamic model. Particles retain velocity during the necessary time to perform the random movement, which is dependent on the local turbulent mixing length.

The increase in volume is associated with small-scale turbulence and is reasonable to assume it as isotropic. In these conditions, small particles keep their initial form and their increase in volume is a function of the volume itself. In this study every particle is considered as a water parcel whose paths are modelled as their move through the water.

4.2.3 Equations discretization

The MOHID model uses a finite volume approach to discretize the equations in a structured grid. In this approach, the discrete form of the governing equations is applied macroscopically to a cell control volume. This method makes the solution independent of the mesh geometry, allowing the use of a generic vertical mesh [Martins et al., 1998, 2001]. The equations are discretized horizontally using an Arakawa C staggered grid. All types of vertical coordinates have a wetting/drying cell scheme. Temporal discretization is performed by a semi-implicit Alternating Direction Implicit (ADI) algorithm to compute the sea level evolution with two time levels per iteration, following the method proposed by Leendertse [1967]. The two components of the horizontal velocity are globally centred in time, *t+dt/2*, leading to a second order time accuracy [Martins et al., 1998, 2001]

For the baroclinic force, MOHID uses a *z*-level approach for any type of vertical coordinate. This methodology integrates the horizontal density gradient always into the Cartesian space. Advection and diffusion of tracer properties such as water temperature and salinity are computed explicitly in the horizontal and implicitly in the vertical, using a Total Variation Diminishing (TVD) Superbee method. Vertical turbulent mixing is computed using the k-ϵ model, while for the horizontal, constant coefficients are assumed. The MOHID model is coupled to the General Ocean Turbulence Model (GOTM) [Burchard et al., 1998]. GOTM is a water column model which simply allows a choice between some standard turbulence parametrizations. In this work, the parametrization proposed by Canuto et al. [2001] is used.

4.2.4 Boundary conditions

Five different types of boundaries were used in this study: free surface, bottom, lateral closed boundary, lateral opened boundary and moving boundary.

At the free surface boundary, advective fluxes of mass and momentum across the surface are assumed null, imposing a null *W* vertical flux:

$$Wflux|_{surface} = 0 \tag{4.10}$$

Diffusive flux of momentum is imposed explicitly by means of a wind surface stress, $\vec{\tau}_W$:

$$\nu_3 \frac{\partial u_i}{\partial x_3}|_{surface} = \vec{\tau}_W, i = 1, 2 \tag{4.11}$$

where ν_3 is the vertical eddy viscosity. The wind stress is calculated according to a quadratic friction law:

$$\vec{\tau}_W = C_D \rho_a \vec{W} |\vec{W}| \tag{4.12}$$

where C_D is a drag coefficient that is a function of the wind speed (*W*) measured 10 m above the sea surface and ρ_a is the air density.

At the bottom boundary, the water flux is also assumed null and a quadratic law is used to calculate the bottom stress:

$$\nu_3 \frac{\partial u_i}{\partial x_3}|_{bottom} = C_D u_i \sqrt{u_1^2 + v_2^2}, i = 1, 2 \tag{4.13}$$

For stability reasons the bottom stress must be calculated implicitly in the momentum equation of the bottom cell.

The closed boundaries of the domain correspond to land. A free slip condition is used to resolve this lateral boundary, imposed by specifying a zero normal component of mass and momentum diffusive fluxes at cell faces in contact with land.

At the ocean open boundary the free surface elevation is imposed and at the river boundaries the flow is specified.

Moving boundaries are closed boundaries whose position varies with time. Intertidal zones generate moving boundaries in the alternate wetting/drying areas. A detailed explanation of the algorithms used in MOHID can be found in Martins et al. [2001] and Leitão [2002].

4.3 Model implementation

To investigate the dynamics of the Minho estuarine plume two downscaling methodologies similar to the one proposed by Leitão et al. [2005] and Vaz et al. [2009b], for simulating the Algarve coastal circulation and Tagus estuarine plume were developed. Two nested configurations with three levels one-way nested grids and an estuarine model were implemented. The nested configurations are used to simulate the propagation of the Minho River plume towards the Rias Baixas and analyse the effects of the plume intrusion into these estuaries. The estuarine model runs offline and was developed to reproduce the Minho estuary-ocean interaction, computing the estuarine outflow which is introduce as a point discharge in the coastal model. A coarse model for the entire coast of the Iberian Peninsula (‘”father” model) supplies boundary conditions for finer models applied to the Rias Baixas and the adjacent coastal area (”son” model). The communication between the ”father” and ”son” models is made by relaxation of the horizontal and meridional components, through an eleven cell band adjacent to the lateral boundary. The ”son” model did not exchange information with the ”father” model.

The two configurations only differ in the source of the initial forcing conditions. The first one comes from Levitus climatology (called Configuration #1 hereafter) and the second one comes from Mercator Open Global Solution (called Configuration #2 hereafter), respectively. There was a need to test and implement these two configurations, in order to check which configuration best represents the Minho estuarine plume propagation.

The two nested models comprise a large domain, used to compute the barotropic tide, and two smaller baroclinic domains, which are used to simulate the estuarine plume advection (schematized in Figure 4.1). The main difference between the second and third domains is the horizontal resolution, which is coarser for the second domain, and also that the third domain comprises a smaller region. The downscaling approach was implemented to smooth the transition between first and third solutions. Therefore, the second domain can be seen as the transition between the low-frequency solutions, while the third extracts information from the larger-scale models to provide adequate boundary conditions for its open boundaries as well as initial conditions.

4.3.1 Configuration of the coastal nested model including the Rias Baixas

4.3.1.1 Configuration #1

The first domain (L1) (Figure 4.2) ranges from 13.5°W to 1° E and 33.5°N to 50°N, with a variable horizontal resolution changing from 0.02° ($\sim$ 2 km) near the coast to 0.06° ($\sim$ 6 km) offshore and was constructed based on the ETOPO1 global database. This domain is a 2D

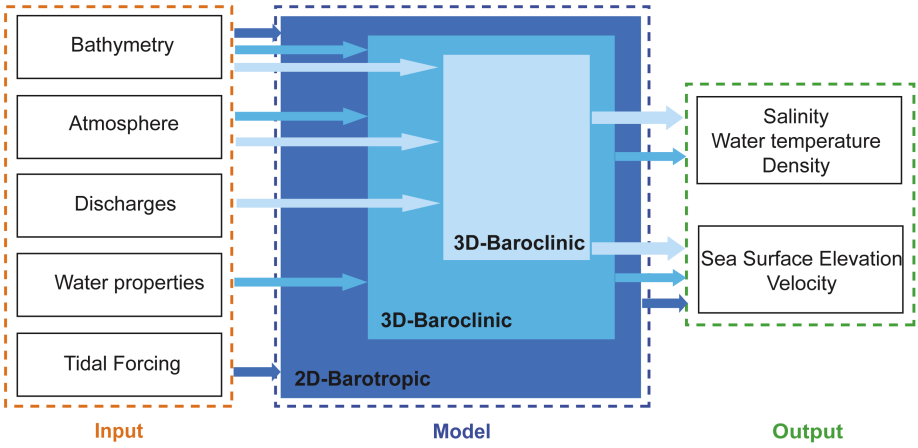

Figure 4.1: Schematic diagram of the MOHID.

barotropic tidal driven model using the FES2004 (Finite Element Solution) global solution as forcing [Lyard et al., 2006]. The time step is 180 s and the horizontal eddy viscosity is 100 m^2 s^{-1}. For the levels, at the open boundary a radiation boundary scheme was used [Blumberg and Kantha, 1985]. The ocean boundary conditions are given in cascade starting at the first level.

The second domain (L2) (Figure 4.2) comprises a region from 10.08°W to 8.40°W and 40.92°N to 43.5°N with a horizontal resolution of 0.02° (∼ 2 km). The third domain

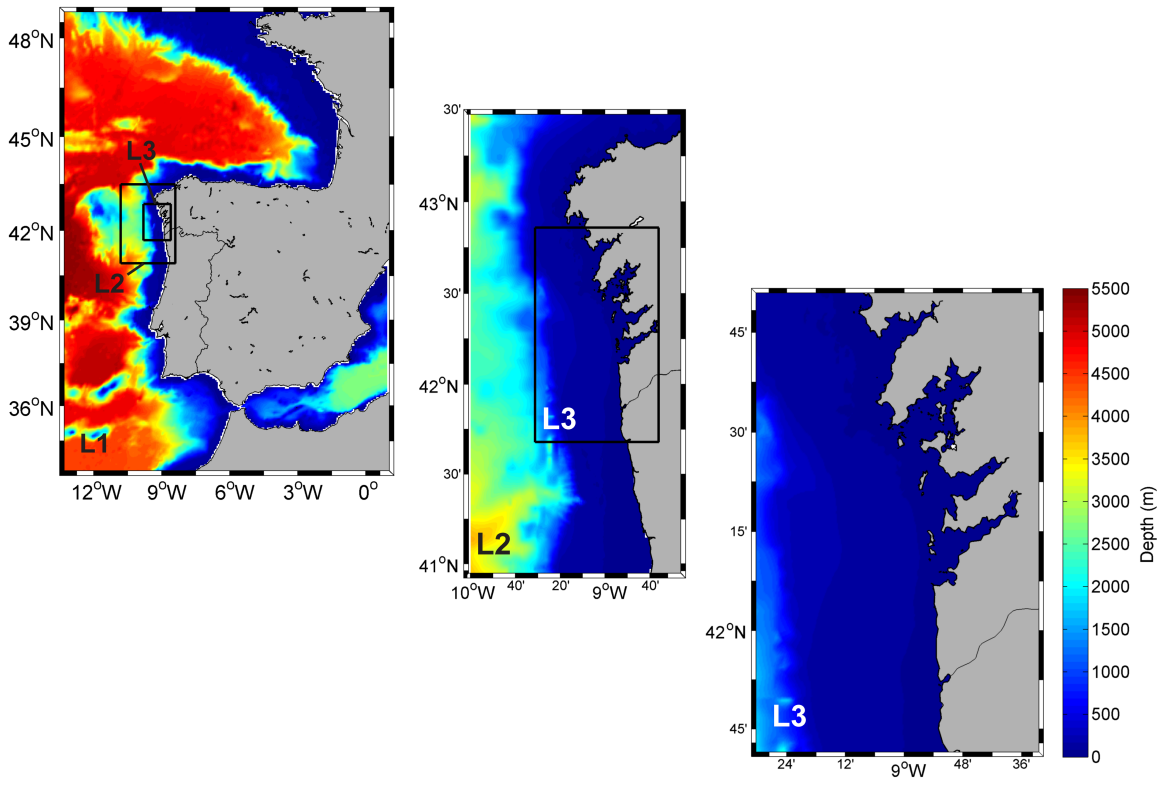

Figure 4.2: The MOHID nesting system implemented for Configuration #1.

(L3) (Figure 4.2) is from 9.52°W to 8.60°W and 41.68°N to 42.86°N with a horizontal step of 0.005° ($\sim$ 500 m) and includes the Rias Baixas adjacent coastal area and it is directly coupled to L2 at the open boundaries. Higher resolution is used in order to properly simulate the small scale processes inside the estuary and also the plume dispersion. The L2 and L3 bathymetries were constructed based on the General Bathymetric Chart of the Oceans (GEBCO), with some corrections on the continental shelf. A *z*-level vertical discretization was adopted, with L2 and L3 having 46 and 42 vertical layers, where the bottom 39 (L2), 35 (L3) are in Cartesian coordinates and the top 10 m are 7 sigma coordinate layers.

To obtain the initial ocean stratification, L2 and L3 are forced at the open boundaries with monthly mean climatologies from Levitus (`http://www.nodc.noaa.gov/OC5/WOA09/pr_woa09.html`) [Antonov et al., 2010; Locarnini et al., 2010]. In the second level a time step of 60 s is used, and the turbulent horizontal eddy viscosity inside the domain is set to 20 m^2 s^{-1}. The third level uses a time step of 15 s and a turbulent horizontal eddy viscosity of 5 m^2 s^{-1}. Furthermore, in both levels, the zonal and meridional velocity components, salinity and water temperature in boundary cells are relaxed from the previous level down. For relaxation, the Flow Relation Scheme [Martinsen and Engedahl, 1987], which consist to apply a relaxation time at the boundary in an extension of ten cells is used. The baroclinic force is slowly active over 10 inertia periods. The biharmonic filter coefficients are set to 1×10^7 m^4 s^{-1} and 1×10^4 m^4 s^{-1} for Levels 2 and 3, respectively.

The surface boundary condition is imposed using the high resolution results from the WRF [Skamarock et al., 2008] with a spatial resolution of 5 km. These fields were interpolated into hourly fields for the two last model domains using triangulation interpolation in space and linear interpolation in time. At the surface, the sensible and latent heat fluxes are calculated using the Bowen and Dalton laws, respectively [Chapra, 1997]. For the bottom boundary condition, a constant value of the bottom rugosity was considered. The 3D momentum (zonal and meridional velocities), heat and salt balance equations are computed implicitly in the vertical direction, while in the horizontal directions are computed explicitly.

As landward boundary condition (L3 grid), the freshwater input from Rias Baixas and the Minho estuary outflow are considered. The Oitabén-Verdugo, Lérez, Umia and Ulla River discharges were obtained from estimations presented by Otero et al. [2010]. The Minho estuarine outflow is imposed offline in L3. This outflow is computed by the Minho estuary model developed in this study, and directly imposed as momentum, water and mass discharge to the coastal model.

4.3.1.2 Configuration #2

The first domain (L1) (Figure 4.3) ranges from 12.60°W to 5.10°W and 34.38°N to 45.00°N with a horizontal resolution of 0.06° ($\sim$ 6 km). This domain corresponds to the

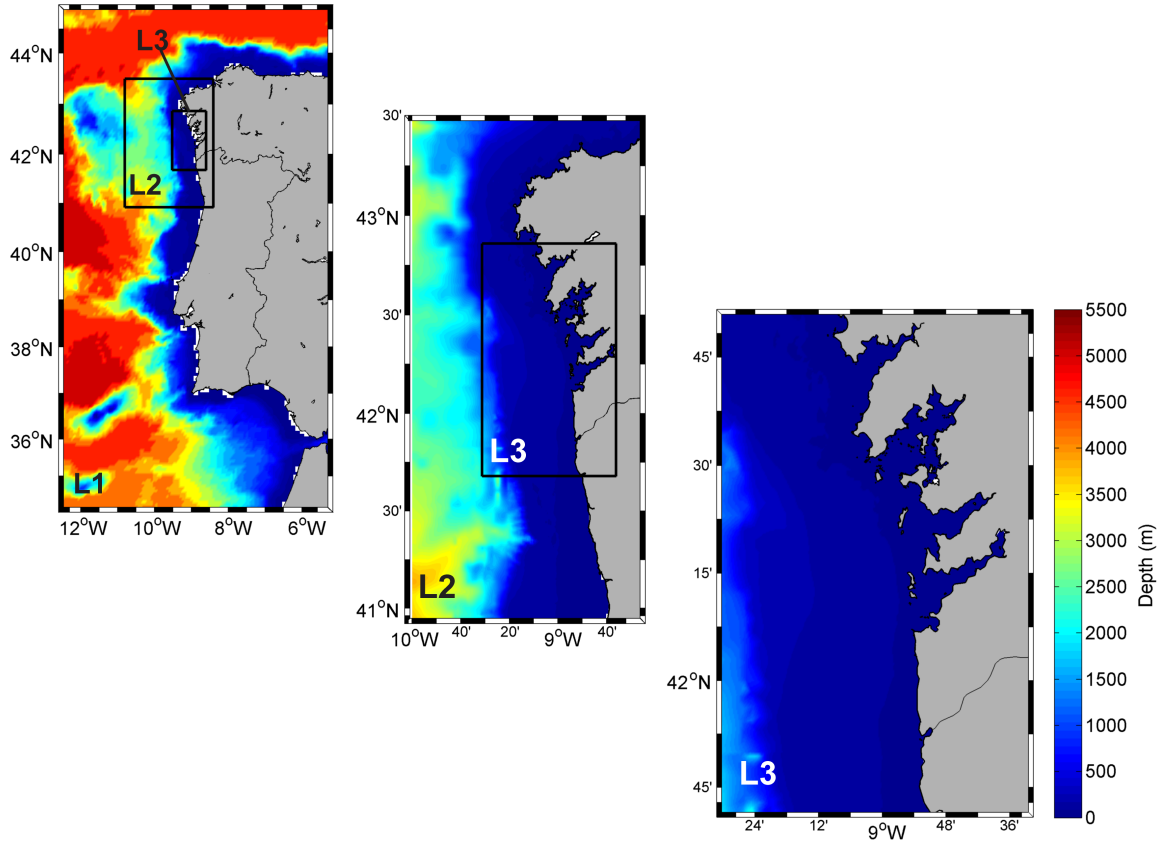

Figure 4.3: The MOHID nesting system implemented for Configuration #2.

Portuguese Coast Operational Modelling System (PCOMS) (`http://forecast.maretec.org/`) predictions [Mateus et al., 2012]. The system provides 3 days forecast of hourly ocean currents, sea surface height, water temperature and salinity.

The vertical resolution comprises 50 vertical layers, where the top are 7 sigma coordinate layers and the remaining 43 to the bottom are cartesian coordinates layers. The bathymetry is calculated by interpolation of the SRTM30 dataset. At the open boundary, the model downscales the solution of the General Circulation Model Mercator Ocean PSY2SV4. Tidal forcing results from a 2D barotropic model domain with 0.06° ($\sim$ 6 km) of resolution forced only with the FES2004 tidal atlas solution, using a Blumberg and Kantha [1985] radiation scheme. The surface forcing is provided by MM5 regional and local atmospheric forecasting model, supported by Instituto Superior Técnico. The variables used are air temperature, relative humidity, wind velocity at 10 m, solar radiation and downward long wave radiation. Bulk formulas are used to compute heat transfer between the atmosphere and the ocean.

The L2 and L3 have the same configuration as in Configuration #1 (Figure 4.3). The only difference is that the L2 and L3 are forced at the open boundaries with salinity, water temperature, three components of velocities and sea level from the father model (L1-PCOMS solution).

4.3.2 The Minho estuary model

Due to the low depth ($\sim$ 2 m) of Minho River estuary, the estuarine model was implemented in a 2D depth integrated mode. This procedure follows a methodology similar to that used by Vaz et al. [2007] for the Ria de Aveiro. In this configuration, a variable spatial step grid was developed due to the geometry of the estuary, which is characterized by several sand banks and islands. The grid has 119$\times$100 cells, with dimensions of 100 m in the inner part of the estuary and 650 m (300 m in the direction *y*) at the western boundary. The numerical bathymetry was interpolated from topo-hydrographic data measured by the Hydrographic Institute of the Portuguese Navy in 1978/1989/1999 (Figure 4.4). The model is forced by tides at the offshore open boundary and by river flow at the upstream end of the Minho River estuary. Tidal forcing at the oceanic open boundary is specified using a global tidal model [Le Provost et al., 1998].

The Minho river freshwater input was supplied by the "Confederación Hidrográfica del Miño-Sil". At the ocean and river boundaries, the water temperature and salinity are considered fixed, with typical values for the season of the simulation. At the surface, heat fluxes were imposed, using latent and sensible heat fluxes parametrizations based on the Dalton and Bowen laws, respectively [Chapra, 1997]. The meteorological data used for heat fluxes calculation were obtained from MeteoGalicia (`www.meteogalicia.es`). The time step defined for this application is 10 s, the horizontal eddy viscosity is 10 m^2 s^{-1}, and a constant value of 0.0025 is assumed for bottom rugosity. Initial conditions for the hydrodynamic model are null free surface gradient and null velocity in all grid points. For the transport model the initial conditions are constant values of salinity and water temperature.

The Minho estuarine model was developed to produce outflow properties (hydrodynamic and hydrographic variables) at the mouth of the estuary, as well as to maintain the computational efficiency. This outflow was computed along the section shown in Figure 4.4 (red rectangle). Hourly discharges flow were determined using the velocity

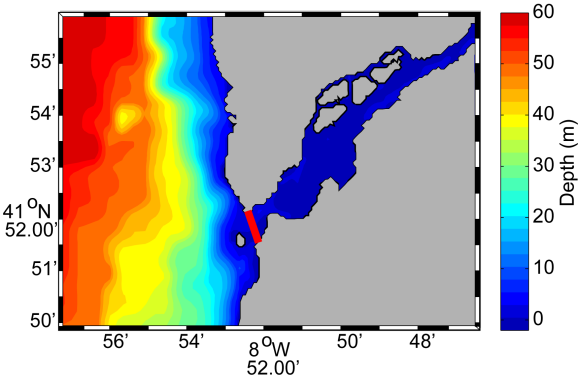

Figure 4.4: Minho estuary bathymetry with the location of the section (red rectangle) used to compute the Minho River outflow.

magnitude, depth and water level on the cells that define the section. The salinity and water temperature along the section were determined by the mean value for these cells. The outflow is imposed offline in the coastal nested models (Configurations #1 and #2). This methodology presents clear advantages in the reproduction of the Minho estuary-ocean interaction. Indeed, it takes into account the estuarine dynamics (e. g. tide and ocean-atmosphere interaction) and not a river represented by a point source with a constant outflow.

4.3.3 Comparison between Configurations #1 and #2

As it was previously mentioned, the Configurations #1 and #2 only differ in the source of the initial forcing conditions, more specifically in the salinity and water temperature patterns. As initial conditions, Configuration #1 uses Levitus climatology and the Configuration #2 uses Mercator Open Global Solution as boundary conditions. In order to evaluate which configuration is more accurate in order to represent the Minho estuarine plume propagation, model results were compared with remote sensing data covering the region under analysis and *in situ* data collected close to the Ria de Vigo mouth. The comparison between Configurations #1 and #2 was made for the period from January to March 2010. It was used six months and five days as spin-up for Configurations #1 and #2, respectively. The Configuration #1 has a longer spin-up than Configuration #2, because it initializes with a climatological solution, while Configuration #2 initializes with PCOMS model results. The spin-up is defined as the period after which each is considered that there is no significant spurious perturbation in the solution associated with the model initialization process [Leitão et al., 2005]. During these simulations the salinity and water temperature fields are generated. The initial conditions in the third nested model were interpolated from the previous level.

SST was obtained from Moderate-resolution Imaging Spectroradiometer (MODIS) (`http://oceancolor.gsfc.nasa.gov/`). MODIS is a key instrument comprising the Terra (EOS AM) and Aqua (EOS PM) satellites. The orbit is sun-synchronous, meaning that the satellite always passes over a particular part of the Earth at about the same local time each day. MODIS Aqua always crosses the equator from south to north at about 1:30 PM local time. One of the instruments on Aqua, MODIS, measures 36 spectral frequencies of light reflected off the Earth in a 2300-kilometers wide swath along this orbit, so that MODIS measures almost the entire surface of the Earth every day. The measurements can only be taken in ocean regions that are free of clouds. For the spatial comparison of the model results, predicted data (500 m) were interpolated for the satellite grid (1 km) using a cubic interpolation. Figure 4.5 shows SST maps obtained from satellite data and model predictions for Configurations #1 and #2 for the L3 domain.

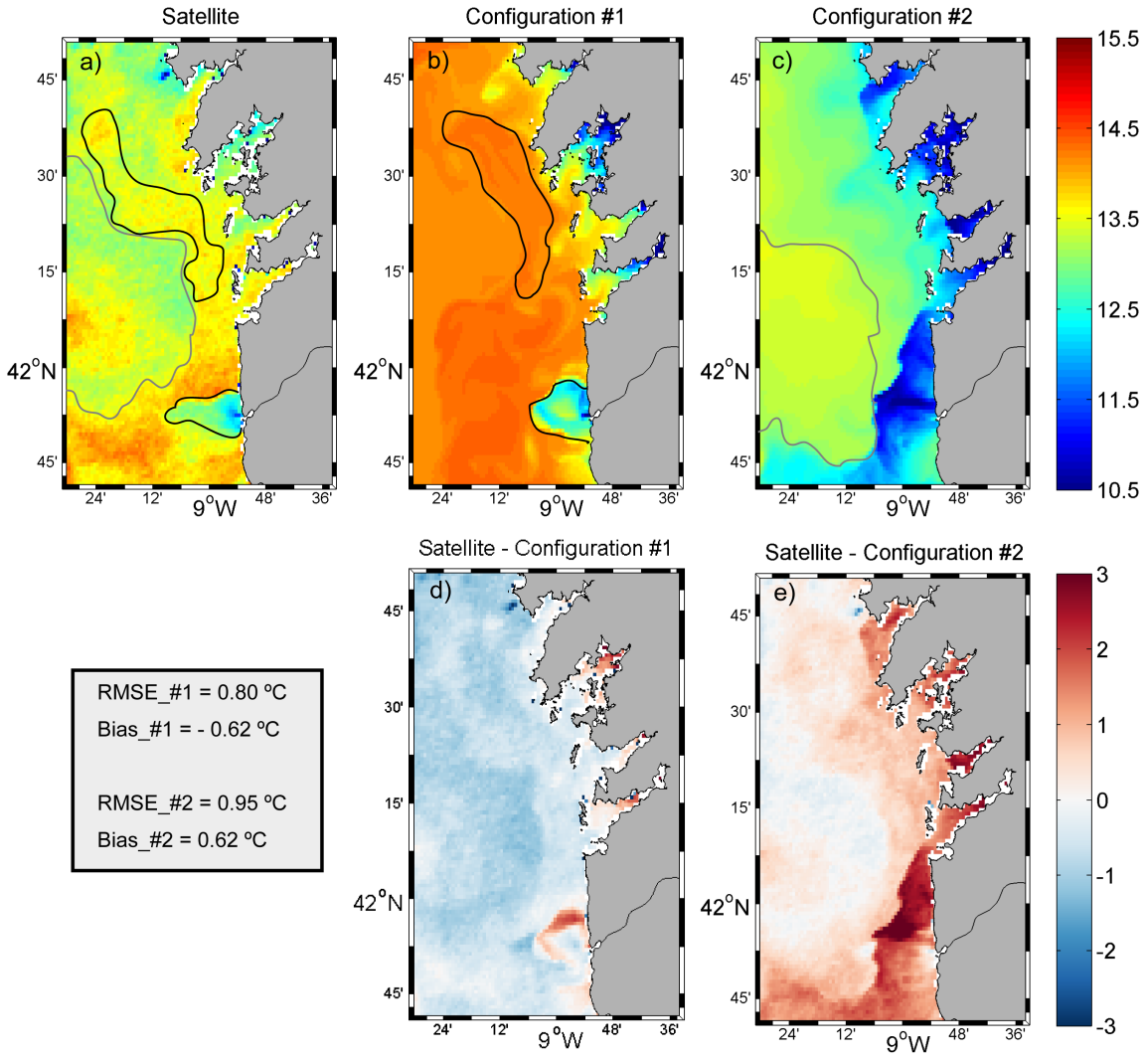

Figure 4.5: Sea surface temperature (ºC) on 1 February 2010 obtained from satellite data (a), model predictions (Configurations #1 and #2) (b,c) and respective difference (d,e). The computed RMSE and bias between satellite and model data are also shown.

In general, both configurations show the same spatial pattern of the Minho estuarine plume. In Configuration #1, the area of propagation of the plume is very similar to the observations (Figures 4.5a and 4.5b, black line), showing the same extension and water temperature values. In this configuration, in front of Rias Baixas the water temperature pattern (Figures 4.5a and 4.5b, black line) is also very well represented. On the other hand, the water temperature pattern offshore (Figures 4.5a and 4.5c, gray line) is better represented in Configuration #2.

The difference between satellite and model predicted SST and error analyses (RMSE and bias) were performed for both configurations. The RMSE and bias are also computed in order to quantify the difference between satellite and model data. In most of the region, the difference distribution shows negative values in Configuration #1 (Figure 4.5d), meaning that the model overestimates the SST (bias of -0.62 ºC). However, the lowest values (close to

zero) are observed in the area of propagation of the plume and close to the coast, revealing a good fit between predictions and satellite data. In Configuration #2 (Figure 4.5e) an underestimation of the SST (bias of 0.62 ºC) is observed in the entire region. However, Configuration #1 (0.80 ºC) has a RMSE slightly lower than the Configuration #2 (0.95 ºC), showing that the Configuration #1 represents better the main features of the surface water temperature field in the region under analysis. This result is very similar to the one obtained by Leitão et al. [2005] in the Algarve coast, revealing that the climatological solution is a good alternative to obtain the ocean salinity and water temperature.

Regarding the plume propagation, the configurations accuracy was also verified using salinity and water temperature data on a buoy moored at Cíes (44.16ºN, 8.91ºW, close to Ria de Vigo mouth) (Figure 4.6).

Generally, according to the results presented in Figure 4.6, the predictions obtained by Configuration #1 are more accurate for the salinity and water temperature. The bias (RMSE) for the salinity is 0.12 (1.16) and 1.55 (1.92) in the Configurations #1 and #2, respectively (Figure 4.6a). For the water temperature, the RMSE for Configuration #1 is 0.65 ºC, while for Configuration #2 is 1.78 ºC (Figure 4.6b). While the Configuration #1 results show a slightly warm (-0.47 ºC) bias, the Configuration #2 results show a significant cold bias (1.72 ºC). These high errors values obtained in Configuration #2 may be related to the initial conditions differences [Mateus et al., 2012], showing that the climatological solution fits the data better than the Mercator solution.

Considering the previous results, the Configuration #1 allows a better agreement with the water temperature and salinity data in the area of propagation of the Minho estuarine plume. Thus, in the next chapters, this nesting numerical modelling methodology

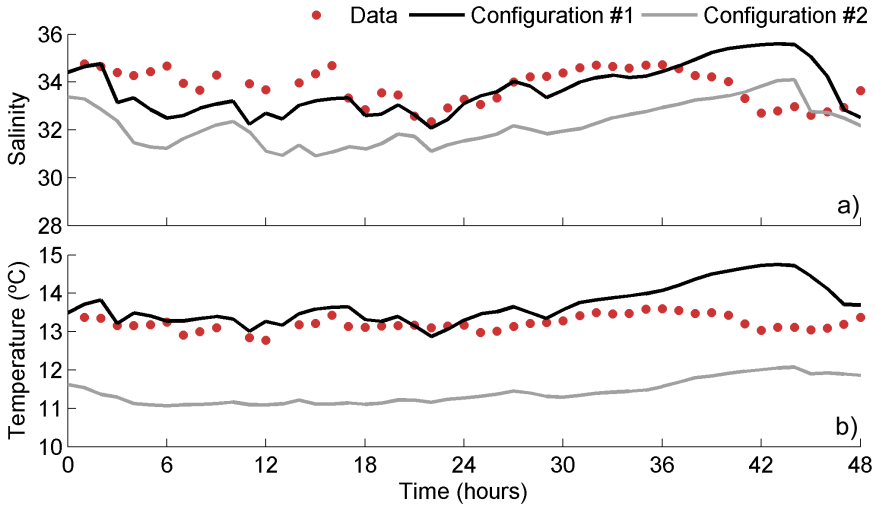

Figure 4.6: Observed and predicted (Configurations #1 and #2) salinity (a) and water temperature (b) time series at Cíes from 2 to 3 February, 2010.

(Configuration #1) will be used to study the evolution of the Minho estuarine plume, as well as its effect on the hydrography of the Rias Baixas.

Chapter 5

Model application on Minho River plume intrusion into the Rias Baixas

5.1 Introduction

The buoyancy generated by the Minho plume can flood the Rias Baixas for long periods, reversing the normal estuarine density gradients [Fiedler and Laurs, 1990; Alvarez et al., 2006], and motivating the research of its influence on these estuaries through several studies [Mourino and Fraga, 1982; Alvarez et al., 2006]. Their results show that the plume intrusion can generate an important salinity decrease at the estuaries mouth, with the water fresher than at the middle estuaries [Mourino and Fraga, 1982; Otero et al., 2013]. Consequently, the plume intrusion reverses the normal circulation pattern, with near bed water moving seawards and near surface water moving landwards, which tends to stop water exchange between estuaries and shelf [Alvarez et al., 2006; deCastro et al., 2006a]. In addition, the nutrient salts, the oxygen, the chlorophyll and the phytoplankton patterns can be modified suggesting the existence of blooms penetrating the Ria from the shelf, embedded in a water mass that is fresher than the estuarine one. According to deCastro et al. [2006a] the effects of the Minho river freshwater intrusion in the Ria de Pontevedra are characterized by a peculiar pattern of nutrient salt and oxygen distribution. The nutrient salt patterns show a decrease of nitrate down to undetectable values in the photic layer, while the oxygen distribution shows high oxygen saturation near the surface in the middle part of the estuary. This pattern results from the surface water mass originated from the mixing of coastal water and low-salinity nutrient-rich freshwater from the Minho River. Thus, the high concentration of nutrients from the Minho River fertilized the external and middle estuary leading to the development of diatom blooms and resulting in an extra feeding source for the main shellfish in the area. These studies show the relevance and need of the detailed

analysis of the effects of the Minho River plume on the Galician estuaries.

In fact, this area is characterized by a high primary productivity mainly due to spring-summer upwelling events that can support the high fishery and aquaculture yields in this region [Tenore et al., 1995]. Indeed, the Galician area produces around 250000 tons of mussels per year, i.e., around 15% of the world production. Consequently, knowledge of freshwater effects in these areas greatly facilitates the management of many exploited and protected species. Due to the lack of continuous and simultaneous *in situ* measurements along coastal estuaries as the Rias Baixas, the use of numerical models is therefore a reliable and useful tool to understand the complex structure of the oceanographic variables and circulation patterns that characterize these particular environments.

The present review of the literature showed that the Minho river plume influence inside the western Galician estuaries has not been previously studied in detail, namely by means of numerical model applications specifically designed for this purpose. Thus, this chapter aims to study the propagation and influence of Minho estuarine plume on the Rias Baixas circulation and hydrography. Additionally, it describes the validation of a nesting numerical modelling methodology (Configuration #1) developed to reproduce the propagation of the Minho estuarine plume towards the Rias Baixas, using a downscaling approach. In this context, the model ability to reproduce the Minho River plume intrusion into the Rias Baixas is analysed for the spring of 1998, since in this year was reported a high Minho River discharge as well as favourable wind patterns to advect the river plume towards the Rias Baixas, inducing an inverse circulation [Alvarez et al., 2006]. Field data is compared to the profiles predicted by the model in this situation to validate the model results. Finally, the possible effect of this high discharge and wind on the Rias Baixas circulation and hydrography is also analysed.

5.2 Methodology

5.2.1 Model validation

Two sets of simulations were performed to validate the settings of the model in reproducing the evolution and fate of the estuarine plume originated from the Minho freshwater discharge, using the initial and boundary conditions described in Section 4.3.1.1 (Configuration #1). The first one was dedicated to evaluate the Minho estuary model accuracy and the second one to evaluate the coastal nested model including the Rias Baixas (L3) (Figure 5.1a) under a high Minho River discharge.

The sets of simulation of the Minho estuarine model covers the period between February (model spin-up) and March 2006, and only the results of March 2006 were used for the validation.

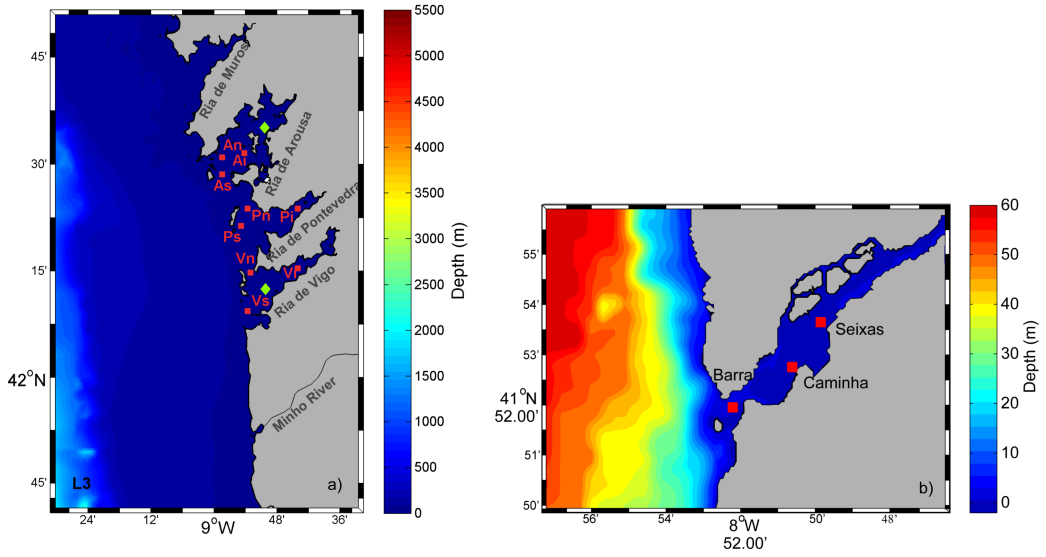

Figure 5.1: Rias Baixas (a) and Minho estuary (b) bathymetries with indication of sampling stations position (red squares) and tide gauges (green diamonds). The *n*, *s* and *i* indices correspond to the northern mouth, southern mouth and inner-middle areas of the Rias, respectively.

The model prediction skill for the Minho estuary is evaluated through a qualitative and quantitative comparison of the temporal evolution of predicted sea surface elevation (SSE), salinity and water temperature and concurrent *in situ* data. First, a visual comparison between observed and predicted times series of SSE at Barra (41° 52.0'N, 8° 51.2'W), Caminha (41° 52.4'N, 8° 50.5'W) and Seixas (41° 54.0'N, 8° 48.2'W) (Figure 5.1b, red squares) was done. Next, in order to quantify the model accuracy in reproducing *in situ* data, RMSE and predictive skill [Warner et al., 2005] at same stations are computed following the methodology proposed by Sousa and Dias [2007] and Dias et al. [2009]. The comparison between harmonic constituents [Pawlowicz et al., 2002] computed from the model results and observations is another quantification method used to perform the evaluation of the model accuracy. This methodology was applied in this study, by comparing the harmonic constants of the major tidal constituents in the Minho River estuary (M_2, S_2, K_1 and O_1) for the stations shown in Figure 5.1b. Computed and observed salinity and water temperature were also compared to evaluate the transport model accuracy. These comparisons were performed at two locations (Figure 5.1b) inside the estuary.

The validation of L3 is performed in two steps: first, the propagation of the astronomical tidal wave is evaluated and second, the Minho estuarine plume dispersion is analysed over the period 1-13 May 1998. This simulation was made for the period of November 1997 to May 1998, and the first six months of the simulation are considered as spin-up.

To verify the accuracy of model predictions for the Rias Baixas (L3, Figure 5.1a), SSE outputs from a hydrodynamic simulation from 1 to 18 May 1998 are compared with synthesized tides for Vigo (42° 14.4'N, 8° 43.8'W) and Villagarcia (42° 36.0'N, 8° 46.2'W)

(Figure 5.1a, green diamonds). The tide was synthesized from local tidal constituents. The RMSE, predictive skill and harmonic analysis are also computed.

The model ability to reproduce the pattern of the Minho estuarine plume dispersion is also analysed, comparing SST horizontal fields and salinity vertical profiles predicted by the model with satellite measurements and results obtained by Alvarez et al. [2006] inside the Rias Baixas. SST data was obtained by the Advanced Very High Resolution Radiometer (AVHRR) sensors provided by the AVHRR/Pathfinder. SST daily data are available from 1986 to 2006 with a high spatial resolution of 4.5 km. The *in situ* salinity data available was measured weekly at three sampling stations located at the southern (wider and deeper) and northern mouths, and in the inner-middle areas of the Rias de Vigo, Pontevedra and Arousa, during May 1998 (Figure 5.1a, red squares). These measurements were made using conductivity-temperature-depth (CTD) instruments (Seabird19 and 25). Salinity calibration was previously performed by means of an "Autosal" salinometer. Regarding the circulation pattern, the accuracy of the model is also analysed using current meter data taken at the inner-middle part of the Ria de Pontevedra (42° 23.51'N, 8° 44.29'W) during eight hours on 12-13 May 1998. Current velocity data was measured *in situ* by means of an Electromagnetic Current Meter (Valeport Model 808) at six different depths during 5 min at each depth. The same protocol was repeated every 30 minutes during a tidal cycle.

5.2.2 Influence of Minho estuarine plume on Rias Baixas circulation and hydrography

The impact of the buoyant plume in the circulation and thermohaline patterns of Rias Baixas is also evaluated from 1 to 18 May 1998. Figure 5.2 shows the daily Minho River discharge (black line) and the meridional wind component at a point located close to the Minho River mouth (42°N, 9°W) for the period 19 April-17 May 1998. The river discharge shows an atypical pattern with high values during early May (1600 m^3 s^{-1}; Figure 5.2a, black line). The meridional wind component is variable, with strong fluctuations in direction and intensity. The prevailing winds are from the north, with intensities higher than 5 m s^{-1}.

Thus, in order to assess the individual effect of Minho outflow and wind forcing on the establishment of negative circulation in Rias Baixas, two new simple simulations were designed, keeping most of the setups described in previous section, but changing the wind and river discharge characteristics. The first one was run considering essentially the wind effect, adopting a river discharge where the maximum values from 1 to 3 May were removed, and a constant average value (833 m^3 s^{-1}) between 30 April and 4 May was considered (Figure 5.2a, dashed gray line). The second one analysis essentially the river discharge effect, considering the real discharge (Figure 5.2a, black line), but removing the wind from 1 to 13 May 1998. With this procedure is also studied the effect of the Minho estuarine outflow

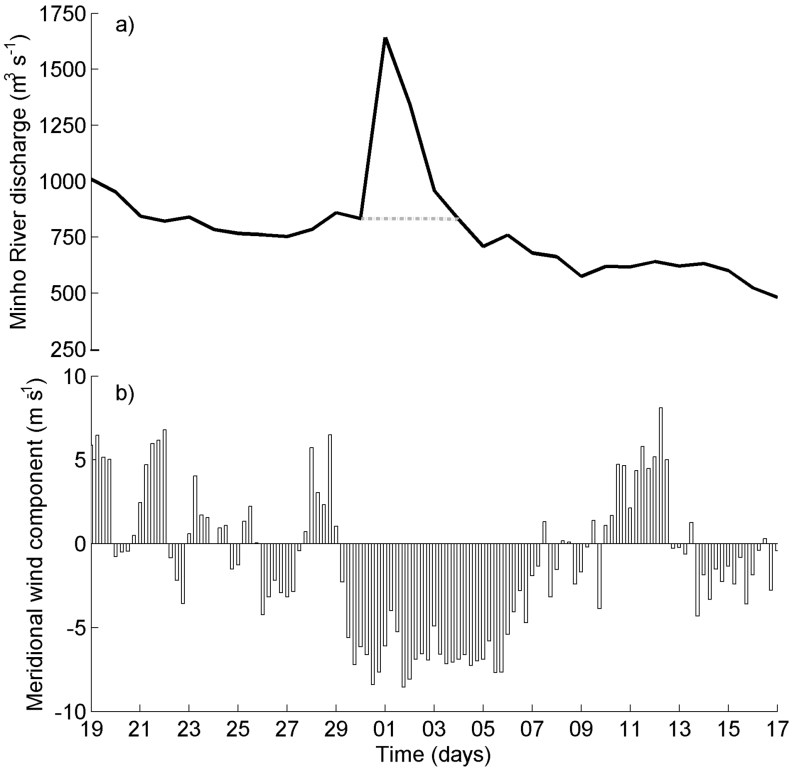

Figure 5.2: Minho River discharge between 19 April and 17 May 1998 (black line) (a). Meridional wind component (b).

in the circulation and hydrography of the Rias Baixas and understood the effects of its main driving forces.

5.3 Results and discussion

5.3.1 Model validation

5.3.1.1 Minho estuary

SSE, salinity and water temperature data sampled at the Minho estuary during February 2006 by the Hydrographic Institute of Portugal under the project ”Estuarine Contributions to Inner Shelf Dynamics (ECOIS)” were used to validate the 2D estuarine model.

Figure 5.3 shows the observed and predicted SSE at three tidal stations (Figure 5.1b). The predicted tidal elevations closely follow the observed records, revealing that the numerical model reproduces the tidal propagation inside the estuary. The average RMSE and the predictive skill are 0.16 m and 0.96, respectively. These values are very similar to those obtained in previous numerical modelling works for other estuaries, such as the Ria

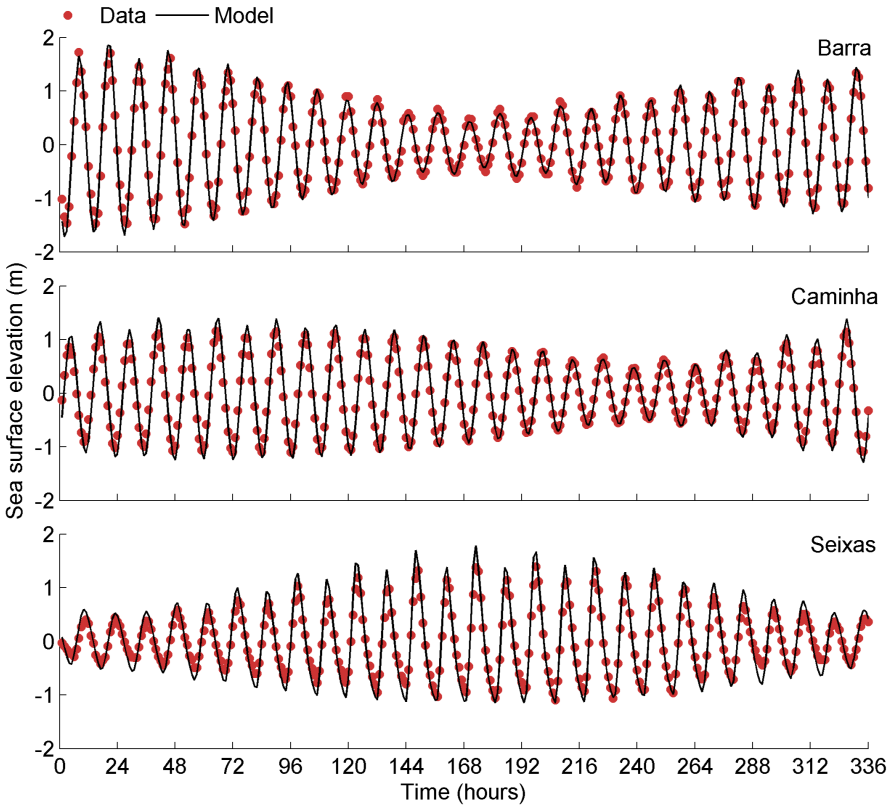

Figure 5.3: Observed and predicted sea surface elevation time series at Barra, Caminha and Seixas.

de Aveiro [Sousa and Dias, 2007; Vaz et al., 2009a] and the Ria Formosa [Dias et al., 2009], and show that the estuarine model accuracy is excellent.

The amplitudes and phases for M_2, S_2, K_1 and O_1 constituents at Barra, Caminha and Seixas are determined (Table 5.1) through harmonic analysis [Pawlowicz et al., 2002] of 30 days time series for both observed and predicted SSE.

The distributions of both observed and predicted amplitude and phase are very similar. The tide is semi-diurnal with low diurnal inequality, with form number of about 0.08. At all stations, M_2 presents the highest amplitude decreasing upstream. For this constituent, the phase errors range from 9 to 30 min in Barra and Caminha, respectively (Table 5.1). The model predictions for Barra are more accurate than for the remaining stations, with amplitude errors of 0.06 m for both semidiurnal constituents. Both in amplitude and phase, the highest differences between model predictions and observed data correspond to Caminha and Seixas stations. These differences are due to bathymetric constraints that are more significant between Caminha and Vila Nova de Cerveira [Reis et al., 2009]. The results for the diurnal constituents reveal a good agreement between model predictions and observations, with average amplitude (phase) errors of about 10% (11.5°) and 17% (10.6°) for the constituents K_1 and O_1, respectively. In summary, the harmonic analysis results

Table 5.1: Harmonic analysis results comparison of observed and predicted sea surface elevation data for Barra, Caminha and Seixas (M_2, S_2, O_1 and K_1 constituents).

	Tide gauge	Amplitude (m)			Phase (°)		
		Data	Model	Difference	Data	Model	Difference
M_2	Barra	0.98	1.04	-0.06	84.74	80.65	4.09
	Caminha	0.87	0.98	-0.11	95.62	80.94	14.68
	Seixas	0.72	0.84	-0.12	106.87	99.63	7.24
S_2	Barra	0.43	0.49	-0.06	122.55	114.97	7.58
	Caminha	0.37	0.45	-0.08	137.91	116.30	21.61
	Seixas	0.26	0.36	-0.10	156.07	139.98	16.09
O_1	Barra	0.05	0.06	-0.01	324.53	320.03	4.50
	Caminha	0.06	0.06	0.00	338.96	324.47	14.49
	Seixas	0.04	0.05	-0.01	325.60	341.11	-15.51
K_1	Barra	0.05	0.05	0.00	64.17	79.17	-15.00
	Caminha	0.05	0.05	0.00	94.28	84.11	10.17
	Seixas	0.07	0.05	0.03	93.57	100.42	-6.85

show that the amplitude and phase of the major tidal constituents are well reproduced by the model.

The water temperature and salinity predictions accuracy is also investigated at the Minho estuary. These variables can be strongly influenced by the freshwater discharge and the validation of the salt and heat transport becomes an interesting and challenging issue. Salinity and water temperature data sampled at Barra and Seixas during two tidal cycles was available for comparison with model predictions (Figure 5.4). This comparison shows that the model reproduces the variability of the thermohaline properties, with small differences in water temperature values. The maximum RMSE value was determined for Barra station, with a value of 0.89 ℃, which represents about 30 % of the local water temperature amplitude. For the salinity, the RMSE values are typically about 8% of the local salinity amplitude. According to these results is considered that the model reproduces the heat and salt transport inside the Minho estuary and consequently was considered validated.

5.3.1.2 Rias Baixas

The dataset used in the validation of the Rias Baixas model comprises harmonic constants of the main tidal constituents obtained at the mouth of the Rias Baixas (available from Puertos del Estado) and hydrographic parameters surveyed in the Rias during May 1998.

In Figure 5.5 the predicted and synthesized SSE at Vigo and Villagarcia stations are represented. In general, a good agreement between the predicted and synthesized SSE for both stations is achieved, revealing the ability of the model to reproduce the data. The RMSE between computed and synthesized time series is 0.06 m and 0.05 m for Villagarcia and Vigo stations, respectively. The predictive skills are close to 1 for both stations, confirming

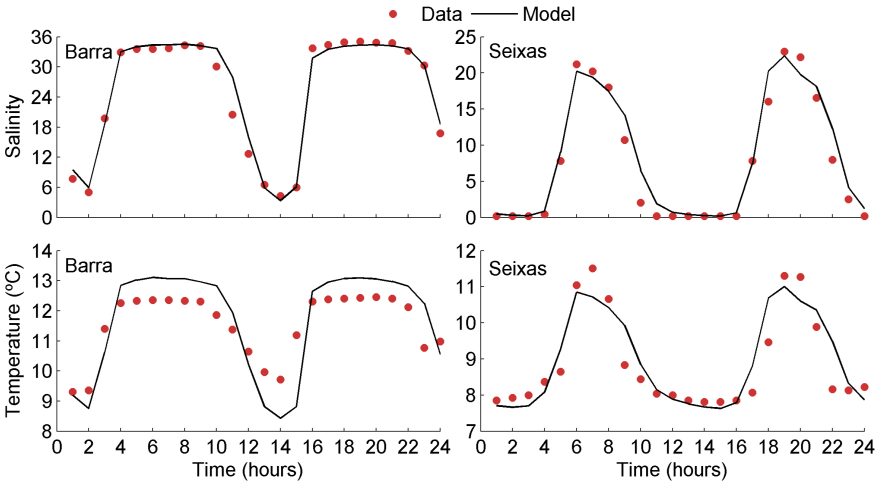

Figure 5.4: Observed and predicted salinity and water temperature time series for Barra and Seixas.

the excellent agreement between both datasets.

Harmonic analysis was also applied to predict SSE for Rias Baixas, to comparison with the harmonic constants available from Puertos del Estado for the Villagarcia and Vigo. Results of the amplitude and phase of the harmonic constants M_2, S_2, O_1 and K_1 determined are presented in Table 5.2.

The agreement between predicted and observed values is very good both in amplitude and in phase for the semi-diurnal and diurnal constituents, which are the major tidal

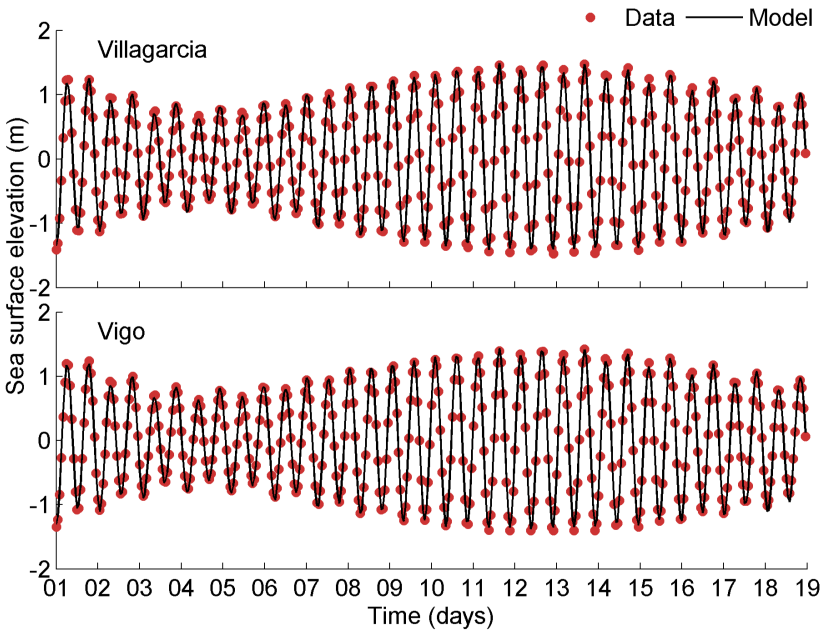

Figure 5.5: Model results and predicted sea surface elevation time series at Villagarcia and Vigo.

constituents in the Rias Baixas and near coastal region [Marta-Almeida and Dubert, 2006; Herrera et al., 2008].

For the M_2 constituent, whose amplitude is the largest, the difference between datasets is 0.01 m. In Villagarcia, the phase difference is 2.6°, which means an average delay between the observed and predicted tide of about 5.5 minutes for this constituent. For the Vigo station, the average delay is lower (about 2.5 minutes), revealing a good phase agreement. For the diurnal constituents the amplitude and phase agreement may be considered good for both stations (about 0.01 m for amplitude and 10° for phase in Vigo). The results from the harmonic analysis show that the tide should be classified as semidiurnal (form number $\approx$ 0.07) and that semidiurnal constituents together determine about 90% of the astronomic tide in Western Galician coast. This last result is in accordance with findings from previous studies [Marta-Almeida and Dubert, 2006; Herrera et al., 2008].

The wind and river runoff affects the dispersal of estuarine plumes, influencing the transport and mixing of plume waters [Choi and Wilkin, 2007]. Thereby, it is important to evaluate the model accuracy to reproduce the Minho estuarine plume under different conditions.

One way of validating the accuracy of model results spatial variability consists in comparing model predicted SST horizontal fields with satellite measurements. For the spatial comparison, model data were interpolated for the satellite grid (4.5 km) using a cubic interpolation. The modeled SST is calculated by daily averaging the model predictions at each grid cell. Thus, Figure 5.6 shows SST patterns obtained from model predictions and satellite data on 3 May 1998 (northerly winds, Figure 5.2b) and 11 May 1998 (southerly winds, Figure 5.2b).

The results show that wind plays an important role in the dispersion of the Minho estuarine plume. When the wind blows southwards (Figure 5.6, upper panel), the main feature is the offshore extension of the plume. Otherwise, northward wind (Figure 5.6, lower panel) spreads the river plume towards the Rias Baixas, confining it close to the coast. In this case the plume reaches the mouth of the Ria de Pontevedra, influencing its inner

Table 5.2: Harmonic analysis results comparison of observed and predicted sea surface elevation data for Villagarcia and Vigo (M_2, S_2, O_1 and K_1 constituents).

	Tide gauge	Amplitude (m)			Phase (°)		
		Data	Model	Difference	Data	Model	Difference
M_2	Villagarcia	1.06	1.07	-0.01	83.07	80.47	2.60
	Vigo	1.02	1.03	-0.01	80.25	79.06	1.19
S_2	Villagarcia	0.44	0.41	0.03	100.89	97.32	3.57
	Vigo	0.42	0.40	0.02	97.66	95.78	1.88
O_1	Villagarcia	0.06	0.07	-0.01	323.22	323.59	-0.37
	Vigo	0.06	0.07	-0.01	318.96	332.52	-13.56
K_1	Villagarcia	0.05	0.08	-0.03	32.86	42.98	-10.12
	Vigo	0.06	0.08	-0.02	47.87	42.60	5.27

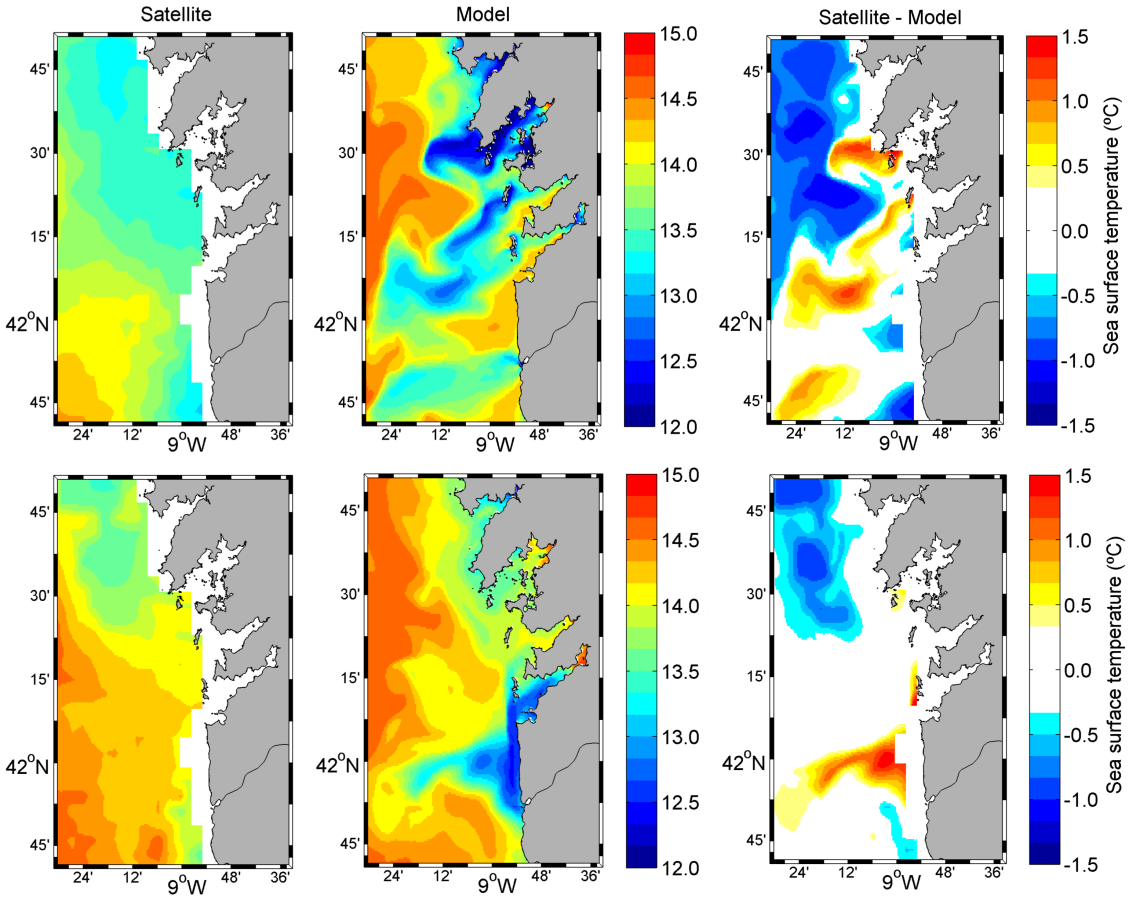

Figure 5.6: Sea surface temperature maps obtained from satellite data, model predictions and respective difference on 3 May 1998 (upper panel) and 11 May 1998 (lower panel).

physical properties.

Both the measured and predicted SST patterns show approximately the expected main features of the water temperature field in the region under analysis, which is characterized by higher temperatures offshore that decrease toward the coast (Figure 5.6).

In both periods there is a satisfactory agreement between the observations and predictions of the plume, although the adjustment quality tends to decrease offshore and close to the river mouth (Figure 5.6, lower panel). More specifically, in the area of spread of the plume it should be considered the existence of a small satellite land mask near shore and the satellite coarse resolution. These results are very similar to those obtained in previous numerical modelling works [Otero and Ruiz-Villarreal, 2008; Marta-Almeida et al., 2012], revealing that the numerical model developed reproduces adequately the plume propagation.

The difference between satellite and model predicted SST was determined to evaluate and quantify the model accuracy (Figure 5.6). The difference distribution shows negative values in the northwestern Galician coast for both scenarios, meaning that the model underestimates SST in this region. However, the lowest values (close to zero) are

observed in the area of spread of the plume, revealing a good fit between predictions and measurements in the reproduction of the estuarine plume. Nevertheless, it is necessary to keep in mind that the predicted water temperature is the average of the surface layer, whose thickness is about 1 m, while the satellite data refers to the ”skin” temperature. The top ocean ”skin” has approximately 0.01 mm or less, which may not represent the bulk temperature of the upper ocean layer due primarily to effects of solar surface heating, reflected radiation, as well as sensible heat loss and surface evaporation. All these factors make it somewhat difficult to compare satellite data with predicted SST [Robinson, 2004]. Considering that the temperature measured by the satellite is usually lower, it is reasonable to assume that the model simulates adequately the thermodynamics of the top sea layer. These differences between model and satellite data are consistent with values described in the literature, where differences of the order of 1-1.5 ℃ are found.

Figure 5.6 shows that when the wind blows from the south the Minho estuarine plume reaches the Rias Baixas. To investigate this freshwater intrusion, the salinity vertical profiles predicted by the model were compared with salinity measurements at the sampling stations shown in Figure 5.1a (Figure 5.7). According to Alvarez et al. [2006] the waters from the Minho River modulate an abnormal horizontal salinity gradient along the axis direction of the Ria de Vigo and Pontevedra, corresponding to fresher water at the mouth of both Rias

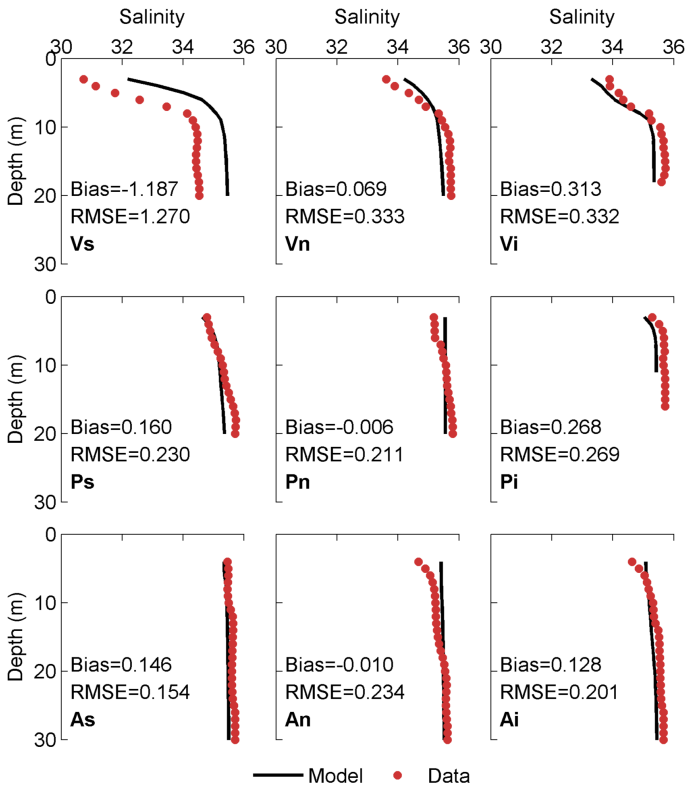

Figure 5.7: Observed and predicted salinity vertical profiles for the sampling stations shown in Figure 5.1.

than at the inner-middle region. This situation contrasts with the typical salinity pattern, corresponding to the normal Rias Baixas dynamics, with saltier water near the mouth.

The *in situ* salinity data reveals an abnormal salinity gradient along the axis direction for the Rias de Vigo and Pontevedra. The southern mouths of the Rias are less saline than the innner region, i.e. an inverse circulation is observed. This difference is more marked in the Ria de Vigo. On the contrary, the Ria de Arousa shows a different salinity gradient, being the water near the mouth saltier than in the inner part of the estuary, corresponding to the typical pattern of an estuarine system. A similar situation is observed in the model predictions. The increase in salinity from south to north shows that the low salinity values are not generated by the rivers inside the Rias, since the highest river runoff corresponds to the Ria de Arousa (the northernmost one) [Alvarez et al., 2006].

Analysis of Figure 5.7 shows that the model overestimates salinity values in the southern mouth of the Ria de Vigo. Nonetheless, the halocline is well reproduced by the model for all stations, being predicted at the same depth.

The maxima RMSE values (1.27) between model predictions and measurements are observed in the Ria de Vigo. For the other stations, RMSE values range from 0.15 to 0.33. The bias was also determined, showing positive values for most of the stations, which indicate that the model predictions tend to overestimate *in situ* salinity. The highest biases (about -1.19) are also observed in the Ria de Vigo. These values can be explained by an improper prescription of the landward boundary condition or a malfunction of the CTD instrument.

The observed and predicted along estuarine circulation in the inner-middle part of Ria de Pontevedra between 12 and 13 May 1998 is also shown in Figure 5.8. Both measured and predicted currents patterns show a negative estuarine circulation in the inner-middle part of Ria de Pontevedra (Figure 5.1), which is characterized by near surface water moving landward and near bed water moving seaward, in accordance with previous findings presented by deCastro et al. [2004].

In general, the predictions reproduce the main features of the observed velocity vertical structure, although the adjustment quality tends to decrease near the surface. The observed maxima velocities are 0.10 m s^{-1} on the surface, while the predicted velocities are 0.06 m s^{-1}, meaning that the model underestimates the velocity in this region. No significant differences are observed near bed, showing a good agreement between predictions and measurements. It is important to note that, according to previous research in the area [deCastro et al., 2000], the wind effects inside the estuary may dominate the current at surface layers, while bottom layers are mainly controlled by tide. Nevertheless, it should be considered that the wind field used in this implementation (5 km resolution) does not have enough resolution to properly solve the associated features of the estuary.

Although the errors are not negligible, especially on the surface layers, the validation results show that the model developed in this study adequately reproduces the

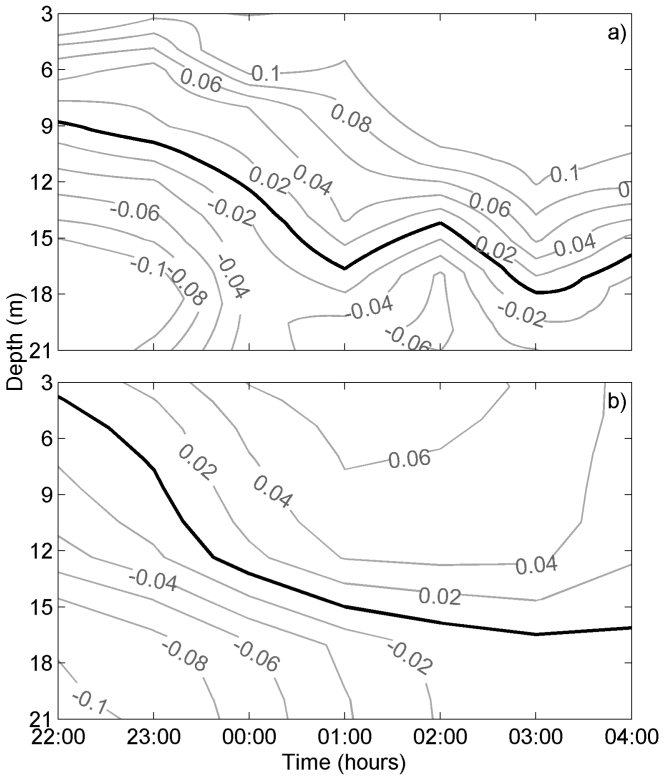

Figure 5.8: Observed (a) and predicted (b) along estuarine circulation (m s^{-1}) in the inner-middle part of Ria de Pontevedra on 12-13 May 1998. Black line corresponds to 0 m s^{-1}.

hydrodynamic behaviour of the Rias Baixas. Therefore, the model is a useful and suitable tool to study of Rias Baixas circulation and hydrography, and in particular for the analysis of the intrusion of the Minho estuarine plume in these coastal regions.

5.3.2 Negative circulation in Rias Baixas

The model developed in this study was used to investigate the influence of Minho estuarine plume on the generation of the inverse circulation episodes in Rias Baixas, as the one described by Alvarez et al. [2006]. These authors observed that high Minho River discharge and favourable southern winds spread the Minho river plume towards the Rias Baixas affecting thermohaline properties inside the estuaries on 12-13 May 1998.

Surface salinity maps (Figure 5.9, top) predicted by the model show a northward spread of the Minho River plume reaching the Ria de Vigo on 11 May. During the following days the northward displacement of the plume continued and the plume intrusion is observed in the Ria de Pontevedra on 13-14 May. This situation generates an unusual surface salinity pattern at these locations. The Rias Baixas normal salinity pattern is characterized by the presence of saltier water at the outer part of the estuary and freshwater at the middle-inner part. In contrast with this normal behavior, the existence of an important external freshwater

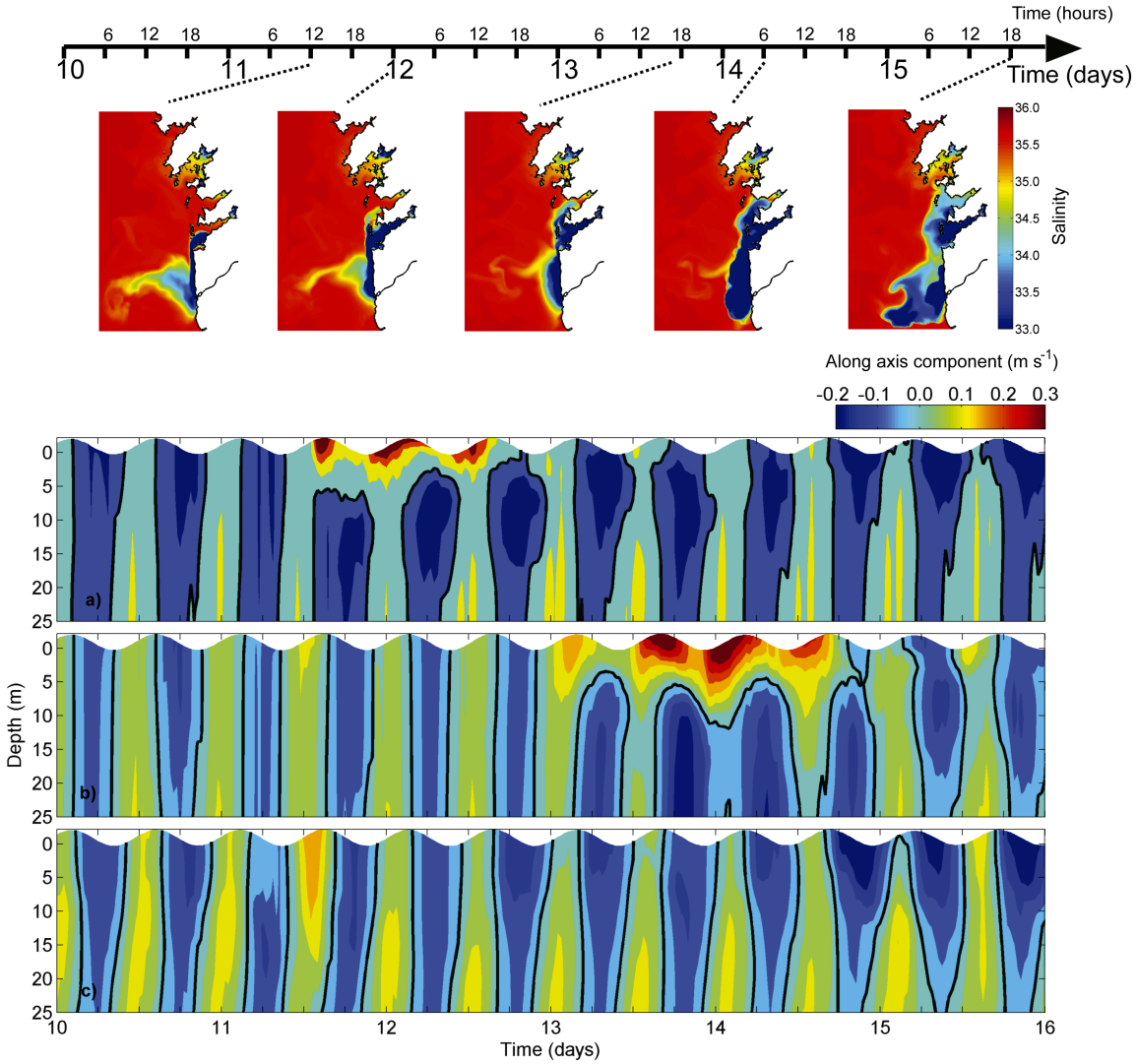

Figure 5.9: Evolution of surface salinity. Along estuarine circulation at stations located at mouths of Rias de Vigo (a), Pontevedra (b) and Arousa (c) between 10 and 15 May 1998. Black line corresponds to 0 m s^{-1}.

supply in an estuary can generate a reversal of the normal salinity and consequently a reversal of the normal estuarine circulation [Alvarez et al., 2006; deCastro et al., 2006a].

The along axis circulation at the mouth of Rias de Vigo, Pontevedra and Arousa is also calculated. Figure 5.9a corresponds to the current pattern at the Ria de Vigo calculated from 10-16 May. Between 11 and 13 May, an unusual circulation (upstream circulation) at the upper layers (up to 5-8 m) with water moving landward is observed, with the highest velocities (0.30 m s^{-1}) between 0-2 m. The presence of southwesterly winds during this period favoured the reversal of the positive circulation resulting in the introduction of the Minho estuarine outflow into the Ria. Chao [1988b], Soares et al. [2007] and Marques et al. [2009] also observed that downwelling winds reverses the surface current, enhancing the mixing processes in their studies for La Plata River and Patos Lagoon. This reverse estuarine circulation may have some ecological consequences. It introduces the

dinoflagellate blooms that are generated in coastal waters into the Rias [Fraga et al., 1988; Sordo et al., 2001], thus decreasing the abundance of marine species in this area.

Thus, the surface current is mainly controlled by the plume intrusion while the tidal effect is only observed at the bottom layers. This pattern is in accordance with the results obtained for the Willapa Bay by Banas et al. [2004], where the Columbia River plume enters the mouth at all depths under a strong tidal flow and the axial gradient can in fact reverse for sustained periods. These forcing conditions confines the Minho plume close to the coast, where a less saline region is developed, as found by Otero and Ruiz-Villarreal [2008].

The Ria de Pontevedra (Figure 5.9b) shows a similar circulation pattern although, in this case, surface water moving landward is observed between 13-15 May. In addition, this unusual circulation is more intense than for the Ria de Vigo with positive values of the along axis current until 10 m. In fact, around 13-14 May it is also possible to see bottom water moving seaward along one tidal cycle, which results in a negative estuarine circulation during this period. The results also agree with those reported by Alvarez et al. [2006], who found this negative estuarine circulation in a station located at the middle-inner estuary. Therefore, the existence of freshwater supplied from the Minho River could generate this unusual circulation, which tends to stop water exchange between this Ria and the shelf, increasing the residence time and consequently changing water quality. This reversal poses a selective force on the phytoplankton assemblage. Diatoms are unable to counteract under these conditions and are therefore removed from the water column [Pitcher et al., 2010]. On the other hand, the high concentration of nutrients from the Minho River could fertilize the external part of the estuary, resulting in an extra feeding source for the main shellfish in the area [deCastro et al., 2006a]. Finally, the Ria de Arousa (Figure 5.9c) shows a normal estuarine circulation (outflow in the surface layer and inflow in the bottom layer) with the whole water column following the tidal cycle, landward during flood and seaward during ebb, without influence of the Minho estuarine plume.

5.3.2.1 Minho outflow and wind effect on Rias Baixas negative circulation

River discharge and wind are important in the modulation of the vertical and horizontal spreading of an estuarine plume. In fact, their temporal variability forces vertical and horizontal mix between buoyant and coastal waters. As it can be observed in the previous results, episodes of moderate-high river discharge combined with southern winds could result in a plume with a northward direction, affecting coastal estuaries located north of the river mouth, and reversing the normal estuarine circulation [Fiedler and Laurs, 1990; Roegner et al., 2002; Hickey and Banas, 2003]. The presence or absence of the plume may provide an important environmental distinction between the estuaries as well as between nearshore coastal regions.

Considering the results of the simulations described in section 5.2.2, for the first scenario (removing the high river discharge from 1 to 3 May), the obtained pattern (Figure 5.10) is very similar to the simulation with real river discharge (Figure 5.9a) with no significant differences at the Rias Baixas mouth. Choi and Wilkin [2007] also demonstrated through numerical modelling a greatest similarity between a steady-low and high discharge events in Hudson River mouth. These results show that the high Minho River discharge, observed at the beginning of May, is not directly responsible for the abnormal hydrographic patterns found at the Rias Baixas, indicating that a continuous and moderate river discharge (500-1000 m^3 s^{-1}) may be enough to produce the negative circulation pattern.

In fact, using wind data provided by the NCEP Climate Forecast System Reanalysis (CFSR; `http://rda.ucar.edu/pub/cfsr.html`) at a control station located near the mouth of the Minho River and river runoff data from 1979 to 2010 (period of available discharge for the Minho River), a percentage analysis of events occurring under northward winds was carried out (Table 5.3). It is found 27% of events at moderate river discharge ($>$ 500 m^3 s^{-1}) under northward wind conditions, showing the importance of studying these situations.

Without wind forcing (second scenario), the plume is displaced over the shelf, creating a bulge in front of the river mouth during the first days. Then, the low salinity waters are

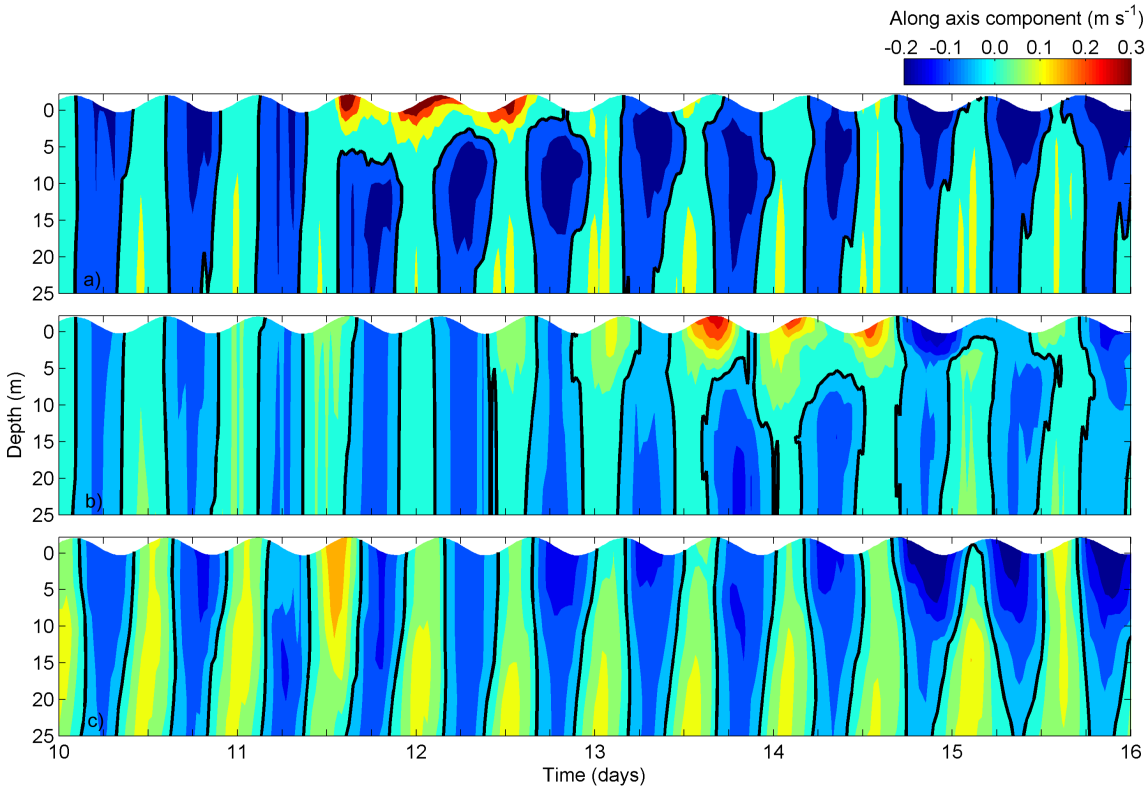

Figure 5.10: Along estuarine circulation at station located at mouths of Ria de Vigo (a), Pontevedra (b) and Arousa (c) between 10 and 15 May 1998, considering constant river discharge. Black line corresponds to 0 m s^{-1}.

Table 5.3: Percentage of events obtained for each range of discharges occurring under northward winds.

Limits of river discharge (m^3 s^{-1})	Percentage of events (%)
<500	73
500-750	17
750-1000	6
1000-1250	2
1250-1500	1
>1500	1

advected to the right extending northward (along the coastline) reaching the Ria de Vigo mouth (Figure 5.11a). In this situation, the plume effect is observed earlier (between 6-8 May) affecting only near surface layers, being surface currents weaker in this case than in the real one (Figure 5.9a), which is consistent with the results by Marques et al. [2009] for the Patos Lagoon. For the other Rias (Figures 5.11b and 5.11c), the classical estuarine pattern is observed, showing that without wind forcing the Minho estuarine plume does not influence their circulation pattern. Therefore, southerly winds tend to mix the water column and to reverse the normal estuarine circulation.

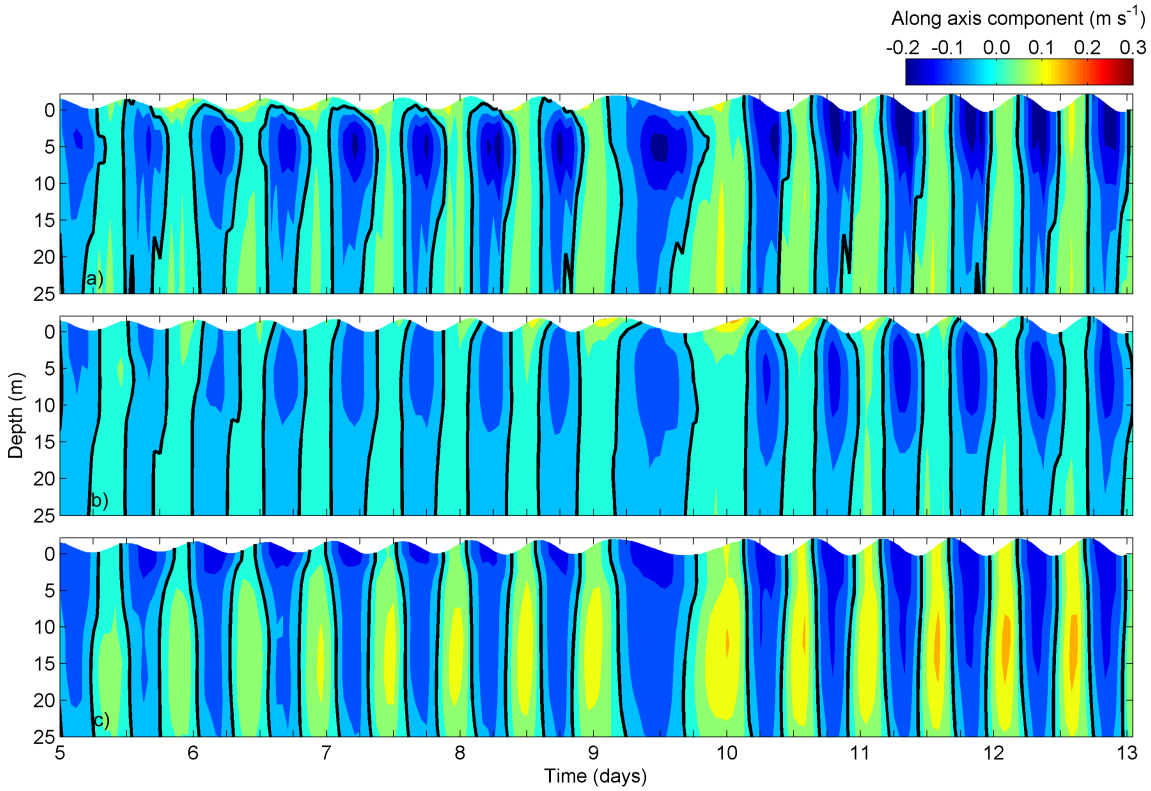

Figure 5.11: Along estuarine circulation at station located at mouths of Ria de Vigo (a), Pontevedra (b) and Arousa (c) between 5 and 12 May 1998, considering no wind forcing. Black line corresponds to 0 m s^{-1}.

5.4 Conclusions

The present chapter aimed to validate the numerical model, and consequently to study the propagation and influence of the Minho estuarine on Rias Baixas circulation and hydrography. The results obtained from this analysis indicate the following:

- The nesting methodology adopted for the Minho estuary and the Rias Baixas was successful implemented. Model predictions reproduce accurately the local hydrodynamics and thermohaline patterns.

- Under certain conditions, the Minho River plume can reach the Rias Baixas and reverse Rias de Vigo and Pontevedra circulation patterns, while the circulation of Ria de Arousa remains unchanged. This situation was observed under northward winds and significant Minho River discharge. The freshwater intrusion of the Minho River into these systems was the main responsible for the unusual horizontal salinity gradient (saltier water near the mouth than in the inner part) and negative circulation pattern characterized at these estuaries on previous research during May 1998.

- The situation observed at the Rias Baixas at the beginning of May was not directly dependent only on the high Minho River discharge observed. Without wind forcing, the Minho estuarine plume does not influence the circulation pattern on Rias Baixas. Furthermore, under northward winds, a continuous moderate Minho River discharge is enough to produce the negative circulation pattern, reducing the importance of specific events of high runoff values.

Chapter 6

Influence of the Minho River plume on the Rias Baixas

6.1 Introduction

The interaction between local seasonal upwelling and estuarine plume intrusion drives the primary productivity in the coastal region of Rias Baixas, supporting an intense raft culture of mussels [Blanton et al., 1987]. Moreover, the plume intrusion can generate an important salinity decrease at the estuary mouth, reversing the normal circulation pattern. On the surface, this reverse pattern is characterized by the intrusion of warm coastal waters, which accumulate within the Rias and finally flow towards the ocean through the bottom. Several works were carried out to analyse changes in thermohaline variables, as salinity, inside the Rias Baixas [Mourino and Fraga, 1982; deCastro et al., 2004; Alvarez et al., 2006; deCastro et al., 2006a]. Some of these studies were performed under a high Minho river discharge and favourable wind in order to spread the river plume northward, toward the Galician coast. In the previous chapter it was observed that under northward winds, a continuous moderate Minho River discharge is enough to produce the negative circulation pattern in Rias Baixas, reducing the importance of the existence of specific events of high estuarine (or river) runoff values. The Minho freshwater intrusion can give rise to both positive and negative effects from a biological point of view. It can generate an inverse estuarine circulation, which tends to stop the water exchange between the Rias and the adjacent shelf, increasing residence time and hence affecting water quality. Conversely, extreme freshwater pulses can induce phytoplankton blooms at the shelf, which penetrates into the Rias embedded in a water mass that was fresher than the estuarine one, contributing to fertilize the area.

As it can be derived from the previous works [García-Berdeal et al., 2002; Choi and Wilkin, 2007; Otero et al., 2008], local wind forcing and river discharges affects significantly

the dispersal of a river plume, namely its trajectory and vertical flux. Moreover, river discharge also affects the location and magnitude of these physical processes. Thus, it becomes important to study the interaction of the wind and river discharge on the Minho estuarine plume propagation, in order to investigate the necessary conditions for the establishment of the reverse circulation at Rias Baixas and also to evaluate water exchange and mixing between Rias Baixas.

Additional insight concerning plume intrusion and the nature of the water exchange between the Rias Baixas can be acquired by looking at particle tracking results. Lagrangian transport constitutes a very useful tool to study the dispersion processes and also to predict the fate of pollutants (e.g. oil spills accidents), allowing the analysis of particle fate through the estimation of its trajectory. The use of particle tracking models in a complex system like the Galician coast is very important, since the Rias Baixas are located along one of the most important maritime routes and numerous merchant ships navigate through its water and even close to the coast. The frequent storms which affect the coast can provoke a larger number of pollutant accidents, affecting the primary production. Therefore, insight of non-dissolved particles dynamics allows the local scientist and managers to improve local policies of ecosystem protection. In the previous chapter, the importance of the Minho River intrusion inside these Rias was analysed, indicating that the possibility of a spill near the river mouth could seriously affect the whole area. Particles transport simulations related to the plume dynamics have been performed worldwide [Whitney and Garvine, 2006; Banas et al., 2009; Xia et al., 2011]. To study the response of the Minho estuarine plume dispersal to an idealized wind forcing during extreme river discharges conditions, several scenarios from weak-to-moderate winds are considered, blowing from each of the main four cardinal points. Three different realistic scenarios of river discharge were chosen: low, moderate and high. A lagrangian particle model is also applied to simulate the transport of released particles at Minho River mouth, in order to assess the water exchange and mixture between Rias Baixas.

6.2 Numerical experimental design: data and methods

A statistical analysis of the maximum annual values of the Minho River discharge was performed to characterize the extreme river discharge events. Estimation of the extreme events is usually carried out by fitting observed data samples with a suitable probability distribution. Thus, the monthly mean Minho River discharge (supplied by the ”Confederación Hidrográfica del Norte”) from January 1971 to December 2010 is depicted in Figure 6.1a, showing a typical pattern with high values during winter and low values during summer. The maximum value corresponds to February (692 m^3 s^{-1}), and the minimum value is reached in August (121 m^3 s^{-1}).

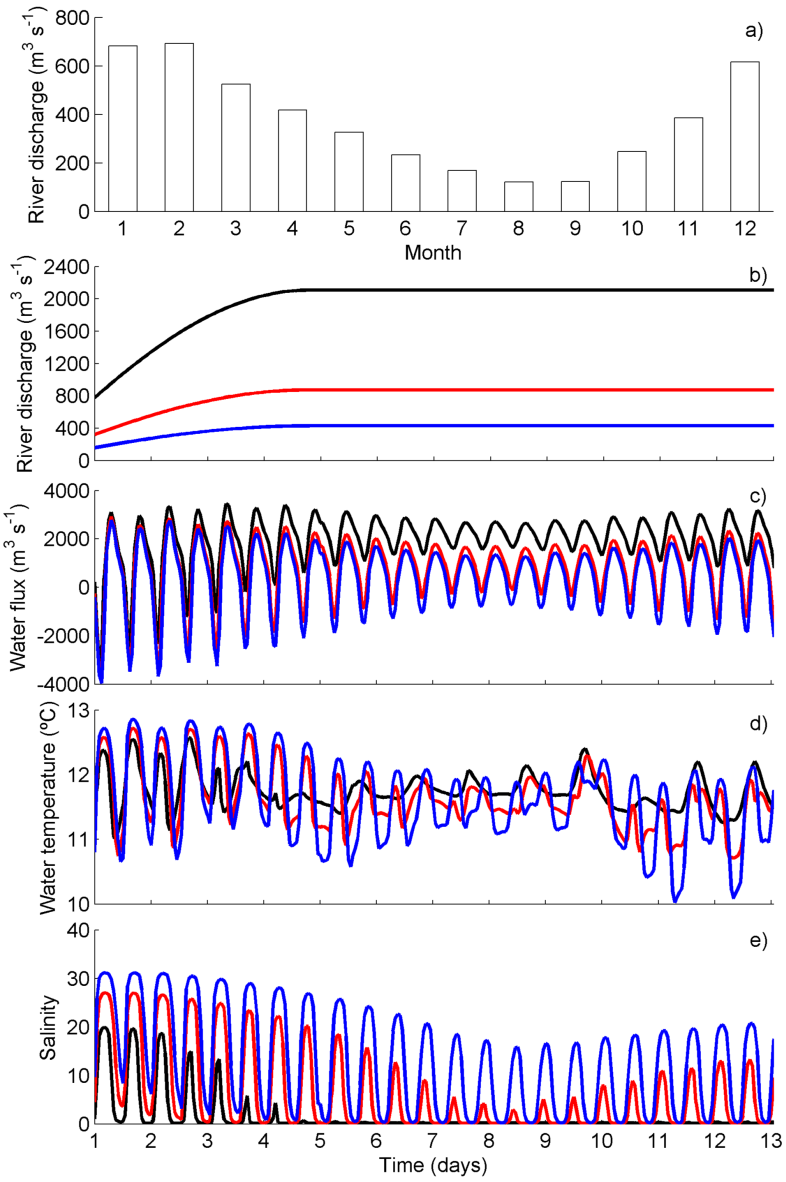

Figure 6.1: Monthly mean Minho River discharge for the period January 1971 to December 2010 (a). Minho River discharge scenarios (black line: high discharge; red line: moderate discharge; blue line: low discharge) (b). Water flux (c), water temperature (d) and salinity (e) computed through the Minho estuary mouth for the three scenarios.

Through the analysis of Figure 6.1a, the mean maximum values occur in February. Therefore, the annual maxima of this month for Minho, Verdugo, Lérez, Umia and Ulla rivers obtained from estimations presented in Otero et al. [2010] were adjusted to five probability distributions. The empirical cumulative distribution function was computed according to Kaplan and Meier [1958], while the theoretical distributions were determined by calculating the location, scale and shape parameters of each annual maximum series. In this study, the following probability distributions were considered: Generalized Extreme Value distribution (GEV), Gamma, Log-normal, Exponential and Weibull. The best distribution

was then selected by testing the quality of the fit using two statistical tests (Chi-squared and the Kolmogorov-Smirnov tests) at the 95% confidence level and the RMSE between the discharges empirical cumulative distribution and each probability cumulative distributions. The GEV distribution is the one that best fits the Minho river discharge, having the lowest RMSE value (0.03 m^3 s^{-1}). Otherwise, the Gamma and Log-normal distributions are the best fits to the Verdugo, Lérez, Umia and Ulla rivers. From these probability distributions, the maxima discharges for non-exceedance probability of 0.05, 0.2, 0.5, 0.8 and 0.95 [Fortunato et al., 2002] were calculated (Table 6.1). These calculations consist in the probability of occurrence of events that are equal to or less than a specific event. Thus, the results suggest maximum (non-exceedance probability of 0.8) of 2108.2 m^3 s^{-1}, 64.0 m^3 s^{-1}, 70.9 m^3 s^{-1}, 53.5 m^3 s^{-1} and 229.8 m^3 $s^{-1}$for the Minho, Verdugo, Lérez, Umia and Ulla rivers, respectively (Table 6.1).

Taking into account these discharge estimates, three scenarios were chosen (Figure 6.1b). The first one considers an idealized high discharge, with an exponential shape for the Minho river discharge starting from 692 m^3 s^{-1} (an average discharge for February), increasing to 2108.2 m^3 s^{-1} (non-exceedance probability of 0.8) over 4 days and then remaining constant (Figure 6.1b, black line). As it can be observed in Figure 6.1b (black line), the exponential beginning is one third of the maximum value, then the second (Figure 6.1b, red line) (moderate discharge) and third (Figure 6.1b, blue line) (low discharge) scenarios were defined considering the same exponential shape, being the starting value one third of the discharge value for the non-exceedance probability of 0.2 and 0.5. Concerning the others rivers, the discharges were kept constant, ranging from each non-exceedance probability scenarios. These Minho River discharge scenarios were imposed in the Minho estuarine model, in order to produce outflow properties at the mouth of the Minho estuary. These outflows (Figures 6.1c, 6.1d and 6.1e) were computed for each scenario and imposed offline in the coastal nested model.

Wind data provided by the NCEP Climate Forecast System Reanalysis (CFSR; `http://rda.ucar.edu/pub/cfsr.html`) at a control station located near the mouth of the Minho River from 1979 to 2010 were used to characterize the wind speed over the area under study. The wind speed statistics reveal that the probability of winds lower than 3 m s^{-1} is 32 % while the probability of moderate winds (between 3 and 6 m s^{-1}) is very high (46 %).

Table 6.1: River discharge estimations for February.

Non-exceedance probability	River discharge (m^3 s^{-1})				
	Minho	Verdugo	Lérez	Umia	Ulla
0.05	237.6	20.0	45.8	14.6	61.0
0.20	429.4	30.6	47.4	23.6	93.6
0.50	873.6	45.3	49.1	36.5	146.7
0.80	2108.2	64.0	70.9	53.5	229.8
0.95	6274.6	86.1	92.7	73.9	352.8

Thus, for the wind scenarios, these intensities were used as representative of the prevailing wind regime of this region.

In order to investigate the distribution and behaviour of the estuarine plume due to external forcing, several numerical experiments were conducted under various external forcing. More than 30 experiments to test the sensitivities of the plume model were simulated, including 4 different wind directions (north, south, west and east); 2 different wind speeds (3 and 6 m s^{-1}) and 3 different river discharges (high, moderate and low). All the simulations run with six months spin-up, covering the period between August 2009 and March 2010, though only the results of February 2010 were considered for the analysis. The wind forcing starts on 5 February 2010, when the river discharge is at its maximum, and is then held steady constant in all scenarios.

At the same time, in order to evaluate the horizontal pattern of plume dispersal, the equivalent depth of freshwater is evaluated by:

$$Fw = \int_{-h}^{\eta} \frac{S_a - S(z)}{S_a} dz \tag{6.1}$$

where S_a is a reference or ambient salinity, which represents the limit of the buoyant plume. Following Peliz et al. [2002] and Otero et al. [2008], it is used 35.6 as the reference salinity. *S(z)* is the salinity of the water column, η is sea level and *h* is the bottom depth.

To identify the temporal and spatial variability of the freshwater transport and compare the effect of the wind and discharge on plume dispersal, the freshwater transport in several sections of the Rias is also evaluated (Figure 6.2, sections II to IV). The freshwater transport, relative to the reference salinity, S_a, is defined as the integral of the freshwater fraction:

$$V_{Fw} = \int \int_{-h}^{\eta} \frac{S_a - S}{S_a} u dz dx \tag{6.2}$$

where *u* is horizontal velocity normal to the section and the integral with respect to *x* is the horizontal distance across the section [Choi and Wilkin, 2007]. The freshwater transport is positive in the direction of the flow.

To assess the water exchange and mixture between Rias Baixas, particles were released continuously close to the Minho river mouth (each simulation time step (15 seconds)), starting 5 and ending 7 February 2010, with a total of 5782 releases. During the next four days, the location of these particles was recorded half-hourly.

6.3 Results and Discussion

The wind forcing and the river discharge play an important role in the dispersion at the Minho estuarine plume, reversing the circulation pattern in Rias Baixas. In this section,

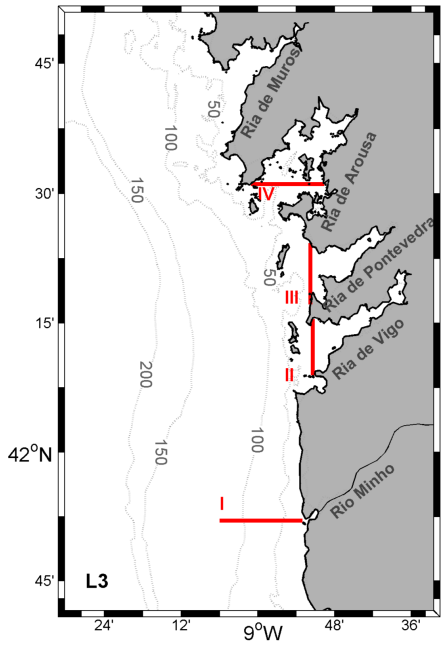

Figure 6.2: Map of Rias Baixas and location of the cross-sections.

a characterization of the Minho estuarine plume and the necessary conditions for the establishment of this reverse circulation were investigated. Different river discharges (high, moderate and low) as well as four scenarios of weak and moderate winds (3 and 6 m s^{-1}) blowing from each of the main four compass points were simulated. The water exchange and mixture between Rias Baixas was also addressed. The details of their influence on Rias Baixas are included as follows.

6.3.1 Characterization of Minho estuarine plume

Firstly, changes in the vertical distribution of salinity and current along the section in front of Minho River mouth (Figure 6.2, section I) after 1 (day 5 in Figure 6.1b) and 4 (day 9 in Figure 6.1b) days of simulation under high river discharges (Figure 6.1b, black line) and considering different wind directions are shown in Figures 6.3 and 6.4, respectively.

Under no wind forcing (Figure 6.3a), the plume expands to the west. The plume becomes about 16.5 km wide offshore, with a thickness of 3 m. The lowest salinity is about 24, because new water joins the plume without being mixed downward by surface winds. After 4 days (Figure 6.4a), the only difference is a greater dispersion of the plume on the surface layers. The northerly winds (Figure 6.3b) also contribute to spread the plume offshore, tilting the isohalines toward the horizontal. These wind conditions enhance the upwelling process, spreading surface waters and intensifying the offshore vertical stratification (Figure 6.4b). Marques et al. [2009] also observed through numerical modelling experiments that the influence of northerly winds contribute to increase the

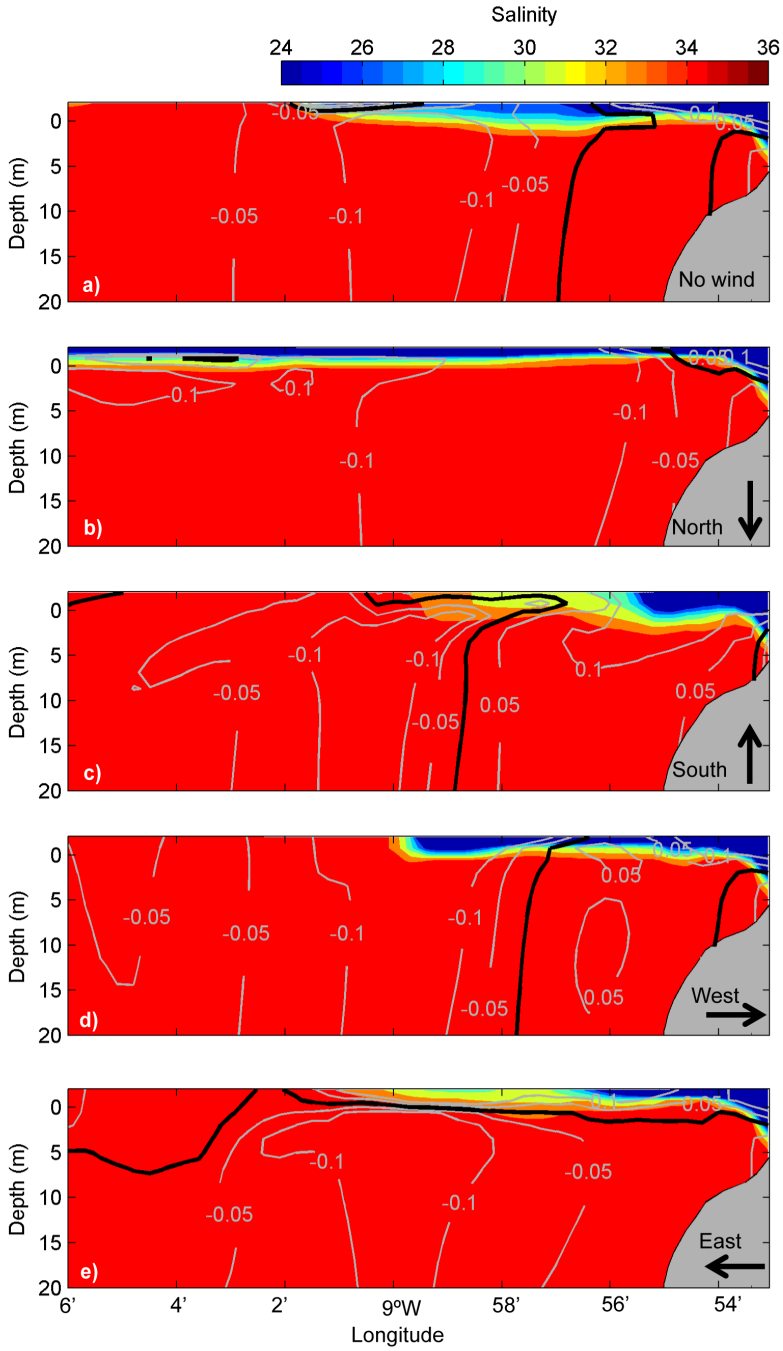

Figure 6.3: Salinity and alongshore velocity (contours) along section I after 1 day under high river discharges and several wind (6 m s^{-1}) directions (no wind (a), north (b), south (c), west (d) and east (e). Black line corresponds to 0 m s^{-1}.

vertical stratification close to the Patos lagoon mouth. In contrast, southerly winds (Figure 6.3c) accelerate the buoyant water along shore (north direction), tilting the isohalines toward the vertical. After 4 days (Figure 6.4c), the plume width and its thickness decrease to 6.5 km and 4 m, respectively. The area of the plume has a salinity of 24 and is well mixed until 5 m. This wind pattern enhances the mixing process within the plume, forming vertically

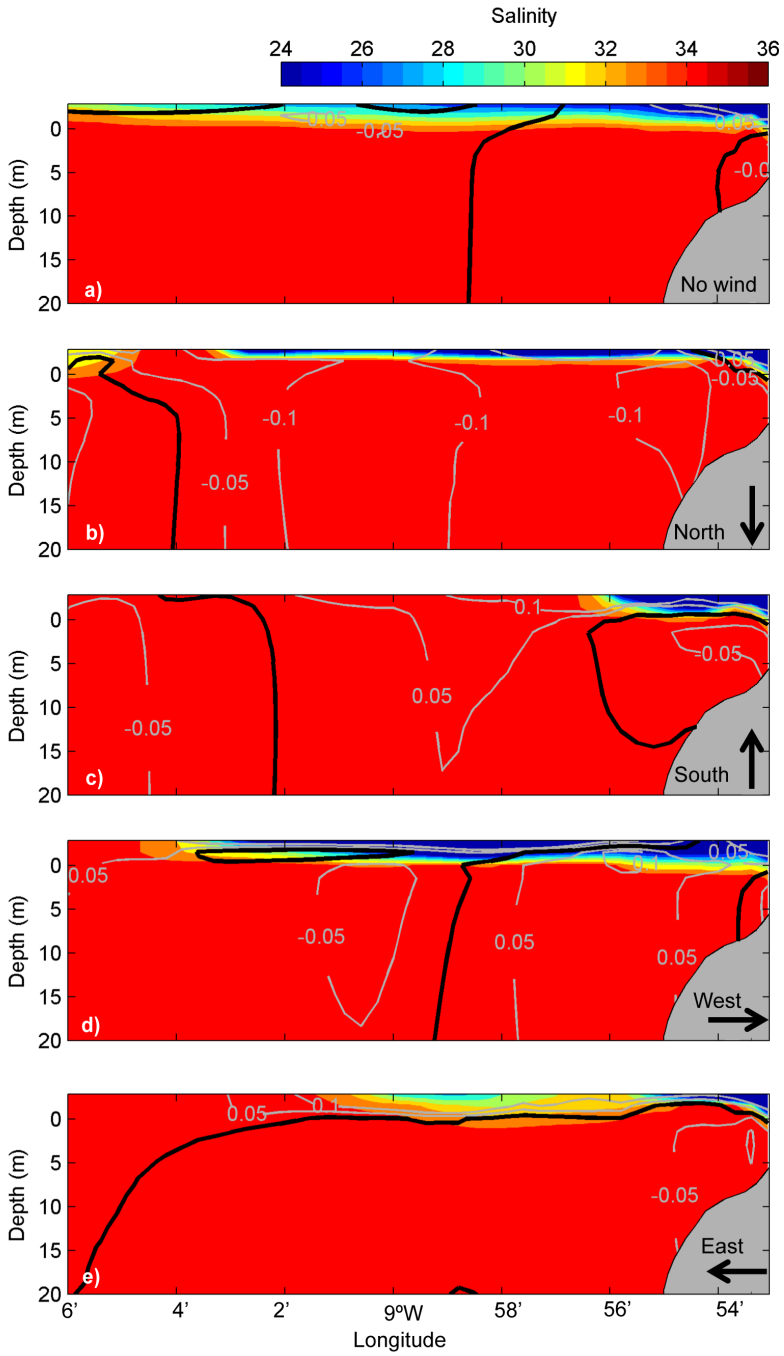

Figure 6.4: Salinity and alongshore velocity (contours) along section I after 4 days under high river discharges and several wind (6 m s^{-1}) directions (no wind (a), north (b), south (c), west (d) and east (e). Black line corresponds to 0 m s^{-1}.

well-mixed and narrow plumes [Soares et al., 2007]. The northward coastal current has a surface speed of about 0.10 m s^{-1} along the salinity front.

During westerly winds (Figure 6.3d), the plume is pushed to the coast and after 4 days (Figure 6.4d) it becomes about 23 km wide and 2.5 m thick. When the wind blows westward (Figures 6.3e and 6.4e), the plume expands about 16 km offshore, about as far the unforced

plume, though the halocline is deeper because of vertical mixing.

Next, the evolution of the surface plume and current structure is analysed (Figures 6.5 and 6.6).

Without wind forcing (Figures 6.5a, 6.5f, 6.6a and 6.5f), the plume expands offshore, creating a bulge in front of the river mouth. The low salinity waters are advected to the right due to the Coriolis effect and after the establishment of the geostrophic balance, the plume water extends northward (along the coastline) [Takano, 1954a,b; Chao and Boicourt, 1986; Zhang et al., 1987; Xia et al., 2007]. However, within 4 days (Figures 6.6a and 6.6f), the plume arrival affects the salinity distribution of the Ria de Arousa and the area of the freshwater plume is expanded offshore. These patterns suggest an approximation to the surface-advected plume presented by Yankovsky and Chapman [1997].

When the wind blows southwards (Figures 6.5b, 6.5g, 6.6b and 6.5g), the main feature is also the offshore extension of the plume due to the Ekman transport . This is related to the development of a surface southwestward flow plume. Otherwise, northward wind (Figures 6.5c, 6.5h, 6.6c and 6.5h) spreads the river plume towards the Rias Baixas (to the north), causing the coastal freshwater band to become more narrow and its thickness to increase ($\sim$ 1.5 m). The northward flow along the coast and inside the Rias Baixas is stronger in this scenario (about 0.5 m s^{-1}) than with any other wind condition, transporting freshwater to the Rias Baixas. The plume reaches the mouth of the Rias de Vigo and Pontevedra after 1 day (Figures 6.5c and 6.5h) and influences the physical properties within the estuaries.

Eastward wind (Figures 6.5d, 6.5i, 6.6d and 6.6i) accumulates freshwater in Rias de Vigo and Pontevedra, showing the importance of the wind direction parallel to the estuarine axis, as found by Choi and Wilkin [2007] in Hudson River. The surface current along the plume is weak ($\sim$ 0.1 m s^{-1}) relative to the northward wind condition (0.5 m s^{-1}). Westward wind (Figures 6.5e, 6.5j, 6.6e and 6.5j) is more effective at pushing freshwater out of the mouth of the Minho River ($\sim$ 13 km). The northwestward flow spreads the plume towards to north, but a small portion accumulates in front of the Rias Baixas mouth.

In general, the numerical results indicate that the horizontal distribution of the Minho estuarine plume is mainly due to the wind forcing, changing under the four different wind directions. These results also indicate that the dynamic response of the Minho estuarine plume to the wind forcing takes less than 1 day, and that moderated wind conditions under high river discharge can reverse the circulation in Rias Baixas.

6.3.1.1 Classification of Minho estuarine plume

The plumes as shown in the previous figures are defined as the surface-advected plumes by Yankovsky and Chapman [1997]. As a wind stress is applied to a buoyant plume, there will come a point when the flow in the plume ceases to be driven by buoyancy and becomes

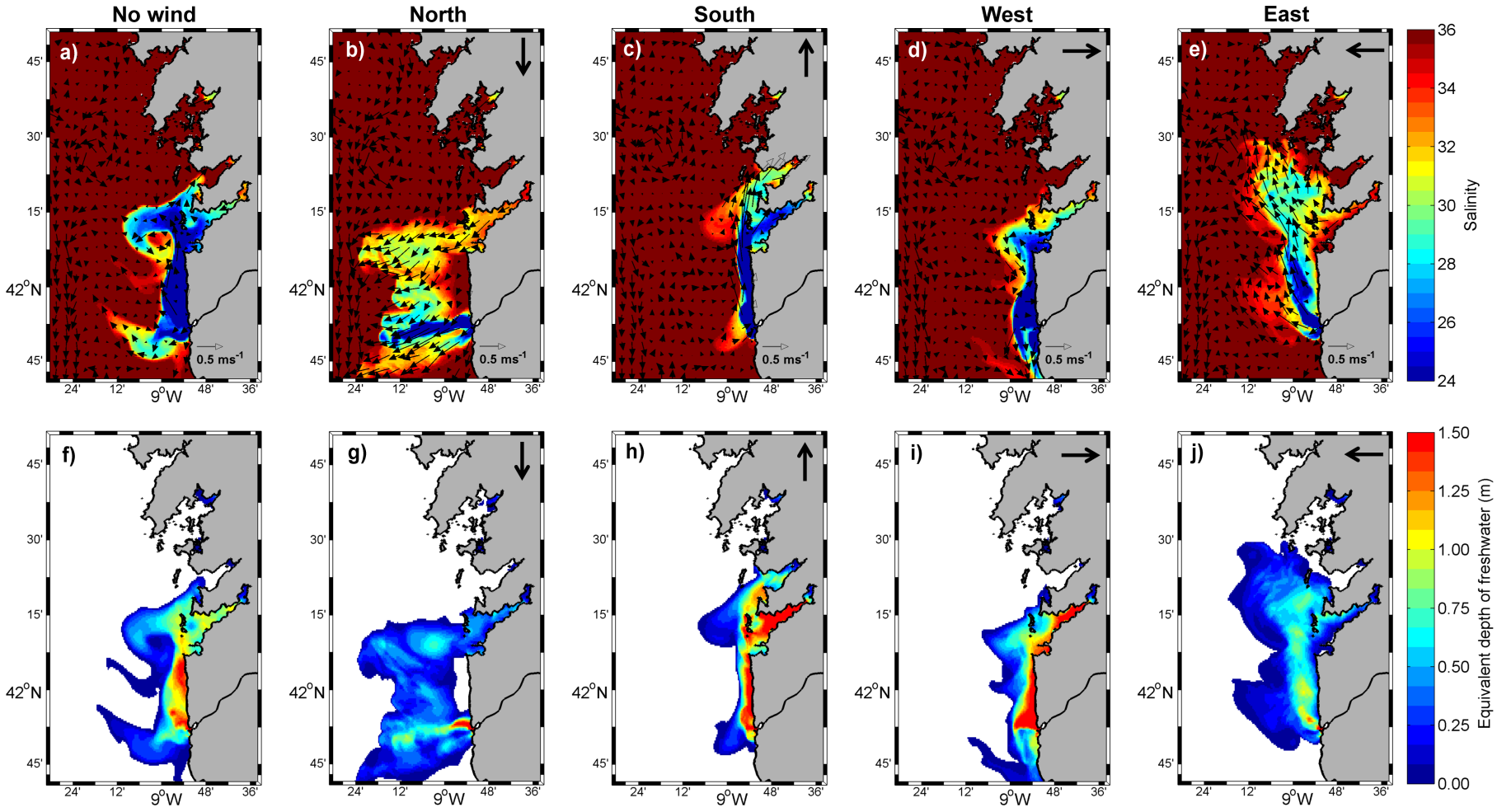

Figure 6.5: Surface currents and salinity (top) and equivalent depth of freshwater (bottom) after 1 day under high river discharges and several wind (6 m s^{-1}) directions (no wind (a,f), north (b,g), south (c,h), west (d,i) and east (e,j)).

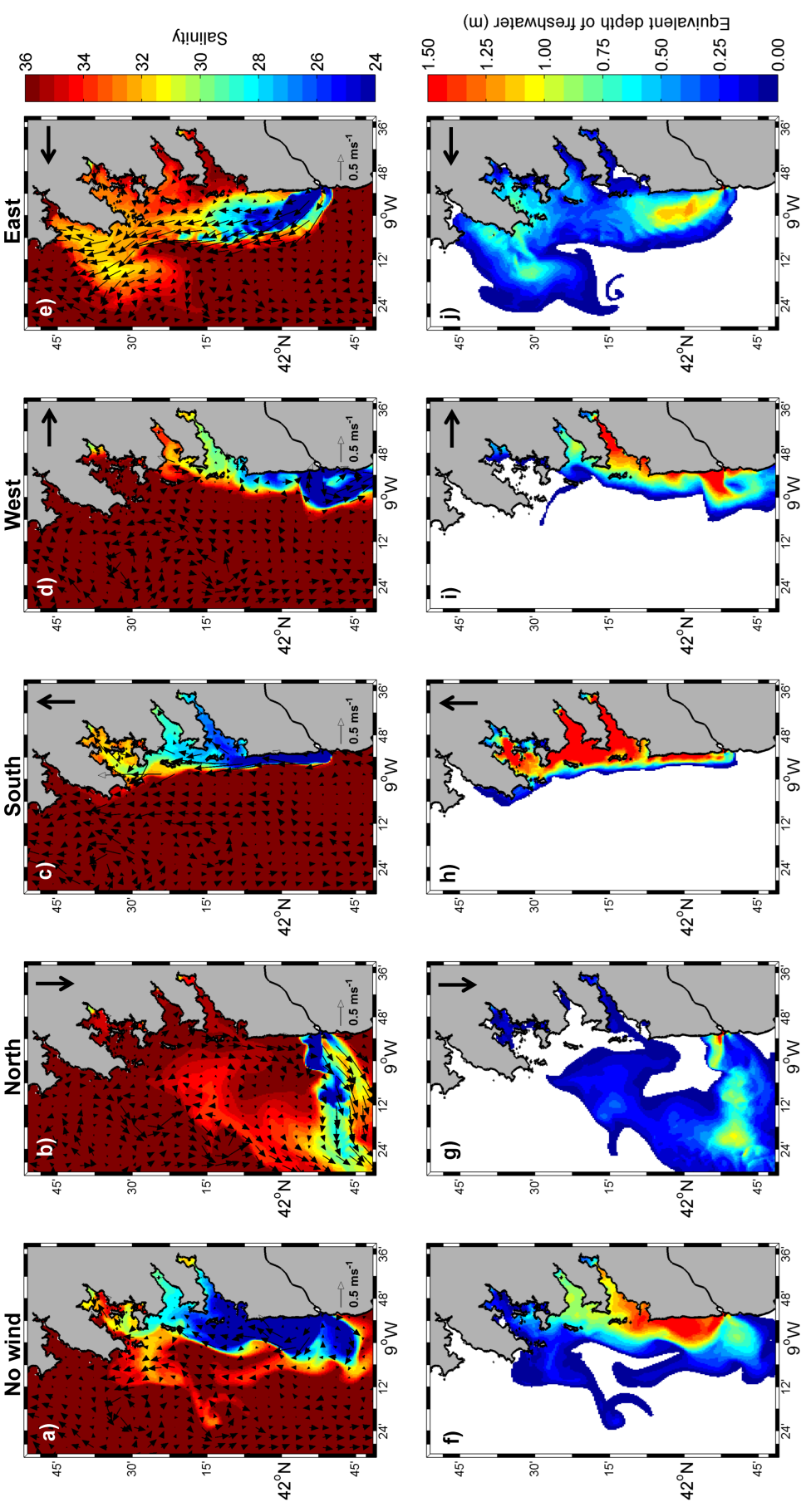

Figure 6.6: Surface currents and salinity (top) and equivalent depth of freshwater (bottom) after 4 days under high river discharges and several wind (6 m s^{-1}) directions (no wind (a,f), north (b,g), south (c,h), west (d,i) and east (e,j)).

heavily influenced by the wind stress [Garvine, 1995]. Here, the theories developed by Yankovsky and Chapman [1997] and Whitney and Garvine [2005] are used to characterize the Minho estuarine plume.

To predict the behaviour of the plume based on the inflow properties, the horizontal length scaling parameter (y_s) and the trapping depth of the plume (h_b), which is considered the depth which the plume remains attached to the bottom are applied:

$$y_s = \frac{2(3g'h_0 + v_i^2)}{f(2g'h_0 + v_i^2)^{\frac{1}{2}}} \tag{6.3}$$

$$h_b = \left(\frac{Lv_i h_0 f}{g'}\right)^{\frac{1}{2}} \tag{6.4}$$

where h_0 is the inflow depth (2 m), L is the inflow width (1 km), v_i is the velocity of buoyant inflow as it enters the shelf, and the reduced gravity g' is given by:

$$g' = g\frac{\rho'}{\rho_0} \tag{6.5}$$

where ρ' is the density anomaly.

To assess the wind impact to the plume shaping, the wind strength index introduced by Whitney and Garvine [2005] is also computed. The wind strength index (W_s) is defined as:

$$W_s = \frac{u_{wind}}{u_{dis}} \tag{6.6}$$

where,

$$u_{wind} = \sqrt{\frac{\rho_a}{\rho}\frac{C_{10}}{C_{Da}}}U_{10} \tag{6.7}$$

$$u_{dis} = \frac{1}{k}(2g'Qf)^{\frac{1}{4}} \tag{6.8}$$

where U_{10} is the wind velocity component at 10 m height (6 m s^{-1}), C_{10} (1.2×10^{-3}) is the surface drag coefficient and C_{Da} (1.3×10^{-3}) is the depth averaged drag coefficient and k is the internal Kelvin number. When $|W_s| > 1$, the flow is heavily influenced by the wind, and when $|W_s| < 1$, the flow is dominated by the buoyant forcing.

For high discharge scenario, the computed trapping depth (h_b) and the predicted y_s are 0.6 m and 36 km, respectively. As $h_b < h_0$, the bottom boundary layer has no significant influence on the buoyant plume transport and the Minho estuarine plume can be classified as surface-advected. In all directions, the W_s is greater than 1, which means that the Minho estuarine plume is heavily influenced by the wind. The Minho estuarine plume shows comparable depth and offshore extension with the findings of Munchow and Garvine [1993] and Lentz and Largier [2006] for the plumes formed in Delaware estuary and Chesapeake bay.

6.3.2 Response of the estuarine plume to wind and river discharge

As it can be observed in Figures 6.5 and 6.6, under high discharge, the Minho estuarine plume reaches the Rias Baixas when the wind blows from the south and west. This could change the hydrographic and circulation features of the Rias Baixas, turning this fact a challenging and important study issue. Thus, in the following only results for these two wind directions will be reported. To examine how this response differs with wind speed and river discharge, northward and westward winds are blown with speeds of 3 and 6 m s^{-1} under high, moderate and low river discharges after 3 days (Figures 6.7, 6.8 and 6.9).

In general, salinity is lower and freshwater occupies a larger area as the river discharge increases, which is consistent with a study on variation of plume size with river discharge performed by Choi and Wilkin [2007] and Shi et al. [2010] for the Hudson River and for an idealized tidal estuary, respectively. The plume area decreases as the wind speed increases from 3 to 6 m s^{-1} due to enhanced surface mixing associated with increased wind speeds.

In the high discharge scenario (Figure 6.7), as a weak northward wind of 3 m s^{-1} (Figures 6.7a and 6.7e) blows during 3 days, freshwater reaches the Rias de Vigo, Pontevedra and Arousa. When the wind increases to 6 m s^{-1}(Figures 6.7c and 6.7g), the plume also reaches the Rias de Vigo, Pontevedra and Arousa. However, in this scenario the plume is more confined to the coast, presenting a higher surface velocity ($\sim$ 0.30 m s^{-1}). Xia et al. [2007] also observed that the intensity of winds tend to reduce the surface plume size and distort the bulge shape due to enhanced wind-surface mixing. Eastward wind (Figures 6.7b, 6.7f, 6.7d and 6.7h) exports freshwater from the estuary and favours the accumulation of freshwater in the recirculating bulge outside the mouth of Minho River. Apart of wind speed, in these conditions, the plume only reaches the Rias de Vigo and Pontevedra.

When the river discharge decreases (Figures 6.8 and 6.9), the patterns are very similar to the previous ones, only with differences in the plume influence area. For example, under low river discharge conditions (Figure 6.9), the Minho estuarine plume does not reach Rias Baixas.

These results show that the wind stress and river discharge are the most important factors determining the size and shape of the Minho estuarine plume.

The influence of wind forcing and river discharges on the freshwater transport in Rias Baixas (Figure 6.10) is illustrated showing the hourly volume transports determined through the cross-sections in front of the Rias Baixas (Figure 6.2, sections II, III and IV).

In general, the freshwater transport is closely related to the river discharges, showing the importance of river discharges in the dispersion of the Minho estuarine plume towards the Rias Baixas. Indeed, the freshwater transport is also related to the wind and tide (the ebb tide produces a decrease of the freshwater flux (outflow)).

When the wind blows eastward during 2 days, an insignificant Minho estuarine influence is observed in Ria de Pontevedra ($\sim$ 0.01 Sv) (Figure 6.10b), showing that this wind direction

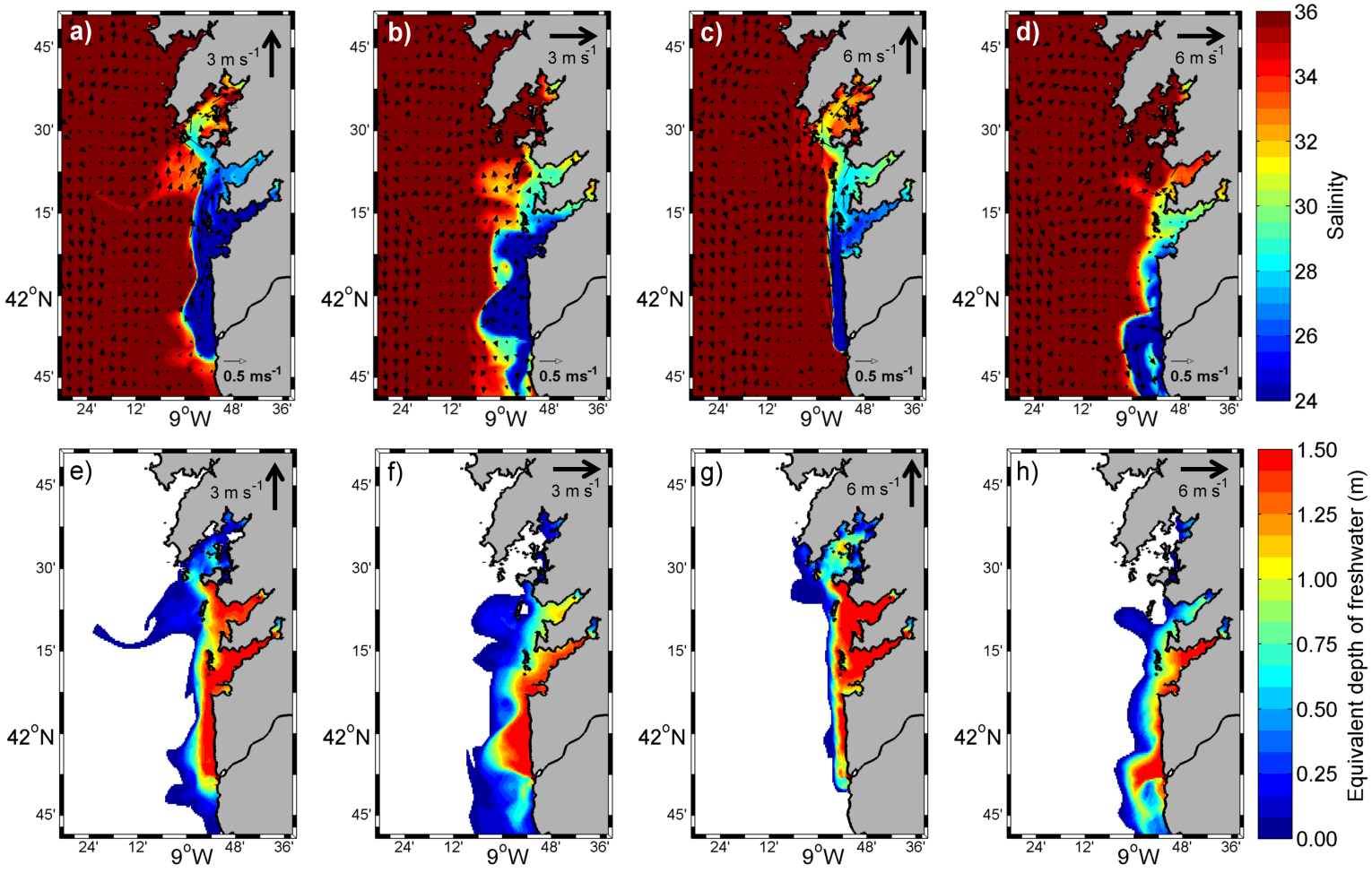

Figure 6.7: Surface salinity (top) and equivalent depth of freshwater (bottom) after 3 days of northward (a,e,c,g) and eastward (b,f,d,h) winds of 3 and 6 m s^{-1} under high river discharges.

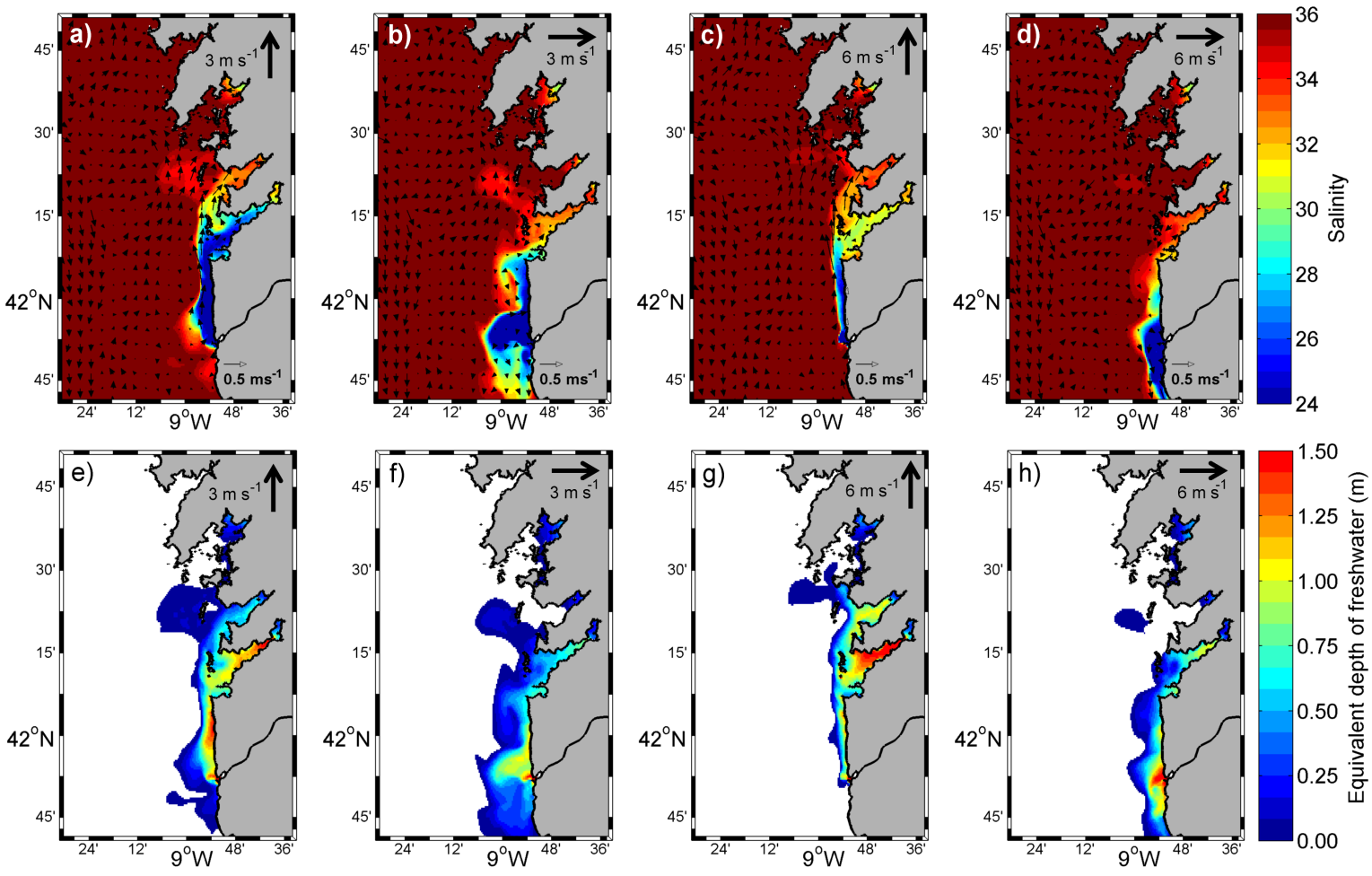

Figure 6.8: Surface salinity (top) and equivalent depth of freshwater (bottom) after 3 days of northward (a,e,c,g) and eastward (b,f,d,h) winds of 3 and 6 m s^{-1} under moderate river discharges.

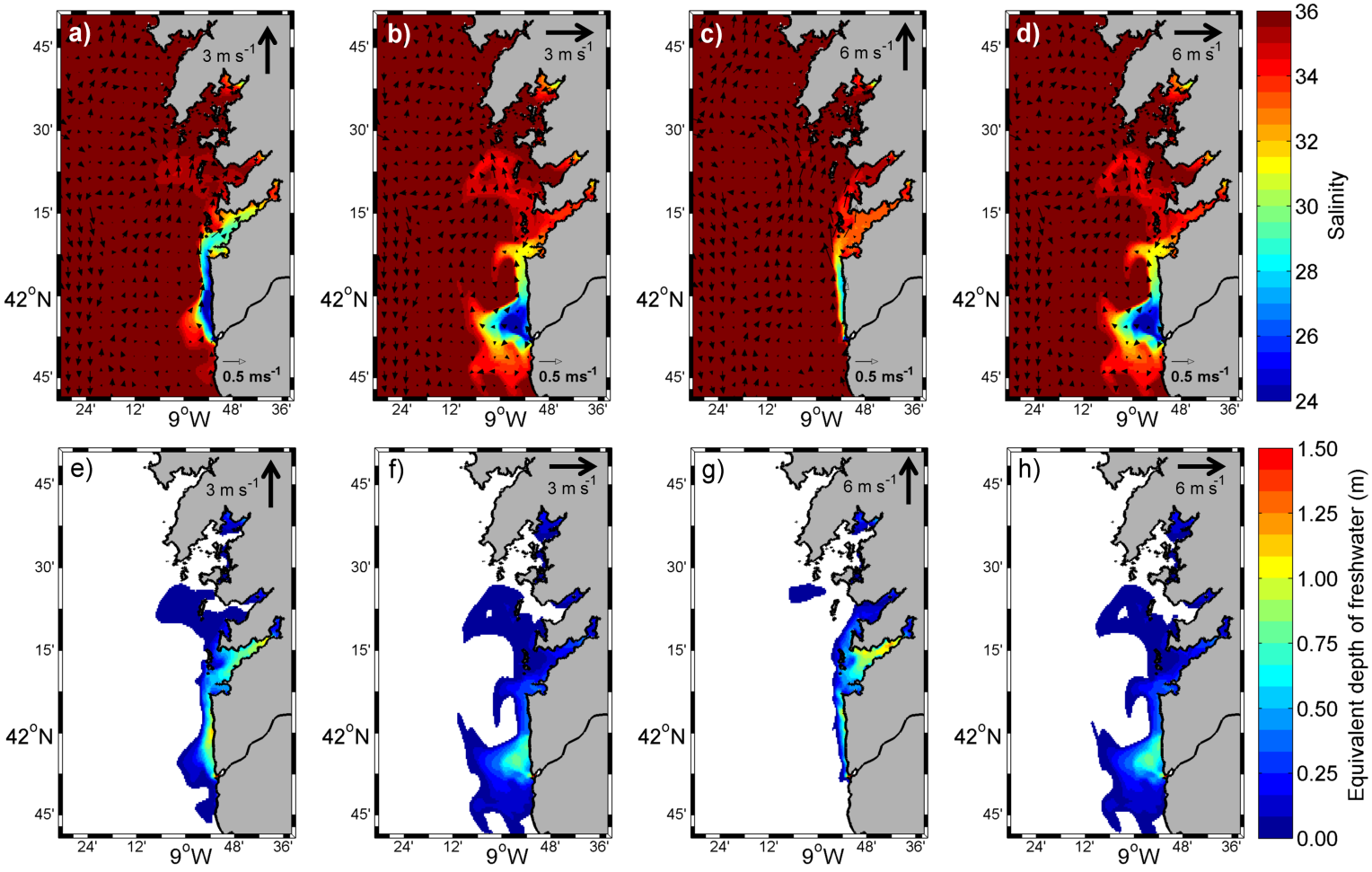

Figure 6.9: Surface salinity (top) and equivalent depth of freshwater (bottom) after 3 days of northward (a,e,c,g) and eastward (b,f,d,h) winds of 3 and 6 m s^{-1} under low river discharges.

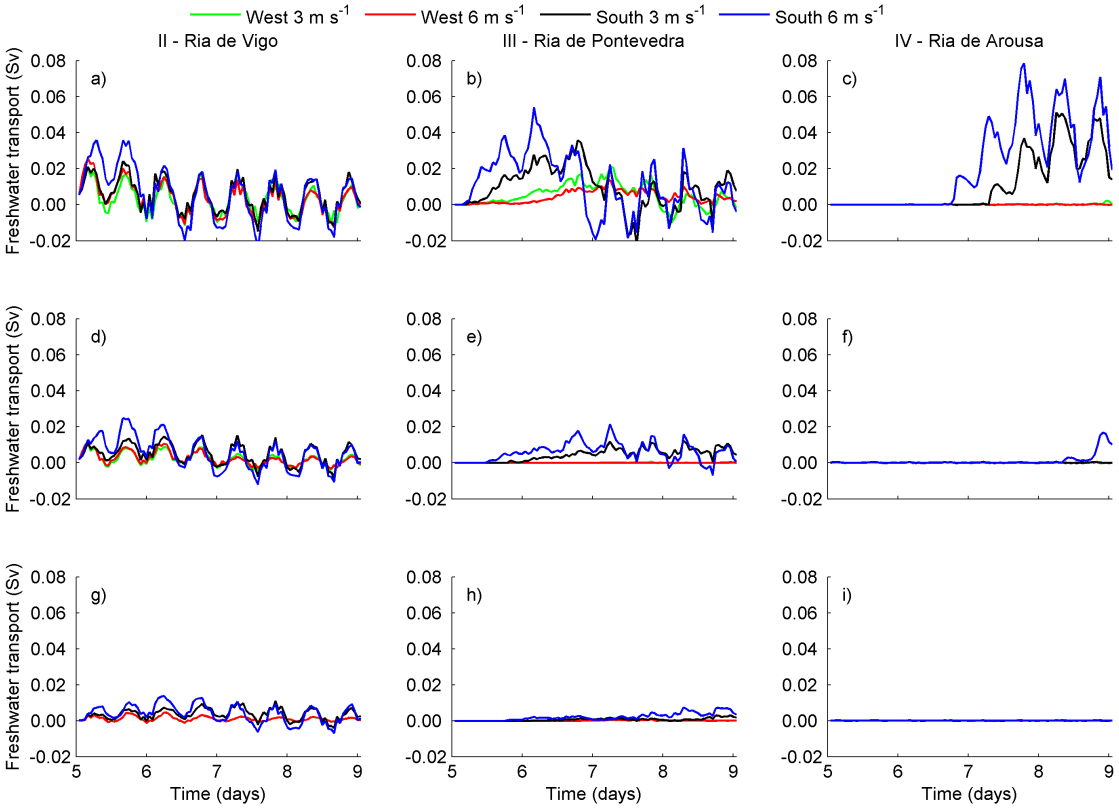

Figure 6.10: Freshwater transport in sections II, III and IV for high (a,b,c), moderate (d,e,f) and low (g,h,i) river discharges scenarios. Positive (negative) freshwater transport means freshwater volume transport into (out of) the domain.

affects with more intensity the Ria de Vigo during high discharge. Otherwise, northward winds have positive freshwater flux (inflow) in all sections, indicating that eastwards currents bring water (on average) with a lower salinity than S_a (35.6). Conversely, when currents turn westward the freshwater is transported to the east. When the winds blow with more intensity (6 m s^{-1}), the freshwater is flushed into the sections more rapidly than with the wind speed of 3 m s^{-1}.

During the high discharge event, in Ria de Vigo (Figure 6.10a), on the first day a maximum freshwater transport of 0.035 Sv is obtained, corresponding to the plume intrusion (Figure 6.5), which reduces to 0.02 Sv on the second day. During the following days, the northward displacement of the plume continued and the plume intrusion is observed in the Ria de Pontevedra (Figure 6.10b) on 5.5-6 days and in the Ria de Arousa (Figure 6.10c) on 7-8 days. It is worth noting that the freshwater transport for the Rias de Pontevedra and Arousa is more intense than for the Ria de Vigo. This situation can be explained by the size difference of the Rias (Ria de Arousa is considerably wider), since the freshwater transport is dependent on the area of the section.

In the moderate river discharge scenario (Figures 6.10d, 6.10e and 6.10f), the results show that the southerly winds promote the introduction of the Minho estuarine outflow into

the Ria de Vigo and Pontevedra and lead to a small introduction in Ria de Arousa. In the low river discharge scenario (Figures 6.10g, 6.10h and 6.10i), only in Ria de Vigo, a small influence of the Minho plume intrusion is observed ($<$ 0.01 Sv) (Figure 6.10g), showing that for these conditions, the Minho estuarine plume does not influence the Rias Baixas circulation pattern.

Taking into account the previous results, events of moderate-to-high river discharge combined with southerly winds result in plume intrusion into the Rias Baixas. As it was previously mentioned in Chapter 5, this plume intrusion can reverse the normal estuarine circulation of these estuaries. Thus, in order to analyse the necessary conditions for the establishment of the reverse circulation, the along axis circulation at the mouth of Rias de Vigo, Pontevedra and Arousa is also computed (Figures 6.11, 6.12, 6.13 and 6.14).

During the high river discharge scenarios (Figures 6.11 and 6.12), in the three estuaries, a negative estuarine circulation with near surface water moving landward (positive values) and near bed water moving seaward (negative values) is observed. However, this negative estuarine circulation results in the propagation of the Minho outflow into the Rias. In Ria de Vigo (Figure 6.12a), a negative estuarine circulation at surface layers is observed during all period. When the weak winds blows northward, this pattern is observed in Ria de Pontevedra from day 5.5 (Figure 6.11b), with the highest velocities (0.5 m s^{-1}) between 0-10 m. After 1.5 days, the plume intrusion effect is observed in Ria de Arousa (Figure 6.11c), with velocities reaching 0.4 m s^{-1} in the upper layers. When the wind increases (Figure 6.12), being the surface currents stronger (0.60 m s^{-1}), the plume effect is observed earlier, affecting deeper layers.

Over the moderate river discharge and both wind scenarios (Figures 6.13 and 6.14), the obtained patterns are very similar to the simulation with high discharge with no significant differences at the Ria de Vigo mouth (Figures 6.13a and 6.14a). The Ria de Pontevedra (Figures 6.13b and 6.14b) also shows a similar pattern although, in this scenario, the surface water moving landward is observed later (day 7). In addition, this pattern is more intense than for the high discharge scenario, with positive values of the along axis current until 20 m (wind of 6 m s^{-1}), increasing in the plume influence area. The Ria de Arousa (Figures 6.13c and 6.14c) presents a normal estuarine circulation, with water moving landward during flood and moving seaward during ebb, for winds of 3 m s^{-1}. Otherwise, for winds of 6 m s^{-1}, the plume intrusion is also observed in Ria de Arousa after 3 days (Figure 6.14c), reversing the circulation pattern.

According to the results, different river discharges play an important role in the plume intrusion into the Rias Baixas. Under moderate freshwater outflow, the plume intrusion velocity tends to be lower than with high river discharges, revealing a reduction of the stratification within the plume. However, the vertical plume area is larger ($\sim$ 20 m) owing to the increase of the water column stability.

The results presented in this section suggest that a moderate river discharge combined

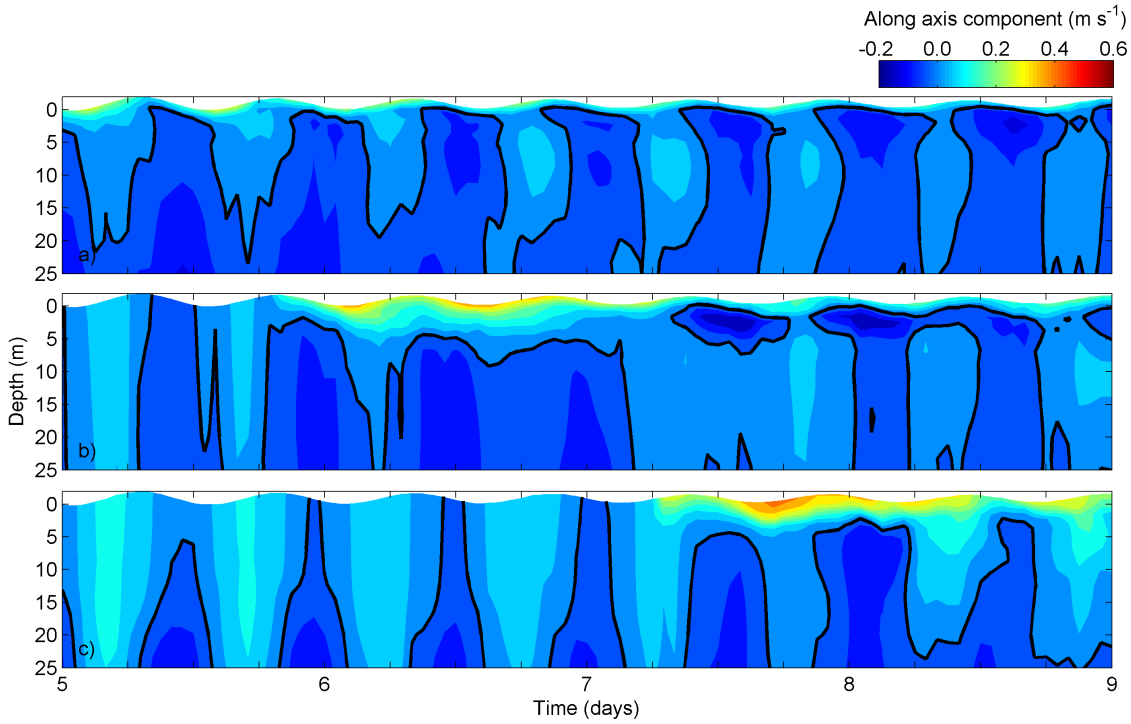

Figure 6.11: Along estuarine circulation at stations located at mouths of Rias de Vigo (a), Pontevedra (b) and Arousa (c), considering high river discharge and southerly winds of 3 m s^{-1}. Positive (negative) current velocity means water moving landward (seaward). Black line corresponds to 0 m s^{-1}.

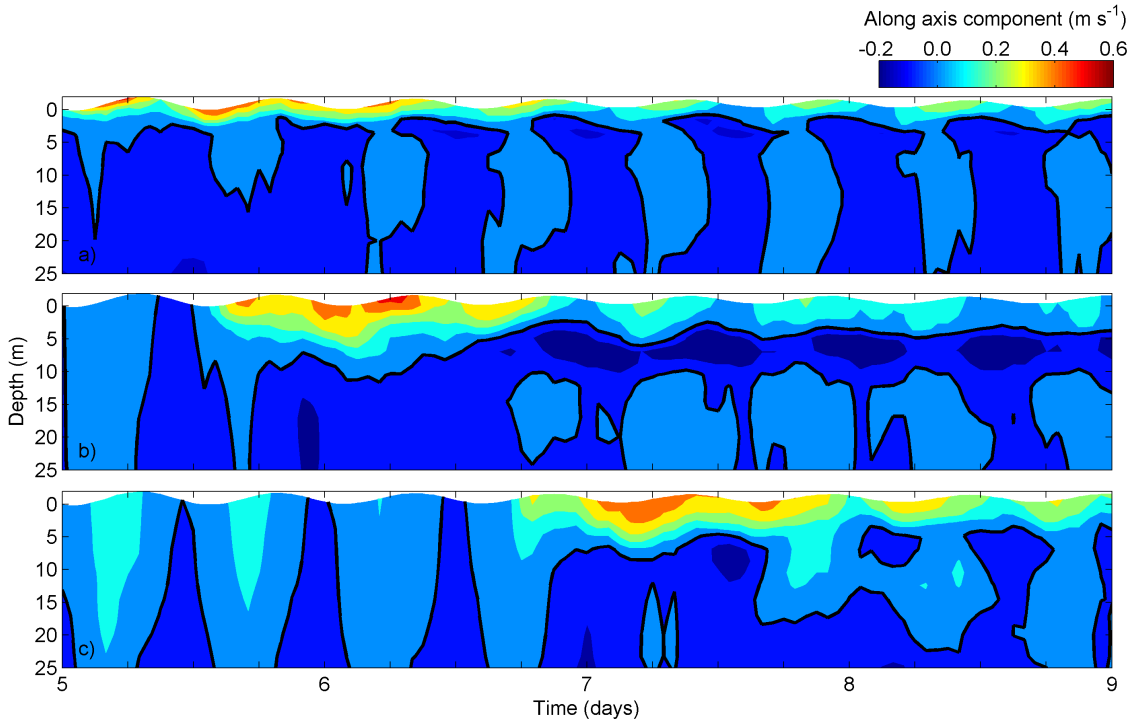

Figure 6.12: Along estuarine circulation at stations located at mouths of Rias de Vigo (a), Pontevedra (b) and Arousa (c), considering high river discharge and southerly winds of 6 m s^{-1}. Positive (negative) current velocity means water moving landward (seaward). Black line corresponds to 0 m s^{-1}.

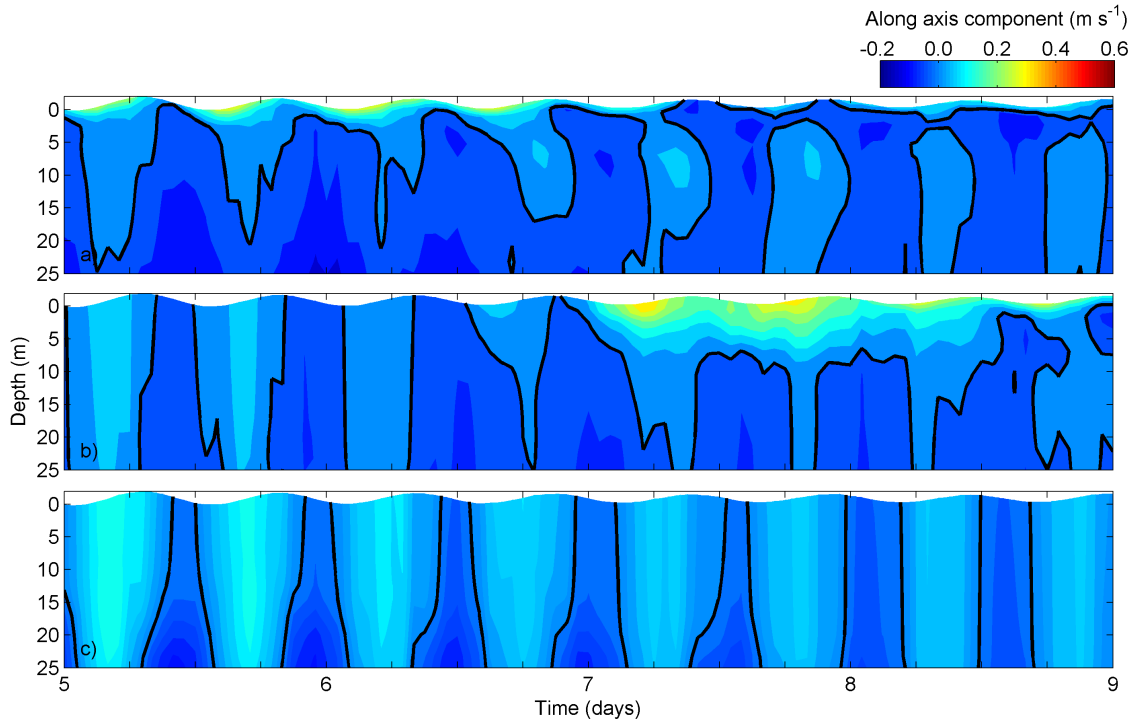

Figure 6.13: Along estuarine circulation at stations located at mouths of Rias de Vigo (a), Pontevedra (b) and Arousa (c), considering moderate river discharge and southerly winds of 3 m s^{-1}. Positive (negative) current velocity means water moving landward (seaward). Black line corresponds to 0 m s^{-1}.

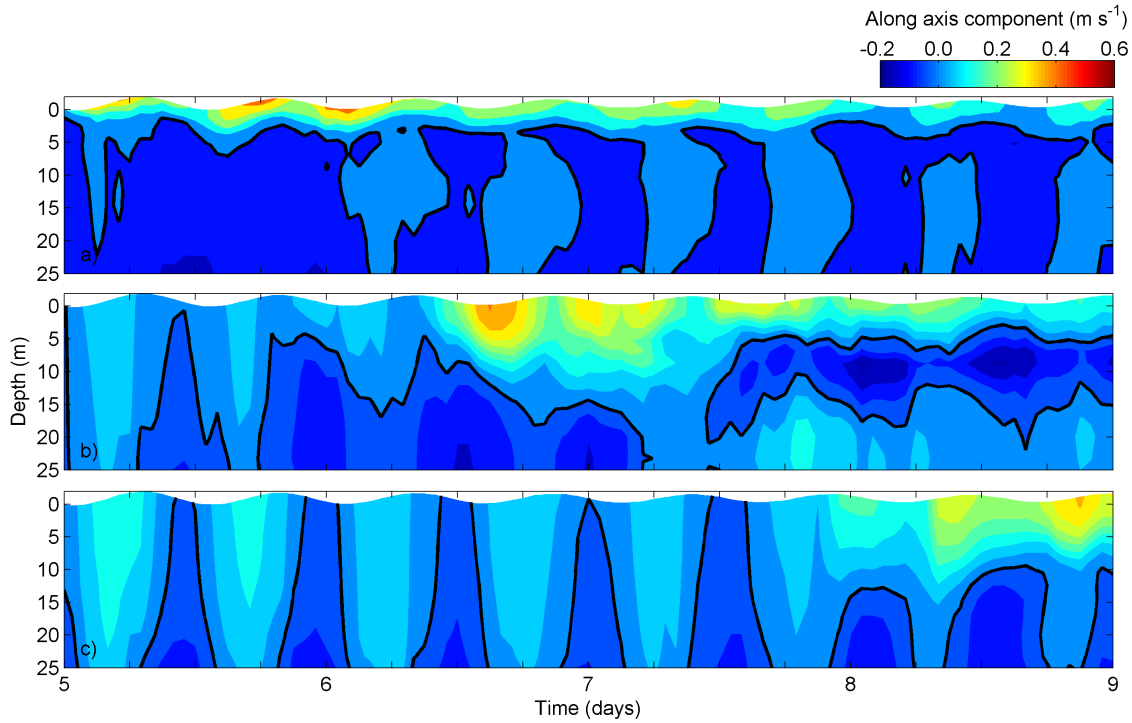

Figure 6.14: Along estuarine circulation at stations located at mouths of Rias de Vigo (a), Pontevedra (b) and Arousa (c), considering moderate river discharge and southerly winds of 6 m s^{-1}. Positive (negative) current velocity means water moving landward (seaward). Black line corresponds to 0 m s^{-1}.

with weak southerly winds only influence the Rias de Vigo and Pontevedra circulation patterns, while for wind speed up to 6 m s^{-1} its influence is also observed in Ria de Arousa. Independently of wind speed, a high discharge combined with southerly winds may change the circulation pattern of the all the Rias Baixas. Chao [1988b], Soares et al. [2007] and Marques et al. [2009] observed that southerly winds weakens and reverses the surface current in their studies for La Plata River and Patos Lagoon, promoting the vertical mixing processes and destratification of the water column.

6.3.3 Water exchange and mixture between Rias Baixas

The modelling results of the Lagrangian particles trajectories are depicted in Figure 6.15, showing the position evolution and time since launch of particles released close to the Minho river mouth during two days, under various forcing conditions. As the Minho estuarine plume can be classified as a surface-advected-plume, the particles were released at the surface layer.

In general, as would be expected, a pattern of younger particles close to the Minho river mouth is observed and older particles are kept farther from it. During the entire time period shown, the obtained model results represent the advection of individual water parcels, indicating that freshwater discharge and wind has a significant impact on the transport of released particles, which relates to the plume intrusion discussed before. For example, the surface plume has a relatively large size under weak wind forcing scenario and more particles move to the coastal ocean, floating far from the river mouth. This result is consistent with the findings obtained in the Columbia estuary plume studies [Banas et al., 2009].

For the high flow scenario (Figures 6.15a and 6.15d), the particles are advected northwards and confined close to the coast, corroborating the previous results. They are rapidly transported, reaching the Rias Baixas 1.5 days after being released. The particles trajectory includes not only the Rias de Vigo, Pontevedra and Arousa, but also extends to the Ria de Muros. Concerning the other freshwater outflow scenarios, the trajectories of the particles are not so different from this situation, however there are interesting features that must be pointed out. Under low-moderate flows and weak southerly winds (Figures 6.15b and 6.15c), the particles become limited to the Rias de Vigo and Pontevedra. However, when the wind increases (Figures 6.15e and 6.15f), particles are more tightly confined along the coast and less will reach the coastal ocean due to the increase of the surface current (Figures 6.8 and 6.9). In addition, many particles are concentrated in Ria de Arousa where the southerly winds in combination with the change in the coastline orientation hamper the northward displacement. The results reveal that the particles take longer ($>$ 2 days) to reach the Rias under the low freshwater condition.

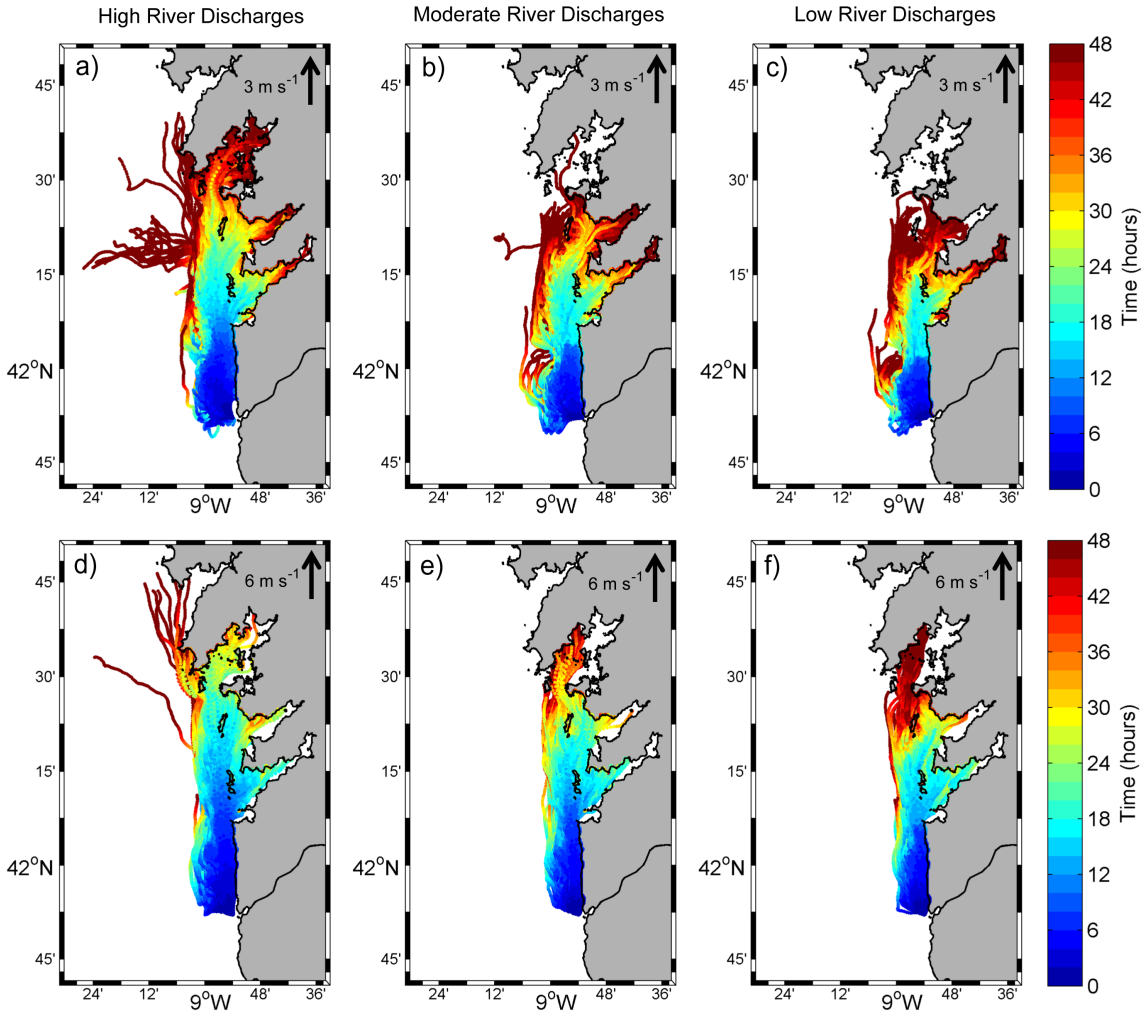

Figure 6.15: Trajectories and time since launch of particles released continuously close to the Minho river mouth, considering different southerly winds and river discharges.

Taking into account Figure 6.15, some particles that cross the Ria de Vigo mouth can turn way and cross the Rias de Pontevedra or Arousa. The fraction of particles arriving at Rias de Vigo, Pontevedra and Arousa (Figure 6.16) is computed considering the sections defined in Figure 6.2 (sections II, III and IV), in order to assess the water renovation and mixture between estuaries.

Over high flow scenario and moderate southerly winds as shown, in Figures 6.16a, 6.16b and 6.16c, about 38.5% of the particles released in the Minho River are transported to the Ria de Vigo (Figure 6.16a) after 5 days, while 37.2% and 59.4% of the particles cross the Rias de Pontevedra (Figure 6.16b) and Arousa (Figure 6.16c), respectively. Nevertheless, only 20.4% and 40.5% of the particles that remain in Rias de Pontevedra and Arousa come directly from the Minho river. These results reveal that there is water exchange between the different estuaries, hence each estuary cannot be considered independent. A similar trend is observed for weak winds , reaching 18.1%, 4.4% and 10.4% of the total particles in Rias

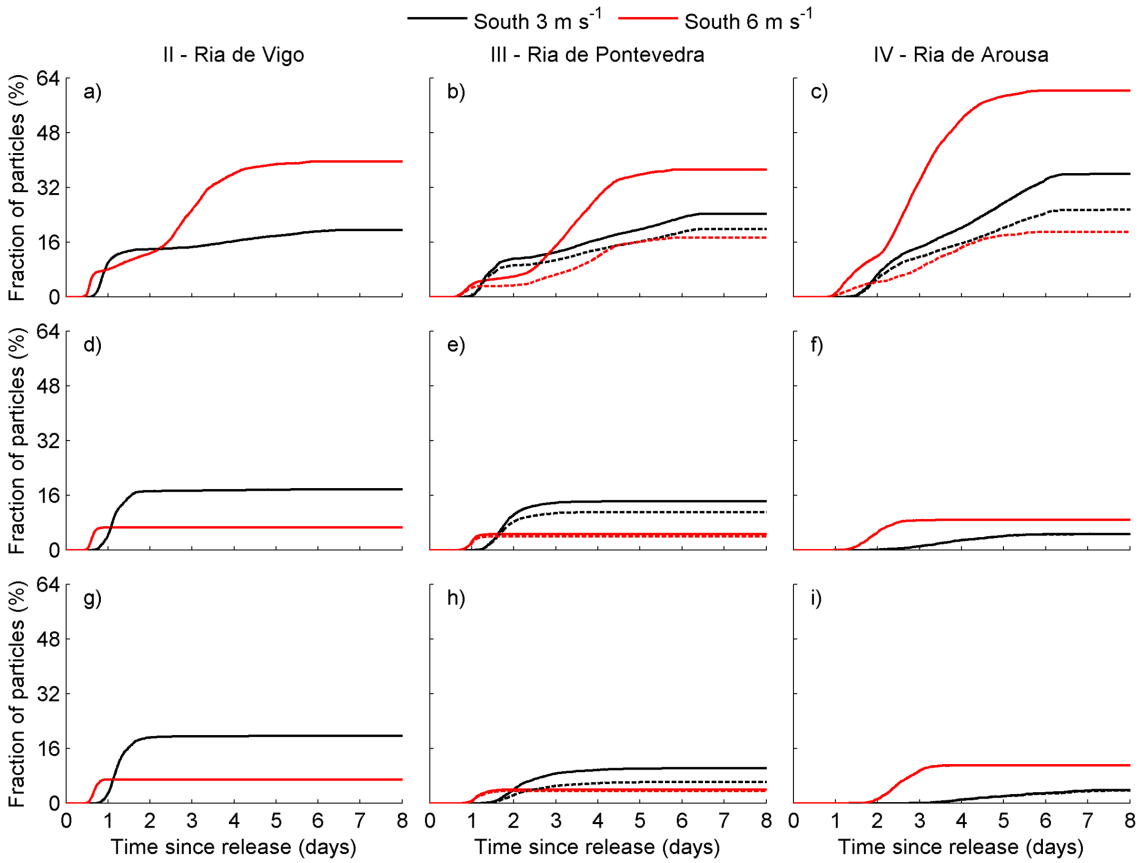

Figure 6.16: Fraction of particles released close to the Minho river mouth arriving at Rias de Vigo (II), Pontevedra (III) and Arousa (IV) under high (a,b,c), moderate (d,e,f) and low (g,h,i) river discharges scenarios. Dashed line corresponds to the particles that cross Rias mouth directly from Minho river.

de Vigo, Pontevedra and Arousa, respectively.

In the Ria de Vigo (Figures 6.16a, 6.16d and 6.16g), no significance differences between river discharges and weak wind scenarios are found. The model results indicate that as the river discharge values decrease, the fraction of particles inside the Rias de Pontevedra (Figures 6.16b, 6.16e and 6.16h) and Arousa (Figures 6.16c, 6.16f and 6.16i) is reduced significantly. Consequently, as results of the lower surface currents, particles spread on a larger area, not being so confined to the coast. This pattern of particle transport is consistent with the previous conclusions that freshwater outflow and wind has important effects on material exchanges.

According to these results, it is important to emphasize that the implementation of a particle tracking model could reveal the significant impact that a continuous emission of a certain pollutant may have, affecting the estuary and its neighbouring coastal ocean, turning this kind of applications a useful tool to marine scientists and managers. Another interesting aspect of these results is the strong effects that wind stress has on particle dispersal, determining the mixing processes during extreme events in this coastal area.

6.4 Conclusions

The main objective of this chapter was to investigate the necessary conditions for the establishment of the reverse circulation pattern in the Rias Baixas and evaluate its impact on Rias Baixas physical properties. Numerical experiments were conducted testing several scenarios with different river discharges, wind directions and intensity. The dispersion and potential pathways of particles released at the Minho river mouth was also assessed according to the previous scenarios. The numerical results obtained from this analysis suggest the following:

- The dispersal of the Minho estuarine plume responds rapidly to wind variations and is also influenced by the bathymetry and morphology of the coastline, being the Minho estuarine plume classified as a surface advected plume and heavily influenced by the wind.

- Under high discharge events, without wind forcing, the plume expands offshore, creating a bulge in front of the river mouth. Then, the low salinity waters are advected to the right due to the Coriolis effect and after the establishment of the geostrophic balance, the plume water extends northward (along the coastline). When the wind blows southwards, the main feature is the offshore extension of the plume. Otherwise, northward wind spreads the river plume, towards the Rias Baixas. The plume is confined close to the coast, reaching the mouth of the Ria de Vigo after 1.5 days and influences its hydrographic and circulation properties. Westward wind is more effective at pushing freshwater out of the mouth of the Minho River than any other wind condition.

- The response of the Minho estuarine plume to the wind forcing takes less than 1 day, and moderate wind conditions under high river discharge reverse the circulation pattern in Rias Baixas.

- The Minho River discharge and wind stress are the most important factors influencing the size and shape of the Minho estuarine plume.

- Under Minho River discharges higher than 800 $m^3\ s^{-1}$ and southerly winds of 3 $m\ s^{-1}$ only the Rias de Vigo and Pontevedra circulation patterns are reversed, while for wind speed higher than 6 $m\ s^{-1}$ the plume influence is also observed in Ria de Arousa. On the other hand, independently of southerly wind speed, under Minho River discharges higher than 2100 $m^3\ s^{-1}$ the circulation patterns are reversed in all Rias Baixas.

- The presented particle tracking model was successfully coupled to the hydrodynamic model, giving an overview of the transport patterns along the Western Galician coast. The freshwater discharge and wind has a significant impact on the transport of released particles.

- Over a period of 5 days, under high river discharge and moderate southerly winds, 38.5%, 37.2% and about 60% of the particles initially in Minho River are exported to the Rias de Vigo, Pontevedra and Arousa, respectively. However, only about 20% and 40% of the particles that remain in Rias de Pontevedra and Arousa come directly from the Minho River, showing the water exchange between the different estuaries. This confirms that the Rias Baixas cannot be considered as independent estuaries.

Chapter 7

Final conclusions

The general objective of this dissertation was to study the propagation of the Minho estuarine plume and its influence on Rias Baixas circulation and hydrography, and consequently to develop and explore an innovative numerical model application, integrating estuarine and coastal models. With this purpose, two numerical models were implemented. The first one is an estuarine model, comprising the whole Minho River estuary and the second one is a 3D baroclinic nested model for the NW Iberian Coast, including the adjacent Rias Baixas. Whereas summary conclusions were presented at the end of each Chapter, an overview of the main results as well as some suggestions that need further research are given in this conclusion section.

In Chapter 2, the hydrographic features of the mouth of each Ria were evaluated. The Rias Baixas are estuarine systems, that have in their downstream area a set of small islands affecting the circulation and hydrography patterns. Due to the existence of these islands, two mouths are considered for each Ria: northern and southern mouths. The results reveal that when comparing both mouths of each Ria, the water temperature is lower at the southern mouth than at the northern one. At the southern mouths, the influence of the upwelling and Minho River discharge is more intense, while at the northern mouths, due to its shallowness, the air temperature acquires a major importance influencing the water temperature. A major conclusion of this Chapter is that the water temperature is weakly dependent on the Minho river discharge and closely related to the air temperature pattern, and that the salinity is closely related to wind variability and to the Minho River discharge. In fact, as in many estuarine and coastal environments, the water temperature follows a daily cycle similar to the air temperature cycle.

In Chapter 3, an assessment of wind data was carried out, allowing to evaluate the applicability to study the dispersal of the Minho estuarine plume. Thus, a comparative analysis between offshore QuikSCAT satellite and *in situ* land meteorological wind data was performed. This comparison showed that the offshore wind from QuikSCAT represents

adequately the wind patterns at land meteorological stations. The results of an weather forecast model (WRF) were also added in the previously study, since the numerical model used throughout this dissertation requires wind data with high spatial and temporal resolution close to the coast. The analysis reveals that the WRF model and QuikSCAT satellite data are consistent tools to obtain representative wind data near the coast, showing good results when comparing with *in situ* wind observations from oceanographic buoys. The results showed that the wind speeds derived from QuikSCAT and the WRF model are similar along the coast, with errors ranging from 1.5 m s^{-1} to 2 m s^{-1}. However, QuikSCAT data tend to overestimate wind speed when compared to the buoys measurements. Regarding the wind direction, the RMSE values are about 35° for the stations under analysis. The bias presents a similar pattern between satellite and modelled data, with positive values at the western coast and negative values at the middle and northern coasts. The satellite data always presents lower absolute values than the model results. A spatial comparison between QuikSCAT and WRF data was also performed over the whole Galician coast to evaluate the differences between the two datasets. This comparison showed that the modelled wind speed tend to be lower than satellite winds over the entire domain, with the highest RMSE and bias values found for the wind speed and direction observed near shoreline.

Due to the near-coastal land contamination of satellite values and the lack of anemometers in the whole coastal region, the weather forecast model presents clear advantages in the representation of the near-shore wind regime. Thus, the wind model predictions becomes a useful tool to analyse the Galician coast, helping to better understand the wind induced phenomena which take place in this region. In fact, the accuracy of the model predictions makes them suitable to perform the precise study of the physical processes driving several coastal phenomena. For example, the study of ocean chlorophyll-*a* concentration distribution and evolution requires the knowledge of accurate wind fields, since chlorophyll-*a* is highly sensitive to changes in wind forcing [Alvarez et al., 2012] and its seasonal variability is mainly related to upwelling events during spring and summer seasons. The study of the dispersal of river plumes also needs the knowledge of accurate wind fields, since estuarine plumes respond rapidly to wind variations, which determine the horizontal buoyancy dispersal pattern [Choi and Wilkin, 2007; Otero et al., 2008; Vaz et al., 2009b].

The modelling task performed throughout this work began by assessing the configuration that better represents the Minho estuarine plume propagation (Chapter 4).Two nested configurations (Configurations #1 and #2) with three levels one-way nested grids and an estuarine model were implemented. The estuarine model runs offline and was developed to reproduce the Minho estuary ocean-interaction. The used configurations only differed in the source of the initial forcing conditions. Both applications were designed using the numerical model MOHID through a downscaling approach, with a three-level one-way nested scheme. The first model domain includes the whole Iberian Peninsula

coast, the second domain is a coarse representation of the Rias Baixas adjacent coastal area, while the third includes the same area with a higher resolution. All domains present realistic coastline and bottom topography. The model results were evaluated against several databases of remote sensing covering the region under analysis and salinity and water temperature *in situ* data collected close to the Ria de Vigo mouth. In the area of propagation of the Minho estuarine plume, the configuration that uses the Levitus climatology as initial condition (Configuration #1) presented a better agreement with the *in situ* data. For the salinity, the RMSE value is close to 1 and the bias is close to zero. The measured water temperature is also well represented by the Configuration #1, with RMSE and bias values lower than 0.6 ºC, revealing a good temporal representation of the hydrographic features of this area.

A good validation of the nesting model was achieved (Chapter 5), revealing the ability in reproducing the local hydrodynamics and thermohaline patterns over the Western Galician coast. At the Minho estuary, the observed and predicted SSE follow a similar pattern, with an average RMSE around 0.20 m and a predictive skill close to 1. The modelled water temperature pattern showed a maximum RMSE about 30% of the local water temperature amplitude, while for salinity the RMSE value was about 8%, showing a good agreement with the *in situ* data. Also, at the Rias Baixas, a good agreement between model predictions and *in situ* data was found. The observed and predicted SSE at both areas follow a similar pattern, with an average RMSE around 0.06-0.20 m and the predictive skill close to 1. The model predictions slightly overestimate salinity, with maximum RMSE values lower than 1.27, whereas the lowest difference between SST model predictions and satellite data (close to zero) are observed in the plume propagation area.

The chosen period for the plume propagation model validation was the spring of 1998, because a high Minho River discharge was reported, as well as favourable wind patterns that spread the river plume towards the Rias Baixas. The importance of the Minho River discharge and the wind forcing in the event of May 1998 was studied considering two scenarios: one with a constant average discharge to evaluate the wind effects and the second removing the wind from 1 to 13 May 1998 to evaluate the river discharge effects. From the model results, it was found that a buoyancy intrusion (in the Rias Baixas) caused by the Minho River reverses the normal estuarine longitudinal gradient of salinity and the normal estuarine circulation of the Rias de Vigo and Pontevedra. Moreover, a continuous moderate Minho River discharge combined with northwards winds is enough to produce the negative circulation pattern in Rias Baixas, reducing the importance of the existence of specific events of high runoff values.

The characterization of the Minho estuarine plume and the necessary conditions (in terms of wind and river discharge) for the establishment of the reverse circulation pattern in Rias Baixas were investigated in Chapter 6. For this purpose, several scenarios with different river discharges (low, moderate and high), wind directions (north, south, west

and east) and intensity (3 and 6 m s^{-1}) were created. According to the Yankovsky and Chapman [1997] and Whitney and Garvine [2005] formulations, the Minho estuarine plume was classified as a surface-advected plume and it is heavily influenced by the wind patterns. In the moderate-to-high river discharge scenarios, the results revealed that the southerly winds promote the introduction of the Minho estuarine outflow into the Rias de Vigo and Pontevedra and lead to a small influence in Ria de Arousa. In the low river discharge scenario, a small influence of the Minho plume intrusion was observed in the Ria de Vigo, showing that for these conditions, the Minho estuarine plume does not influence the Rias Baixas general circulation pattern.

Independently of the wind speed, the response of the Minho estuarine plume to the wind forcing takes less than 1 day and a high estuarine discharge combined with southerly winds reverses the circulation pattern of all the Rias Baixas. However, a moderate river discharge combined with weak southerly winds only reverse the Rias de Vigo and Pontevedra circulation pattern, while for wind speed up to 6 m s^{-1} the plume influence is also extended to the Ria de Arousa. This is an important feature, since, this negative circulation tends to stop water exchange between the Rias and the shelf, increasing the residence time and hence affecting water quality. On one hand, the high concentration of nutrients from the Minho River can induce phytoplankton blooms at the shelf, contributing as an extra feeding source for the main shellfish. One the other hand, the Rias Baixas are more sensitive to freshwater input because the water renewal is lower in these systems, affecting negatively its ecology. The Rias Baixas are recognized as a privilege area of production of marine species of great economical interest [Tenore et al., 1995], especially mussels. The existence of this negative circulation affects the exchange between the Rias and the ocean, changing the input of nutrients.

In order to better understand the surface transport of passive tracers, a particle tracking model was also implemented in Chapter 6. The Lagrangian model has proved to be an useful tool for the study of dispersion phenomena along the Western Galician coast. It was successfully coupled to the hydrodynamic model, allowing the tracking of the path of individual particles released at Minho River mouth. The results of this application revealed that in a time scale higher than 5 days, the particles released close to the Minho River mouth enter both in Rias de Vigo, Pontevedra and Arousa, revealing a high exchange rate between them ($\sim$ 20%). This confirms that the Rias Baixas cannot be considered as independent estuaries.

Overall, the outcome of this work shows that the reverse circulation pattern observed in the Rias Baixas may be induced by a continuous moderate ($>$ 800 m^3 s^{-1}) Minho river discharge under northward winds. Due to the high frequency of these moderate river discharge events, the methodology proposed in this dissertation produces sound and thorough results, and proved to be useful and accurate enough to simulate the dynamics of the Minho estuarine plume along the Galician coast, as well as its effects on Rias Baixas.

The results of this dissertation as well as the methodologies developed are unlikely to be unique for the Rias Baixas and it is suggested that similar modelling approaches could be replicated to other comparable systems, such as Spencer Gulf, Oregon Washington coast, Upper Gulf of California or Patos Lagoon, to improve understanding and characterize coupled estuarine-near coastal systems.

All the aims established at the beginning of the work were fulfilled and even surpassed. It remains for the future several numerical improvements in the numerical model yet to be performed. In particular, the implementation of a model with higher resolution inside the Rias Baixas, allowing an accurate description of the local bathymetry. This implementation will result in more accurate predictions of the circulation and hydrographic features of the Rias Baixas. Also, it should be interesting to add to the model the coastal currents forcing (especially the IPC) to study its influence (or not) in the circulation in Rias Baixas.

Future research must also put an emphasis on the coupling between the hydrodynamic-transport and ecological models, in order to understand the complex structure of the physical and water quality variables.With this methodology it will be possible to study and analyse the upwelling formation as well as the interaction between the Rias Baixas, and to identify the potential risk sources (e.g. decrease of the oxygen in water column or increase of the freshwater input) than can threat the local aquaculture productivity. This ecological implementation will allow to study the effects of the harmful algal blooms generated in the coastal waters, which are introduced into the Rias Baixas at times of downwelling or through the reverse of circulation patterns.

References

Accadia C., Zecchetto S., Lavagnini A. and Speranza A. (2007). Comparison of 10-m wind forecasts from a regional area model and QuikSCAT Scatterometer wind observations over the Mediterranean Sea. *Monthly Weather Review*, 135(5):1945–1960.

Allen C.M. (1982). Numerical simulation of contaminant dispersion in estuary flows. *Proceedings of the Royal Society A*, 381:179–194.

Alonso-Perez F., Ysebaert T. and Castro C.G. (2010). Effects of suspended mussel culture on benthic-pelagic coupling in a coastal upwelling system (Ria de Vigo, NW Iberian Peninsula). *Journal of Experimental Marine Biology and Ecology*, 382(2):96–107.

Alvarez I., deCastro M., Gomez-Gesteira M. and Prego R. (2005a). Inter- and intra-annual analysis of the salinity and temperature evolution in the Galician Rias Baixas-ocean boundary (northwest Spain). *Journal of Geophysical Research-Oceans*, 110(C4).

Alvarez I., deCastro M., Gomez-Gesteira M. and Prego R. (2006). Hydrographic behavior of the Galician Rias Baixas (NW Spain) under the spring intrusion of the Miño River. *Journal of Marine Systems*, 60(1-2):144–152.

Alvarez I., deCastro M., Prego R. and Gomez-Gesteira M. (2003). Hydrographic characterization of a winter-upwelling event in the Ria of Pontevedra (NW Spain). *Estuarine Coastal and Shelf Science*, 56(3-4):869–876.

Alvarez I., Dias J.M., deCastro M., Vaz N., Sousa M.C. and Gomez-Gesteira M. (2013). Influence of upwelling events on the estuaries of the north-western coast of the Iberian Peninsula. *Marine and Freshwater Research*, 64(5):1–12.

Alvarez I., Gomez-Gesteira M., deCastro M. and Dias J. (2008a). Spatio-temporal evoltion of upwelling regime along the western coast of the Iberian Peninsula. *Journal of Geophysical Research*, 113:C07020.

Alvarez I., Gomez-Gesteira M., deCastro M., Lorenzo M.N., Crespo A.J.C. and Dias J.M. (2011). Comparative analysis of upwelling influence between the western and northern coast of the Iberian Peninsula. *Continental Shelf Research*, 31(5):388–399.

Alvarez I., Gomez-Gesteira M., decastro M. and Novoa E.M. (2008b). Ekman transport along the Galician coast (NW, Spain) calculated from QuikSCAT winds. *Journal of Marine Systems*, 72(1-4):101–115.

Alvarez I., Gomez-Gesteira M., deCastro M. and Prego R. (2005b). Variation in upwelling intensity along the Northwest Iberian Peninsula (Galicia). *Journal of Atmospheric & Ocean Science*, 10(4):309–324.

Alvarez I., Lorenzo M.N. and deCastro M. (2012). Analysis of chlorophyll a concentration along the Galician coast: seasonal variability and trends. *ICES Journal of Marine Science*, 69(5):728–738.

Alvarez I., Ospina-Alvarez N., Pazos Y., deCastro M., Bernardez P., Campos M.J., Gomez-Gesteira J.L., Alvarez-Ossorio M.T., Varela M., Gomez-Gesteira M. and Prego R. (2009). A winter upwelling event in the Northern Galician Rias: Frequency and oceanographic implications. *Estuarine Coastal and Shelf Science*, 82(4):573–582.

Alvarez-Salgado X.A., Figueiras F., Perez F.F., Groom S., Nogueira E., Borges A.V., Chou L., Castro C.G., Moncoiffé G., Rios A.F., Miller A.E.J., Frankignoulle M., Savidge G. and Wollast R. (2003). The Portugal coastal counter current off NW Spain: new insights on its biogeochemical variability. *Progress in Oceanography*, 56:281–321.

Alvarez-Salgado X.A., Roson G., Perez F.F., Figueiras F.G. and Pazos Y. (1996a). Nitrogen cycling in a estuarine upwelling system, the Ria de Arousa (NW Spain). *Marine Ecology Progress Series*, 135:259–273.

Alvarez-Salgado X.A., Roson G., Perez F.F., Figueiras F.G. and Rios A.F. (1996b). Nitrogen cycling in a estuarine upwelling system, the Ria de Arousa (NW Spain). II. Spatial differences in the short- timescale evolution of fluxes and net budgets. *Marine Ecology Progress Series*, 135:275–288.

Alvarez-Salgado X.A., Roson G., Perez F.F. and Pazos Y. (1993). Hydrographic variability off the Rias Baixas (NW Spain) during the upwelling season. *Journal of Geophysical Research-Oceans*, 98(C8):14447–14455.

Antonov J.I., Seidov D., Boyer T.P., Locarnini R.A., Mishonov A.V., Garcia H.E., Baranova O.K., Zweng M.M. and Johnson D.R. (2010). *World Ocean Atlas 2009, Volume 2: Salinity*. Tech. Rep. S. Levitus, Ed. NOAA Atlas NESDIS 69, Washington, DC: U.S. Government Printing Office, 184 pp.

Austin S. and Pierson W.J. (1999). Mesoscale and synoptic-scale effects on the validation of NSCAT winds by means of data buoy reports. *Journal of Geophysical Research*, 104(C5):11437–11447.

Banas N.S., Hickey B.M., MacCready P. and Newton J.A. (2004). Dynamics of Willapa Bay, Washington: a highly unsteady, partially mixed estuary. *Journal of Physical Oceanography*, 34(11):2413–2427.

Banas N.S., MacCready P. and Hickey B.M. (2009). The Columbia River plume as cross-shelf exporter and along-coast barrier. *Continental Shelf Research*, 29:292–301.

Bermudez A., Dervieux A., Desideri J.A. and Vazquez E. (1996). Upwind schemes for the two-dimensional shallow water equations with variable depth using unstructured meshes. *Computer Methods in Applied Mechanics and Engineering*, 155:49–72.

Bermudez A., Rodriguez C. and Villar M.A. (1997). A numerical method for resolution of two-dimensional shallow-water equations. *Revista de Geociências*, 8:63–66.

Bettencourt A., Ramos L., Gomes V., Dias J., Ferreira G., Silva M. and Costa L. (2003). *Estuários Portugueses*. Tech. Rep., Ordenamento do Território e Ambiente, INAG, Lisbon, 326 pp.

Blanton J.O., Tenore K.R., Castillejo F., Atkinson L.P., Schwing F.B. and Lavin A. (1987). The relationship of upwelling to mussel production in the Rias on the Western Coast of Spain. *Journal of Marine Research*, 45(2):497–511.

Blumberg A.F. and Kantha L.H. (1985). Open Boundary-Condition for Circulation Models. *Journal of Hydraulic Engineering-Asce*, 111(2):237–255.

Borja A., Uriarte A., Valencia V., Motos L. and Uriarte A. (1996). Relationships between anchovy (Engraulis encrasicolus L) recruitment and the environment in the Bay of Biscay. *Scientia Marina*, 60:179–192.

Braunschweig F., Martins F., Leitão P.C. and Neves R. (2003). A methodology to estimate renewal time scales in estuaries: the Tagus Estuary case. *Ocean Dynamics*, 53(3):137–145.

Bruland K.W., Lohan M.C., Aguilar-Islas A.M., Smith G.J., Sohst B. and Baptista A. (2008). Factors influencing the chemistry of the near-field Columbia River plume: nitrate, silicic acid, dissolved Fe, and dissolved Mn. *Journal of Geophysical Research-Oceans*, 113.

Burchard H., Petersen O. and Rippeth T.P. (1998). Comparing the performance of the Mellor-Yamada and the k-epsilon two-equation turbulence models. *Journal of Geophysical Research-Oceans*, 103(C5):10543–10554.

Cabanas J.M. and Alvarez I. (2005). Ekman transport in the area close to the Galician coast (NW, Spain). *Journal of Atmospheric and Ocean Science*, 10(4):325–341.

Canuto V.M., Howard A., Cheng Y. and Dubovikov M.S. (2001). Ocean turbulence. Part I: One-point closure model - momentum and heat vertical diffusivities. *Journal of Physical Oceanography*, 31(6):1413–1426.

Chao S.Y. (1988a). River-forced estuarine plumes. *Journal of Physical Oceanography*, 18(1):72–88.

Chao S.Y. (1988b). Wind-driven motion of estuarine plumes. *Journal of Physical Oceanography*, 18(8):1144–1166.

Chao S.Y. (1990). Tidal modulation of estuarine plumes. *Journal of Physical Oceanography*, 20(7):1115–1123.

Chao S.Y. and Boicourt W.C. (1986). Onset of estuarine plumes. *Journal of Physical Oceanography*, 16(12):2137–2149.

Chapra S.C. (1997). *Surface Water Quality Modeling*. Civil engineering series, McGraw-Hill, New York.

Chelton D.B. and Freilich M.H. (2005). Scatterometer-based assessment of 10-m wind analyses from the operational ECMWF and NCEP numerical weather prediction models. *Monthly Weather Review*, 133(2):409–429.

Choi B.J. and Wilkin J.L. (2007). The effect of wind on the dispersal of the Hudson River plume. *Journal of Physical Oceanography*, 37(7):1878–1897.

Dagg M., Benner R., Lohrenz S. and Lawrence D. (2004). Transformation of dissolved and particulate materials on continental shelves influenced by large rivers: plume processes. *Continental Shelf Research*, 24(7-8):833–858.

deCastro M., Alvarez I., Varela M., Prego R. and Gomez-Gesteira M. (2006a). Miño river dams discharge on neighbor Galician Rias Baixas (NW Iberian Peninsula): Hydrological, chemical and biological changes in water column. *Estuarine Coastal and Shelf Science*, 70(1-2):52–62.

deCastro M., Gomez-Gesteira M., Alvarez I. and Prego R. (2004). Negative estuarine circulation in the Ria of Pontevedra (NW Spain). *Estuarine Coastal and Shelf Science*, 60(2):301–312.

deCastro M., Gomez-Gesteira M., Alvarez I. and Prego R. (2006b). Seasonal evolution of the transverse thermohaline asymmetry in the Ria de Pontevedra (northwestern Spain). *Estuarine Coastal and Shelf Science*, 60:673–681.

deCastro M., Gomez-Gesteira M., Lorenzo M.N., Alvarez I. and Crespo A.J.C. (2008). Influence of atmospheric modes on coastal upwelling along the western coast of the Iberian Peninsula, 1985 to 2005. *Climate Research*, 36(2):169–179.

deCastro M., Gomez-Gesteira M., Prego R., Taboada J.J., Montero P., Herbello P. and Perez-Villar V. (2000). Wind and tidal influence on water circulation in a Galician ria (NW Spain). *Estuarine Coastal and Shelf Science*, 51(2):161–176.

deCastro M., Lorenzo N., Taboada J.J., Sarmiento M., Alvarez I. and Gomez-Gesteira M. (2006c). Influence of teleconnection patterns on precipitation variability and on river flow regimes in the Miño River basin (NW Iberian Peninsula). *Climate Research*, 32:63–73.

Dias J.M., Sousa M.C., Bertin X., Fortunato A.B. and Oliveira A. (2009). Numerical modeling of the impact of the Ancão Inlet relocation (Ria Formosa, Portugal). *Environmental Modelling & Software*, 24(6):711–725.

Dodet G., Bertin X. and Taborda R. (2010). Wave climate variability in the North-East Atlantic Ocean over the last six decades. *Ocean Modelling*, 31:120–131.

Dortch Q. and Whitledge T.E. (1992). Does nitrogen or silicon limit phytoplankton production in the Mississippi River plume and nearby regions. *Continental Shelf Research*, 12(11):1293–1309.

Doval M.D., Nogueira E. and Perez F. (1998). Spatio-temporal variability of the thermohaline and biogeochemical properties and dissolved organic carbon in a coastal embayment affected by upwelling: the Ria de Vigo (NW Spain). *Journal of Marine Systems*, 14:135–150.

Ebuchi N., Graber H.C. and Caruso M.J. (2002). Evaluation of wind vectors observed by QuikSCAT/SeaWinds using ocean buoy data. *Journal of Atmospheric and Oceanic Technology*, 19(12):2049–2062.

Fiedler P.C. and Laurs R.M. (1990). Variability of the Columbia River plume observed in visible and infrared satellite imagery. *International Journal of Remote Sensing*, 11(6):999–1010.

Figueiras F.G., Jones K., Mosquera A.M., Alvarez-Salgado X.A., Edwards A. and MacDougall N. (1994). Red tide assemblage formation in an estuarine upwelling ecosystem: Ria de Vigo. *Journal of Plankton Research*, 16:857–878.

Figueiras F.G., Labarta U. and Fernández Reiriz M.J. (2002). Coastal upwelling, primary production and mussel growth in the Rias Baixas of Galicia. *Hydrobiologia*, 484:121–131.

Fiuza A.F.G., Hamann M., Ambar I., del Rio G.D., Gonzalez N. and Cabanas J.M. (1998). Water masses and their circulation off western Iberia during May 1993. *Deep-Sea Research Part I-Oceanographic Research Papers*, 45(7):1127–1160.

Fiuza A.F.G., Macedo M.E. and Guerreiro M.R. (1982). Climatological space and time variability of the Portuguese upwelling. *Oceanological Acta*, 5(1):31–40.

Fong D.A. and Geyer W.R. (2001). Response of a river plume during an upwelling favorable wind event. *Journal of Geophysical Research-Oceans*, 106(C1):1067–1084.

Fong D.A. and Geyer W.R. (2002). The alongshore transport of freshwater in a surface-trapped river plume. *Journal of Physical Oceanography*, 32(3):957–972.

Fortunato A.B., Oliveira A. and Alves E.T. (2002). Circulation and salinity intrusion in the Guadiana Estuary. *Thalassas*, 18(2):43–65.

Fraga F. (1981). *Upwelling off the Galician Coast, Northwest Spain*. Tech. Rep., In: Richardson, F.A. (Ed.), Coastal Upwelling, American Geophysical Union, Washington, 176–182.

Fraga F. and Margalef R. (1979). Las rias gallegas. Estudio y Explotacion del mar en Galicia. *Santiago de Compostela*, 101–121.

Fraga S., Anderson, D. M. I. Bravo, Reguera B., Steidinger K.A. and Yentsch C.M. (1988). Influence of upwelling relaxation on dinoflagellates and shellfish toxicity in Ria-De-Vigo, Spain. *Estuarine Coastal and Shelf Science*, 27(4):349–361.

Freitas V., Costa-Dias S., Campos J., Bio A., Santos P. and Antunes C. (2009). Patterns in abundance and distribution of juvenile flounder, Platichthys flesus, in Minho estuary (NW Iberian Peninsula). *Aquatic Ecology*, 43(4):1143–1153.

Frouin R., Fiuza A.F.G., Ambar I. and Boyd T.J. (1990). Observations of a poleward surface current off the coast of Portugal and Spain during winter. *Journal of Geophysical Research*, 95:679–691.

García-Berdeal I., Hickey B.M. and Kawase M. (2002). Influence of wind stress and ambient flow on a high discharge river plume. *Journal of Geophysical Research-Oceans*, 107(C9).

Garvine R.W. (1974). Physical features of Connecticut River outflow during high discharge. *Journal of Geophysical Research*, 79(6):831–846.

Garvine R.W. (1984). Radial spreading of buoyant, surface plumes in coastal waters. *Journal of Geophysical Research-Oceans*, 89(Nc2):1989–1996.

Garvine R.W. (1995). A dynamical system for classifying buoyant coastal discharges. *Continental Shelf Research*, 15(13):1585–1596.

Garvine R.W. (1999). Penetration of buoyant coastal discharge onto the continental shelf: a numerical model experiment. *Journal of Physical Oceanography*, 29:1892–1909.

Garvine R.W. (2001). Artifacts in buoyant coastal discharge models: An observational and model study. *Journal of Marine Research*, 59:193–225.

Gilcoto M., Pardo P.C., Alvarez-Salgado X.A. and Perez F.F. (2007). Exchange fluxes between the Ria de Vigo and the shelf: A bidirectional flow forced by remote wind. *Journal of Geophysical Research-Oceans*, 112(C06001).

Gomez-Gesteira M., deCastro M. and Prego R. (2003). Dependence of the water residence in Ria of Pontevedra (NW Spain) on the seawater inflow and the river discharge. *Estuarine, Coastal and Shelf Science*, 58(555-563).

Gomez-Gesteira M., deCastro M., Prego R. and Perez-Villar V. (2001). An unusual two layered tidal circulation induced by stratification and wind in the Ria of Pontevedra (NW Spain). *Estuarine Coastal and Shelf Science*, 52(5):555–563.

Gomez-Gesteira M., Montero P., Prego R., Taboada J.J., Leitão P., Ruiz-Villarreal M., Neves R. and Perez-Villar V. (1999). A two-dimensional particle tracking model for pollution dispersion in A Coruna and Vigo Rias (NW Spain). *Oceanologica Acta*, 22(2):167–177.

Gomez-Gesteira M., Moreira C., Alvarez I. and deCastro M. (2006). Ekman transport along the Galician coast (northwest Spain) calculated from forecasted winds. *Journal of Geophysical Research-Oceans*, 111(C10).

Guerrero R.A., Acha E.A., Framiñan M.B. and Lasta C.A. (1997). Physical oceanography of the Rio de la Plata Estuary, Argentina. *Continental Shelf Research*, 17(7):717–742.

Guo X.Y. and Valle-Levinson A. (2007). Tidal effects on estuarine circulation and outflow plume in the Chesapeake Bay. *Continental Shelf Research*, 27(1):20–42.

Hanson R.B., Alvarez-Ossorio M.T., Cal R., Campos M.J., Roman M., Santiago G., Varela M. and Yoder J.A. (1986). Plankton response following a spring upwelling event in the Ria de Arosa, Spain. *Marine Ecology Progress Series*, 32:101–113.

Herrera J.L., Varela R.A. and Roson G. (2008). Spatial variability of the barotropic m_2 constituent tidal current over the Rias Baixas Galician shelf (NW Spain). *Journal of Marine Systems*, 72(1-4):189–199.

Hetland R.D. (2005). Relating river plume structure to vertical mixing. *Journal of Physical Oceanography*, 35(9):1667–1688.

Hickey B.M. and Banas N.S. (2003). Oceanography of the US Pacific Northwest Coastal Ocean and estuaries with application to coastal ecology. *Estuaries*, 26(4B):1010–1031.

Horner-Devine A.R., Fong D.A., Monismith S.G. and Maxworthy T. (2006). Laboratory experiments simulating a coastal river outflow. *Journal of Fluid Mechanics*, 555:203–232.

Horner-Devine A.R., Jay D.A., Orton P.M. and Spahn E.Y. (2009). A conceptual model of the strongly tidal Columbia River plume. *Journal of Marine Systems*, 78(3):460–475.

Huthnance J.M., Van Aken H.M., White M., Barton E.D., Le Cann B., Coelho E.F., Fanjul E.A., Miller P. and Vitorino J. (2002). Ocean margin exchange - water flux estimates. *Journal of Marine Systems*, 32(1-3):107–137.

IH (2006). *Tabela de Marés*, Vol. 1. Instituto Hidrográfico, Portugal, 192 pp.

Johnson H.K. (1999). Simple expressions for correcting wind speed data for elevation. *Coastal Engineering*, 36(3):263–269.

JPL (2001). *Seawinds on QuikSCAT level 3 gridded ocean winds vectors (JPL version 2)*. Tech. Rep., JPL Seawinds Project. Jet Propulsion Laboratory.

Jurisa J.T. and Chant R. (2012). The coupled Hudson River estuarine-plume response to variable wind and river forcings. *Ocean Dynamics*, 62(5):771–784.

Kaplan E.L. and Meier P. (1958). Nonparametric-estimation from incomplete observations. *Journal of the American Statistical Association*, 53(282):457–481.

Kortzinger A. (2003). A significant CO2 sink in the tropical Atlantic Ocean associated with the Amazon River plume. *Geophysical Research Letters*, 30(24).

Kourafalou V.H. (1999). Process studies on the Po River plume, North Adriatic Sea. *Journal of Geophysical Research-Oceans*, 104(C12):29963–29985.

Kourafalou V.H., Oey J.D. and Lee T.N. (1996). The fate of river discharge on the continental shelf: 1. Modeling the river plume and the inner shelf coastal current. *Journal of Geophysical Research-Oceans*, 101(C2):3415–3434.

Large W.G., Morzel J. and Crawford G.B. (1995). Accounting for surface-wave distortion of the marine wind-profile in low-level ocean storms wind measurements. *Journal of Physical Oceanography*, 25(11):2959–2971.

Large W.G. and Pond S. (1981). Open ocean momentum flux measurements in moderate to strong winds. *Journal of Physical Oceanography*, 11(3):324–336.

Lavin A., Díaz del Rio G., Cabanas J.M. and Gasas G. (1991). *Afloramiento en el noroeste de la Peninsula Iberica: Indices de afloramiento para el punto 43°N, 11°W período 1966-1989*. Tech. Rep. 91, Instituto Español de Oceanografía, 33.

Lavin A., Díaz del Rio G., Gasas G. and Cabanas J.M. (2000). *Afloramiento en el noroeste de la Peninsula Iberica: Indices de afloramiento para el punto 43°N, 11°W período 1990-1999*. Tech. Rep. 15, Instituto Español de Oceanografía, 25.

Le Provost C., Lyard F., Molines J.M., Genco M.L. and Rabilloud F. (1998). A hydrodynamic ocean tide model improved by assimilating a satellite altimeter-derived data set. *Journal of Geophysical Research-Oceans*, 103(C3):5513–5529.

Leendertse J. (1967). *Aspects of a computational model for long water wave propagation*. Tech. Rep., Memorandum rh-5299-rr, Rand Corporation, 165 pp.

Leendertse J. and Liu S. (1978). A three-dimensional turbulent energy model for non-homogeneous estuaries and coastal sea systems. *In: Nihoul, J. (Ed), Hydrodynamics of estuaries and Fjords, Elsevier, Amsterdam*, 387–405.

Leitão P. (2002). *Integração de Escalas e de Processos na Modelação do Ambiente Marinho*. Phd thesis, Instituto Superior Técnico, Lisboa, 466 pp.

Leitão P., Coelho H., Santos A. and Neves R. (2005). Modelling the main features of the Algarve coastal circulation during July 2004: A downscaling approach. *Journal of Atmospheric and Ocean Science*, 10(4):421–462.

Lentz S.J. and Largier J. (2006). The influence of wind forcing on the Chesapeake Bay buoyant coastal current. *Journal of Physical Oceanography*, 36(7):1305–1316.

Liu W.T., Katsaros K.B. and Businger J.A. (1979). Bulk parameterization of air-sea exchanges of heat and water-vapor including the molecular constraints at the interface. *Journal of the Atmospheric Sciences*, 36(9):1722–1735.

Liu W.T. and Tang W.Q. (1996). *Equivalent neutral winds.* Tech. Rep., Jet Propulsion Laboratory Publication, CA, JPL Pub, 16 pp.

Locarnini R.A., Mishonov A.V., Antonov J.I., Boyer T.P., Garcia H.E., Baranova O.K., Zweng M.M. and Johnson D.R. (2010). *World Ocean Atlas 2009, Volume 1: Temperature*. Tech. Rep. S. Levitus, Ed. NOAA Atlas NESDIS 68, Washington, DC: U.S. Government Printing Office, 184 pp.

Lorenzo M.N., Iglesias I., Taboada J.J. and Gomez-Gesteira M. (2010). Relationship between monthly rainfall in northwest Iberian Peninsula and North Atlantic sea surface temperature. *International Journal of Climatology*, 30:980–990.

Lunven M., Guillaud J.F., Youenou A., Crassous M.P., Berric R., Le Gall E., Kerouel R., Labry C. and Aminot A. (2005). Nutrient and phytoplankton distribution in the Loire River plume (Bay of Biscay, France) resolved by a new fine scale sampler. *Estuarine Coastal and Shelf Science*, 65(1-2):94–108.

Lyard F., Lefevre F., Letellier T. and Francis O. (2006). Modelling the global ocean tides: modern insights from FES2004. *Ocean Dynamics*, 56(5-6):394–415.

Marques W.C., Fernandes E.H., Monteiro I.O. and Moller O.O. (2009). Numerical modeling of the Patos Lagoon coastal plume, Brazil. *Continental Shelf Research*, 29(3):556–571.

Marta-Almeida M. and Dubert J. (2006). The structure of tides in the Western Iberian region. *Continental Shelf Research*, 26(3):385–400.

Marta-Almeida M., Reboreda R., Rocha C., Dubert J., Nolasco R., Cordeiro N., Luna T., Rocha A., Silva J.D.L.E., Queiroga H., Peliz A. and Ruiz-Villarreal M. (2012). Towards operational modeling and forecasting of the Iberian shelves ecosystem. *Plos One*, 7(5).

Martins C.S., Hamann M. and Fiuza A.F.G. (2002). Surface circulation in the eastern North Atlantic from drifters and altimetry. *Journal of Geophysical Research*, 107(C12):3217.

Martins F., Leitão P., Silva A. and Neves R. (2001). 3D modelling in the Sado estuary using a new generic vertical discretization approach. *Oceanologica Acta*, 24:S51–S62.

Martins F., Neves R. and Leitão P. (1998). A three-dimensional hydrodynamic model with generic vertical coordinate. *Hydroinformatics*, 98:1403–1410.

Martinsen E.A. and Engedahl H. (1987). Implementation and testing of a lateral boundary scheme as an open boundary-condition in a barotropic ocean model. *Coastal Engineering*, 11(5-6):603–627.

Mateus M., Riflet G., Chambel P., Fernandes L., Fernandes R., Juliano M., Campuzano F., de Pablo H. and Neves R. (2012). An operational model for the West Iberian coast: products and services. *Ocean Science*, 8(4):713–732.

Mazé J.P., Arhan M. and Mercier H. (1997). Volume budget of the eastern boundary layer off the Iberian Peninsula. *Deep-Sea Research I*, 44:1543–1574.

McClain C.R., Chao S.Y., Atkinson L.P., Blanton J.O. and Decastillejo F. (1986). Wind-driven upwelling in the vicinity of Cape Finisterre, Spain. *Journal of Geophysical Research-Oceans*, 91(C7):8470–8486.

Milliff R.F., Morzel J., Chelton D.B. and Freilich M.H. (2004). Wind stress curl and wind stress divergence biases from rain effects on QSCAT surface wind retrievals. *Journal of Atmospheric and Oceanic Technology*, 21(8):1216–1231.

Monteiro I.O., Marques W.C., Fernandes E.H., Goncalves R.C. and Moller O.O. (2011). On the effect of earth rotation, river discharge, tidal oscillations, and wind in the dynamics of the Patos Lagoon coastal plume. *Journal of Coastal Research*, 27(1):120–130.

Montero M., Lloret A. and Ruiz-Mateo A. (1992). Water renovation rate in Bouzas basins. *Hydraulic and Environmental Modelling: Coastal Waters*, 263–276.

Montero P., Gomez-Gesteira M., Taboada J.J., Ruiz-Villarreal. M., Santos A.P., Neves R.J.J., Prego R. and Perez-Villar V. (1999). On residual circulation of Ria de Vigo using a 3D baroclinic model. *Boletín Instituto Español de Oceanografía*, 15:Suplumento 1.

Montero P., Prego M. R.and Gomez-Gesteira, Neves R., Taboada J.J. and Perez-Villar V. (1997). Aplicación de un modelo 2D al transporte de partículas en la bahía de la Coruña. *In Actas del VIII Seminário Ibérico de Química Marina*, 131–136.

Mourino C. and Fraga F. (1982). Hydrography of the Ria of Vigo - 1976-1977 - abnormal influence of the Miño River. *Investigacion Pesquera*, 46(3):459–468.

Munchow A. and Garvine R.W. (1993). Buoyancy and wind forcing of a coastal current. *Journal of Marine Research*, 51(2):293–322.

Nogueira E., Pérez F.F. and Rios A.F. (1997a). Modelling Thermohaline Properties in an Estuarine Upwelling Ecosystem (Ria de Vigo: NW Spain) using Box-Jenkins Transfer Function Models. *Estuarine, Coastal and Shelf Science*, 44:685–702.

Nogueira E., Perez F.F. and Rios A.F. (1997b). Seasonal patterns and long-term trends in a estuarine upwelling Ecosystem (Ria de Vigo: NW Spain). *Estuarine, Coastal and Shelf Science*, 44:285–300.

Ospina-Alvarez N., Prego R., Alvarez I., deCastro M., Alvarez-Ossorio M.T., Pazos Y., Campos M.J., Bernardez P., Garcia-Soto C., Gomez-Gesteira M. and Varela M. (2010). Oceanographical patterns during a summer upwelling-downwelling event in the Northern Galician Rias: Comparison with the whole Ria system (NW of Iberian Peninsula). *Continental Shelf Research*, 30(12):1362–1372.

Otero P. and Ruiz-Villarreal M. (2008). Wind forcing of the coastal circulation off north and northwest Iberia: Comparison of atmospheric models. *Journal of Geophysical Research-Oceans*, 113(C10).

Otero P., Ruiz-Villarreal M., García-García L., González-Nuevo G. and Cabanas J.M. (2013). Coastal dynamics off Northwest Iberia during a stormy winter period. *Ocean Dynamics*, 63:115–129.

Otero P., Ruiz-Villarreal M. and Peliz A. (2008). Variability of river plumes off Northwest Iberia in response to wind events. *Journal of Marine Systems*, 72(1-4):238–255.

Otero P., Ruiz-Villarreal M., Peliz A. and Cabanas J.M. (2010). Climatology and reconstruction of runoff time series in northwest Iberia: influence in the shelf buoyancy budget off Ria de Vigo. *Scientia Marina*, 74(2):247–266.

Otto L. (1975). *Oceanography of the Ria de Arosa (NW Spain)*. University of Leiden, Holland, 210 pp.

Park K. (1966). Columbia River plume identification by specific alkalinity. *Limnology and Oceanography*, 11:118–120.

Pascual J. (1987a). Un modelo de circulación inducida por el viento en la Ria de Arosa. *Instituto Español de Oceanografia*, 4:107–120.

Pascual J. (1987b). The vertical and horizontal m_2 tide in the Ria de arosa (Galicia, Spain NW). *Revista de Geofísica, Universidade Complutense Madrid*, 57–64.

Pawlowicz R., Beardsley B. and Lentz S. (2002). Classical tidal harmonic analysis including error estimates in MATLAB using T-TIDE. *Computers & Geosciences*, 28(8):929–937.

Pearcy W.G. (1992). *Ocean Ecology of North Pacific Salmonids*. University of Washington Press, Seattle, WA.

Peliz A., Dubert J. and Haidvogel D.A. (2003). Subinertial response of a density-driven Eastern Boundary Poleward Current to wind forcing. *Journal of Physical Oceanography*, 33:1633–1650.

Peliz A., Dubert J., Santos A.M.P., Oliveira P.B. and LeCann B. (2005). Winter upper ocean circulation in the Western Iberian Basin-Fronts, Eddies and Poleward Flows: an overview. *Deep-Sea Research I*, 52:621–646.

Peliz A., Rosa T.L., Santos A.M.P. and Pissarra J.L. (2002). Fronts, jets, and counter-flows in the Western Iberian upwelling system. *Journal of Marine Systems*, 35(1-2):61–77.

Penabad E., Alvarez I., Balseiro C.F., deCastro M., Gomez B., Perez-Munuzuri V. and Gomez-Gesteira M. (2008). Comparative analysis between operational weather prediction models and QuikSCAT wind data near the Galician coast. *Journal of Marine Systems*, 72(1-4):256–270.

Pensieri S., Bozzano R. and Schiano M.E. (2010). Comparison between QuikSCAT and buoy wind data in the Ligurian Sea. *Journal of Marine Systems*, 81(4):286–296.

Perez F.F., Álvarez Salgado X.A., Rosón G. and Rios A.F. (1992). Carbonic-calcium system, nutrients and total organic nitrogen incontinental runoff to the Galician Rias Baixas, NW Spain. *Oceanologica Acta*, 15:595–602.

Perez F.F., Rios A.F., King B.A. and Pollard R.T. (1995). Decadal changes of the θ - s relationship of the eastern North Atlantic central water. *Deep-Sea Research Part I-Oceanographic Research Papers*, 42(11-12):1849–1864.

Pickett M.H., Tang W.Q., Rosenfeld L.K. and Wash C.H. (2003). QuikSCAT satellite comparisons with nearshore buoy wind data off the US West Coast. *Journal of Atmospheric and Oceanic Technology*, 20(12):1869–1879.

Pitcher G.C., Figueiras F.G., Hickey B.M. and Moita M.T. (2010). The physical oceanography of upwelling systems and the development of harmful algal blooms. *Progress in Oceanography*, 85(1-2):5–32.

Pollard R. and Pu S. (1985). Structure and circulation of the upper Atlantic Ocean northeast of the Azores. *Progress in Oceanography*, 14:443–462.

Portabella M. and Stoffelen A. (2001). Rain detection and quality control of SeaWinds. *Journal of Atmospheric and Oceanic Technology*, 18(7):1171–1183.

Prego R., Barciela C. and Varela M. (1999). Nutrient dynamics in the Galician coastal area (Northwestern Iberian Peninsula): do the Rias Bajas receive more nutrient salts than the Rias Altas? *Continental Shelf Research*, 19:317–334.

Prego R., Dale A.W., deCastro M., Gomez-Gesteira M., Taboada J.J., Montero P., Villareal M.R. and Perez-Villar V. (2001). Hydrography of the Pontevedra Ria: Intra-annual spatial and temporal variability in a Galician coastal system (NW Spain). *Journal of Geophysical Research-Oceans*, 106(C9):19845–19857.

Prego R. and Fraga F. (1992). A simple-model to calculate the residual flows in a Spanish Ria-Hydrographic Consequences in the Ria-De-Vigo. *Estuarine Coastal and Shelf Science*, 34(6):603–615.

Prego R., Guzman-Zuniga D., Varela M., deCastro M. and Gomez-Gesteira M. (2007). Consequences of winter upwelling events on biogeochemical and phytoplankton patterns in a western Galician ria (NW Iberian Peninsula). *Estuarine Coastal and Shelf Science*, 73(3-4):409–422.

Reifel K.M., Johnson S.C., DiGiacomo P.M., Mengel M.J., Nezlin N.P., Warrick J.A. and Jones B.H. (2009). Impacts of stormwater runoff in the Southern California Bight: Relationships among plume constituents. *Continental Shelf Research*, 29(15):1821–1835.

Reis J.L., Martinho A.S., Pires-Silva A.A. and Silva A.J. (2009). Assessing the influence of the river discharge on the Minho estuary tidal regime. *Journal of Coastal Research*, 1405–1409.

Rio-Barja F.X. and Rodriguez-Lestegas F. (1996). *Os ríos, in as augas de Galicia*. Consello de Cultura, 611 pp.

Rios A.F., Nombela M.A., Perez F.F., Roson G. and Fraga F. (1992a). Calculation of runoff to an estuary, Ria de Vigo. *Scientia Marina*, 56:29–33.

Rios A.F., Perez F.F. and Fraga F. (1992b). Water Masses in the Upper and Middle North-Atlantic Ocean East of the Azores. *Deep-Sea Research Part a-Oceanographic Research Papers*, 39(3-4A):645–658.

Robinson I.S. (2004). *Measuring the oceans from space: the principles and methods of satellite oceanography*. Springer, 655 pp.

Roegner G.C., Hickey B.M., Newton J.A., Shanks A.L. and Armstrong D.A. (2002). Wind-induced plume and bloom intrusions into Willapa Bay, Washington. *Limnology and oceanography*, 47(4):1033–1042.

Roson G., Perez F.F., Alvarez-Salgado X.A. and Figueiras F.G. (1995). Variation of both thermohaline and chemical properties in an estuarine upwelling ecosystem: Ria de Arousa; I. Time Evolution. *Estuarine Coastal and Shelf Science*, 41:195–213.

Royer L. and Emery W.J. (1982). Variations of the Fraser River Plume and their relationship to forcing by tide, wind and discharge. *Atmosphere-Ocean*, 20(4):357–372.

Ruiz-Villarreal M., Montero P., Taboada J.J., Prego R., Leitao P.C. and Perez-Villar V. (2002). Hydrodynamic model study of the Ria de Pontevedra under estuarine conditions. *Estuarine Coastal and Shelf Science*, 54(1):101–113.

Ruti P.M., Marullo S., D'Ortenzio F. and Tremant M. (2008). Comparison of analyzed and measured wind speeds in the perspective of oceanic simulations over the Mediterranean basin: Analyses, QuikSCAT and buoy data. *Journal of Marine Systems*, 70(1-2):33–48.

Sanchez R.F., Relvas P. and Pires H.O. (2007). Comparisons of ocean scatterometer and anemometer winds off the southwestern Iberian Peninsula. *Continental Shelf Research*, 27:155–175.

Santos A.J.P. (1995). *Modelo hidrodinâmico tridimensional de circulação oceânica e estuarina*. Phd thesis, Instituto Superior Técnico, Lisboa, 273 pp.

Santos A.M.P., Peliz A., Dubert J., Oliveira P.B., Angelico M.M. and Re P. (2004). Impact of a winter upwelling event on the distribution and transport of sardine (Sardina pilchardus) eggs and larvae off western Iberia: a retention mechanism. *Continental Shelf Research*, 24(2):149–165.

Santos F., Gomez-Gesteira M., deCastro M. and Alvarez I. (2012). Variability of coastal and ocean water temperature in the upper 700 m along the Western Iberian Peninsula from 1975 to 2006. *Plos One*, 7(1-7):149–165.

Saunders P.M. (1982). Circulation in the eastern North Atlantic. *Journal of Marine Research*, 40:641–657.

Shi J.Z., Lu L.F. and Liu Y.N. (2010). The hydrodynamics of an idealized estuarine plume along a straight coast: a numerical study. *Environmental Modelling and Software*, 15(6):487–502.

Skamarock W., Klemp J., Dudhia J., Gill D., Barker D., Duda M., Huang X., Wang W. and Powers J.G. (2008). *A description of the Advanced Research WRF Version 3*. Tech. Rep., NCAR Technical Note NCAR/TN-475+STR, 113 pp.

Soares I.D., Kourafalou V. and Lee T.N. (2007). Circulation on the western South Atlantic continental shelf: 2. spring and autumn realistic simulations. *Journal of Geophysical Research: Oceans*, 112(C4).

Soomere T. and Keevallik S. (2003). Directional and extreme wind properties in the Gulf of Finland. *Proceedings Estonian Academy of Sciences, Enginering*, 9(2):73–90.

Sordo I., Barton E.D., Cotos J.M. and Pazos Y. (2001). An inshore poleward current in the NW of the Iberian Peninsula detected from satellite images, and its relation with G-catenatum and D-acuminata blooms in the Galician Rias. *Estuarine Coastal and Shelf Science*, 53(6):787–799.

Sousa M.C. and Dias J.M. (2007). Hydrodynamic model calibration for a mesotidal lagoon: the case of Ria de Aveiro (Portugal). *Journal of Coastal Research*, SI50:1075–1080.

Sousa R., Guilhermino L. and Antunes C. (2005). Molluscan fauna in the freshwater tidal area of the River Minho estuary, NW of Iberian Peninsula. *Annales De Limnologie-International Journal of Limnology*, 41(2):141–147.

Souto C., Gilcoto M., Farina-Busto L. and Perez F.F. (2003). Modeling the residual circulation of a coastal embayment affected by wind-driven upwelling: Circulation of the Ria de Vigo (NW Spain). *Journal of Geophysical Research-Oceans*, 108(C11).

Stefansson U. and Richards F.A. (1963). Processes contributing to the nutrient distribution off the Columbia River and Strait of Juan de Fuca. *Limnology and Oceanography*, 8:394–410.

Stiles B.W. and Yueh S.H. (2002). Impact of rain on spaceborne Ku-band wind scatterometer data. *Ieee Transactions on Geoscience and Remote Sensing*, 40(9):1973–1983.

Szekielda K.H. and Kupferman S. (1973). Heterogeneities in salinity in a river plume. *Estuarine and Coastal Marine Science*, 1(4):419–424.

Taboada J.J., Prego R., Ruiz-Villarreal M., Gomez-Gesteira M., Montero P., Santos A.P. and Perez-Villar V. (1998). Evaluation of the seasonal variations in the residual circulation in the Ria of Vigo (NW Spain) by means of a 3D baroclinic model. *Estuarine Coastal and Shelf Science*, 47(5):661–670.

Takano K. (1954a). On the salinity and the velocity distributions off the mouth of a river. *Journal of the Oceanographical Society of Japan*, 10(3):92–98.

Takano K. (1954b). On the velocity distribution off the mouth of a river. *Journal of the Oceanographical Society of Japan*, 10(2):60–64.

Takano K. (1955). A complementary note on the diffusion of the seaward river flow off the mouth. *Journal of the Oceanographical Society of Japan*, 11(4):147–149.

Tang W.Q., Liu W.T. and Stiles B.W. (2004). Evaluations of high-resolution ocean surface vector winds measured by QuikSCAT scatterometer in coastal regions. *Ieee Transactions on Geoscience and Remote Sensing*, 42(8):1762–1769.

Tenore K.R., Alonsonoval M., Alvarezossorio M., Atkinson L.P., Cabanas J.M., Cal R.M., Campos H.J., Castillejo F., Chesney E.J., Gonzalez N., Hanson R.B., Mcclain C.R., Miranda A., Roman M.R., Sanchez J., Santiago G., Valdes L., Varela M. and Yoder J. (1995). Fisheries and oceanography off Galicia, NW Spain - mesoscale spatial and temporal changes in physical processes and resultant patterns of biological productivity. *Journal of Geophysical Research-Oceans*, 100(C6):10943–10966.

Tenore K.R., Boyer L.F., Cal R.M., Corral J., Garciafernandez C., Gonzalez N., Gonzalezgurriaran E., Hanson R.B., Iglesias J., Krom M., Lopezjamar E., McClain J., Pamatmat M.M., Perez A., Rhoads D.C., Desantiago G., Tietjen J., Westrich J. and Windom H. (1982). Fisheries and oceanography off Galicia, NW Spain - mesoscale spatial and temporal changes in physical processes and resultant patterns of biological productivity. *Journal of Marine Research*, 40:701–770.

Tian R.C., Hu F.X. and Martin J.M. (1993). Summer nutrient fronts in the Changjiang (Yantze River) estuary. *Estuarine Coastal and Shelf Science*, 37(1):27–41.

Tilstone G.H., Figueiras F.G. and Fraga F. (1994). Upwelling-downwelling sequences in the generation of red tides in a Coastal Upwelling System. *Marine Ecology-Progress Series*, 112(3):241–253.

Torres R., Barton E.D., Miller P. and Fanjul E. (2003). Spatial patterns of wind and sea surface temperature in the Galician upwelling region. *Journal of Geophysical Research-Oceans*, 108(C4).

Torres-López S., Varela R.A. and Delhez E. (2001). Residual circulation and thermohaline distribution of the Ria de Vigo: a 3D hydrodynamical model. *Scientia Marina*, 65:277–289.

van Alphen J.S.L.J., Ruijter W.P.M. and C. B.J. (1988). Outflow and three-dimensional spreading of Rhine River water in the Netherlands coastal zone. *In: Physical Processes in Estuaries, J. Dronkers and W. van Leussen, Eds., Springer*, 70–92.

Varela M., Alvarez-Ossorio M.T., Bode A., Prego R., Bernardez P. and Garcia-Soto C. (2010). The effects of a winter upwelling on biogeochemical and planktonic components in an area close to the Galician Upwelling Core: The Sound of Corcubion (NW Spain). *Journal of Sea Research*, 64(3):260–272.

Varela M., Prego R. and Pazos Y. (2008). Spatial and temporal variability of phytoplankton biomass, primary production and community structure in the Pontevedra Ria (NW Iberian Peninsula): oceanographic periods and possible response to environmental changes. *Marine Biology*, 154(3):483–499.

Varela R.A., Roson G., Herrera J.L., Torres-Lopez S. and Fernandez-Romero A. (2005). A general view of the hydrographic and dynamical patterns of the Rias Baixas adjacent sea area. *Journal of Marine Systems*, 54(1-4):97–113.

Vaz N. (2007). *Study of heat and salt transport processes in the Espinheiro Channel (Ria de Aveiro)*. Phd thesis, Physics Department, University of Aveiro, Aveiro, 151 pp.

Vaz N. and Dias J.M. (2008). Hydrographic characterization of an estuarine tidal channel. *Journal of Marine Systems*, 70:168–181.

Vaz N., Dias J.M. and Leitão P.C. (2009a). Three-dimensional modelling of a tidal channel: The Espinheiro Channel (Portugal). *Continental Shelf Research*, 29(1):29–41.

Vaz N., Dias J.M., Leitão P.C. and Nolasco R. (2007). Application of the Mohid-2D model to a mesotidal temperate coastal lagoon. *Computer ad Geosciences*, 33(9):1204–1209.

Vaz N., Fernandes L., Leitão P.C., Dias J.M. and Neves R. (2009b). The Tagus estuarine plume induced by wind and river runoff: Winter 2007 case study. *Journal of Coastal Research*, SI56:1090–1094.

Vitorino J., Oliveira A., Jouanneau J.M. and Drago T. (2002). Winter dynamics on the northern Portuguese shelf. Part 1: physical processes. *Journal of Geophysical Research*, 108:3130–3143.

Warner J.C., Geyer W.R. and Lerczak J.A. (2005). Numerical modeling of an estuary: A comprehensive skill assessment. *Journal of Geophysical Research-Oceans*, 110(C5).

Warrick J.A. and Milliman J.D. (2003). Hyperpycnal sediment discharge from semiarid southern California rivers: Implications for coastal sediment budgets. *Geology*, 31(9):781–784.

Whitney M. and Garvine R.W. (2005). Wind influence on a coastal buoyant outflow. *Journal of Geophysical Research*, 110(C03014).

Whitney M.M. and Garvine R.W. (2006). Simulating the Delaware Bay buoyant outflow: Comparison with observations. *Journal of Physical Oceanography*, 36(3-21).

Wooster W.S., Bakun A. and Mclain D.R. (1976). Seasonal upwelling cycle along Eastern Boundary of North-Atlantic. *Journal of Marine Research*, 34(2):131–141.

Xia M., Xie L. and Pietrafesa L.J. (2007). Modeling of the Cape Fear River estuary plume. *Estuaries and Coasts*, 30:698–709.

Xia M., Xie L., Pietrafesa L.J. and Whitney M.M. (2011). The ideal response of a Gulf of Mexico estuary plume to wind forcings: Its connection with salt flux and a Lagrangian view. *Journal of Geophysical Research*, 116:C08035.

Yankovsky A.E. and Chapman D.C. (1997). A simple theory for the fate of buoyant coastal discharges. *Journal of Physical Oceanography*, 27(7):1386–1401.

Zhang Q.H., Janowitz G.S. and Pietrafesa L.J. (1987). The interaction of estuarine and shelf waters: A model and applications. *Journal of Physical Oceanography*, 17:455–469.